Study of hydrogen bonding in energy materials using single crystal neutron diffraction

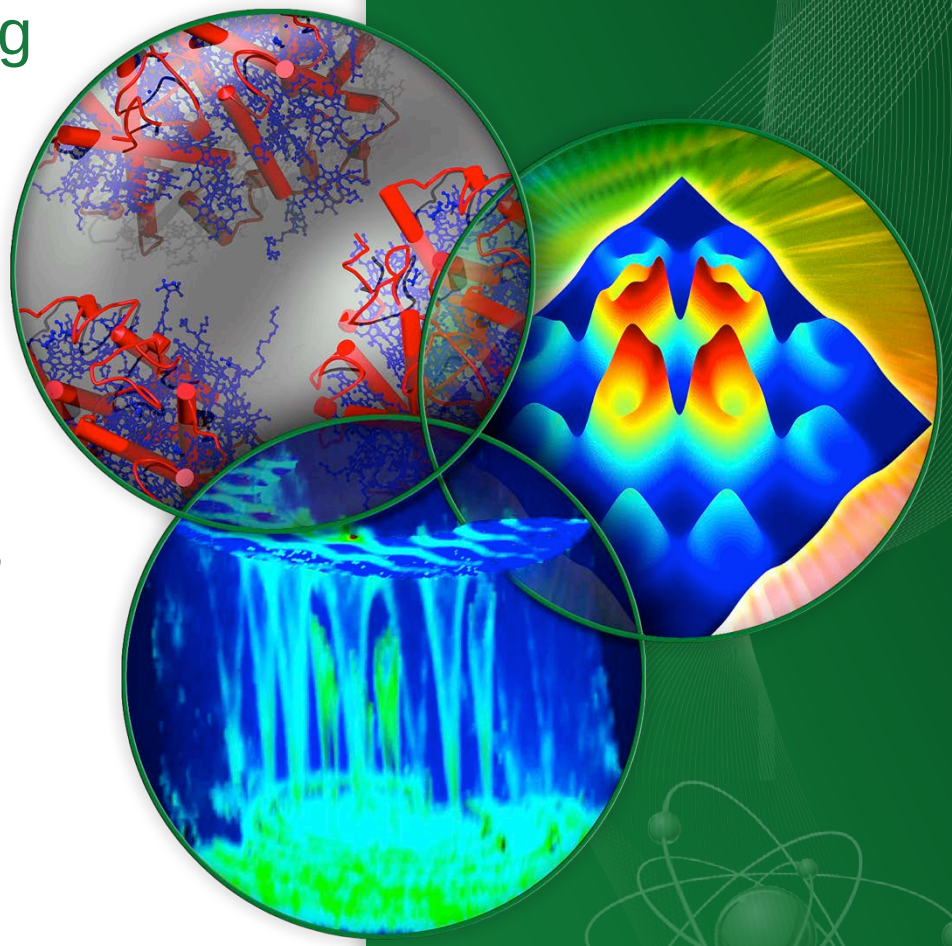

Xiaoping Wang

Chemical and Engineering Materials Division
Neutron Science Directorate
Oak Ridge National Laboratory
Tennessee, USA

ORNL/Georgia Tech Joint Workshop
27 January 2016

The ORNL Spallation Neutron Source

Neutron Time-of-Fligh Laue

- Combine de Broglie's equation with Bragg's law

$$\lambda = \frac{h}{mv} = \frac{ht}{m(L_1 + l_2)} = 2d\sin\theta \qquad t = \frac{m}{h}(L_1 + l_2) \times 2d\sin\theta$$

Neutron Time-of-flight Laue

(**Wavelength-resolved Laue**)

3-*D* Reciprocal Space Mapping

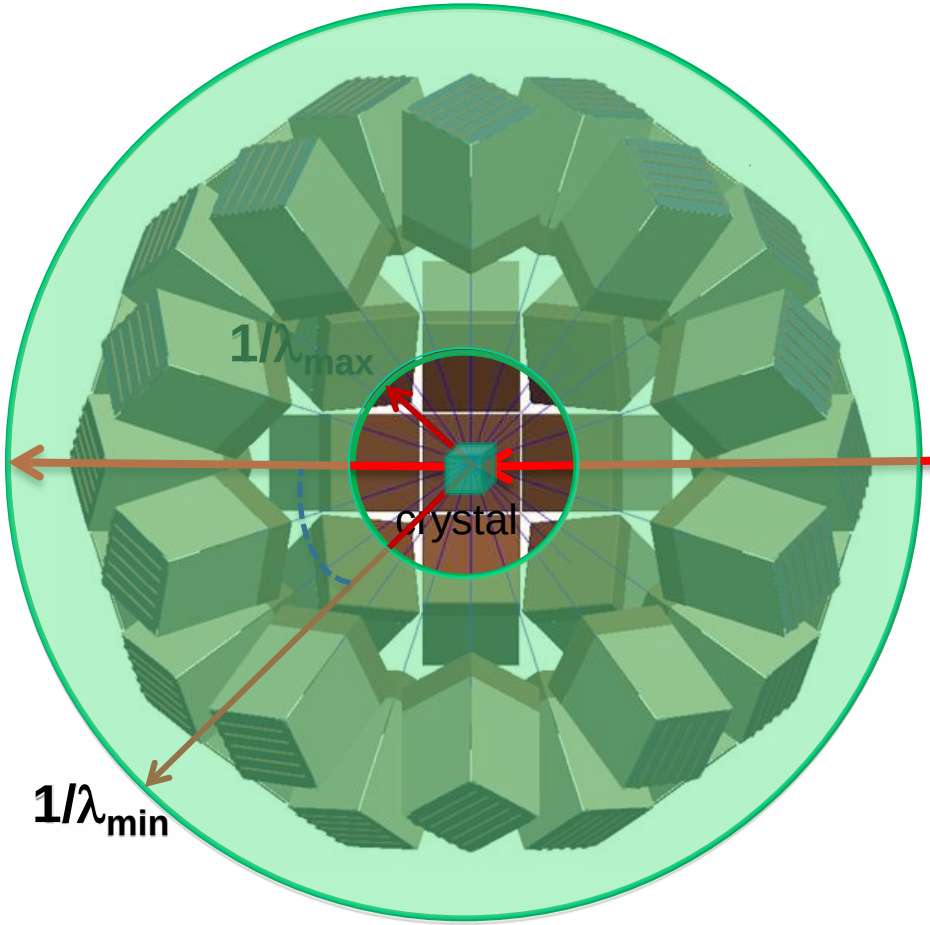

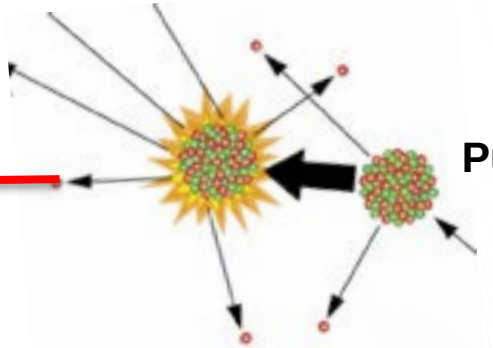

Pulsed Neutron
60 *Hz*

The SNS TOPAZ Instrument

Neutron wavelength-resolved Laue
3*D* Reciprocal space mapping

d_{min} = 0.25 Å

$Q_{max} \approx 25$ Å^{-1}

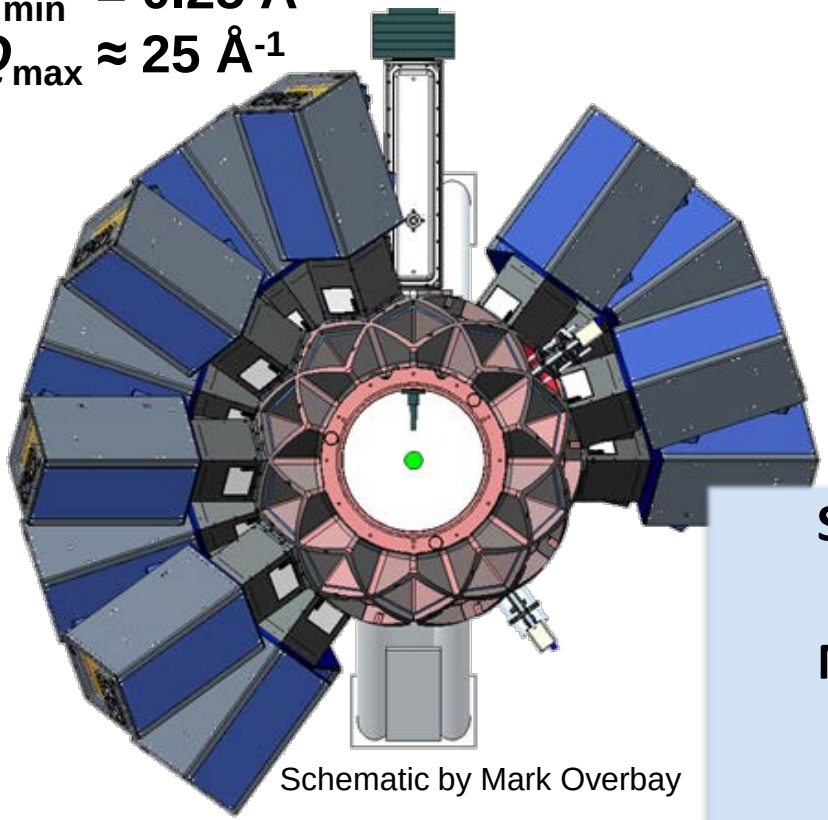

Schematic by Mark Overbay

21 Area Detectors
Installed in 2015

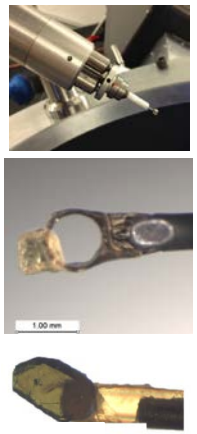

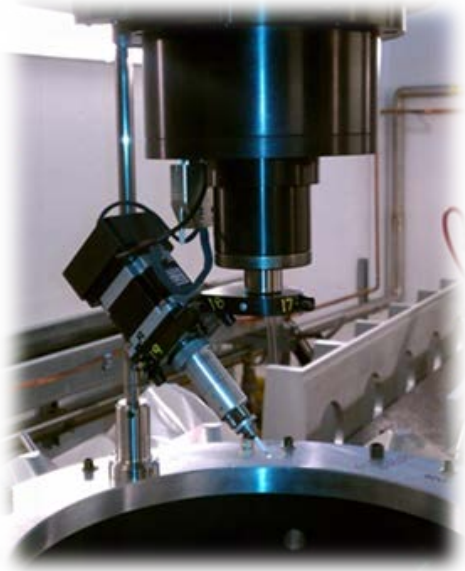

Crystal Logic Goniostat

Sub-Millimeter Sized Crystals

Diameter: 0.10 – 4.0 mm, Volume: > 0.1 mm^3

Multiple Area Detectors

Solid Angle Coverage: 2.4 ster.

Detector 2θ Coverage: 15.0° - 160°

Sample Environment

CryoStream 700 Plus: 90K – 500K

Accurate structural parameters from TOPAZ

Acta Crystallographica Section A
Foundations and Advances
ISSN 2053-2733

Received 26 February 2014
Accepted 3 July 2014

Accurate atomic displacement parameters from time-of-flight neutron-diffraction data at TOPAZ

Mads R. V. Jørgensen,[a] Venkatesha R. Hathwar,[a] Mattia Sist,[a] Xiaoping Wang,[b] Christina M. Hoffmann,[b] Alejandro L. Briseno,[c] Jacob Overgaard[a]* and Bo B. Iversen[a]*

[a]Center for Materials Crystallography, Department of Chemistry and iNano, Aarhus University, Langelandsgade 140, Aarhus C, DK-8000, Denmark, [b]Chemical and Engineering Materials Division, BL-12 TOPAZ, Oak Ridge National Laboratory, PO Box 2008 - MS 6475, Oak Ridge, TN 37831, USA, and [c]Department of Polymer Science and Engineering, University of Massachusetts, 120 Governors Drive, Amherst, MA 01003, USA. Correspondence e-mail: jacobo@chem.au.dk, bo@chem.au.dk

Accurate atomic displacement parameters (ADPs) are a good indication of high-quality diffraction data. Results from the newly commissioned time-of-flight Laue diffractometer TOPAZ at the SNS are presented. Excellent agreement is found between ADPs derived independently from the neutron and X-ray data emphasizing the high quality of the data from the time-of-flight Laue diffractometer.

Jorgensen, M. R. V.; *et. al*. *Acta Cryst. A* **2014**, *70*, 679

Neutron Single Crystal Crystallography

- **Complementary to X-ray**
  - X-ray ➔ electron density distribution
  - Neutron ➔ nuclear / magnetic density distribution

X-ray Scattering power ∝ Atomic No.

Hydrogen atoms are not visible

C and N atoms are difficult to locate

Neutron Scattering powder ⊃ Isotope specific

H -3.74 fm, D 6.67 fm

N and Pb atoms are comparable

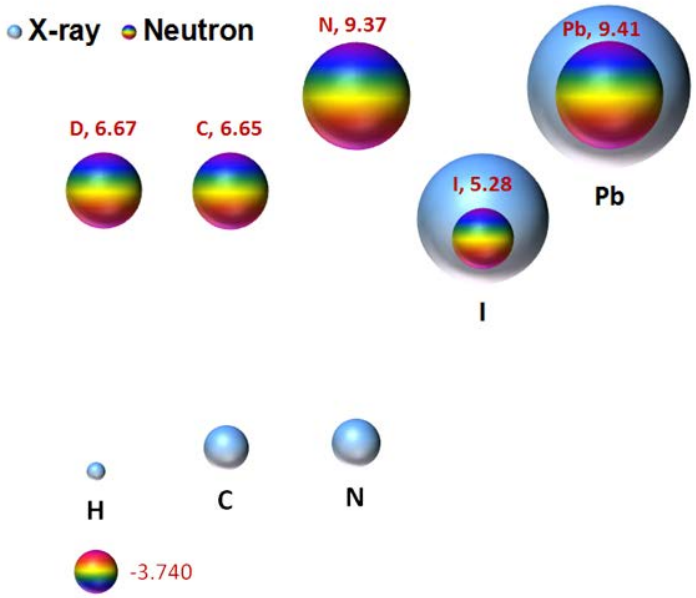

Notes: Neutron elastic scattering amplitude, known as the scattering length (*fm*), can be positive or negative, depending on whether the neutron-nuclear interaction is attractive or repulsive.

www.ncnr.nist.gov/resources/n-lengths/

Hydrogen bonding in hybrid perovskite $CH_3NH_3PbI_3$

- High power conversion efficiencies (> 20%) for solar cell applications
  - Heavy elements with very high X-ray absorption μ = **526.82** cm^{-1}
  - **Transparent to neutrons** μ = **0.654 + 0.508λ** cm^{-1}
- Effect of H-bonding on structural phase transitions

Cubic

↕

Tetragonal

↕

Orthorhombic

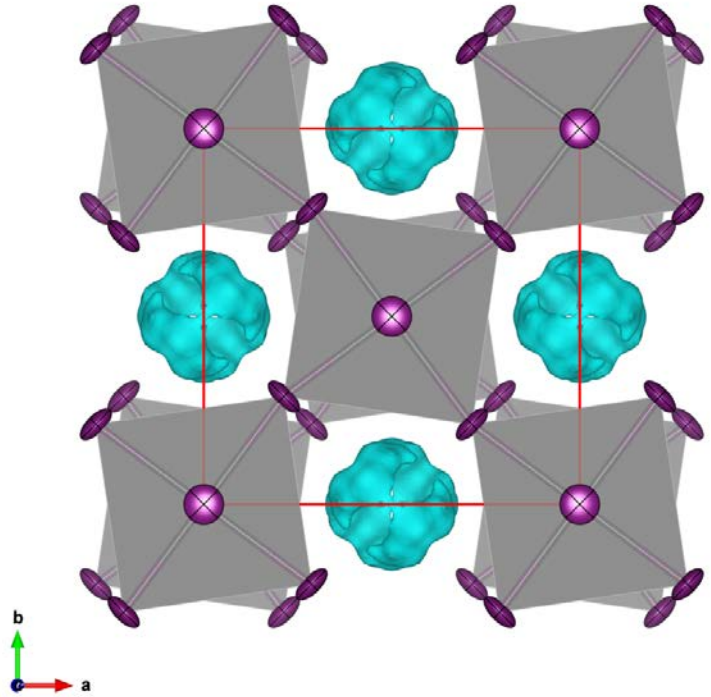

J. Chan, UTD, *TOPAZ data*

Quantitative analysis of hydrogen bonding

- **Isotope contrast study**
  - Nuclear density map [*difference Fourier*] reveals H atom positions

Occupancy	D (6.671 fm)	H (-3.739 fm)
HF	0.969(6)	0.031(6)
Pyrazine	0.080(3)	0.920(3)

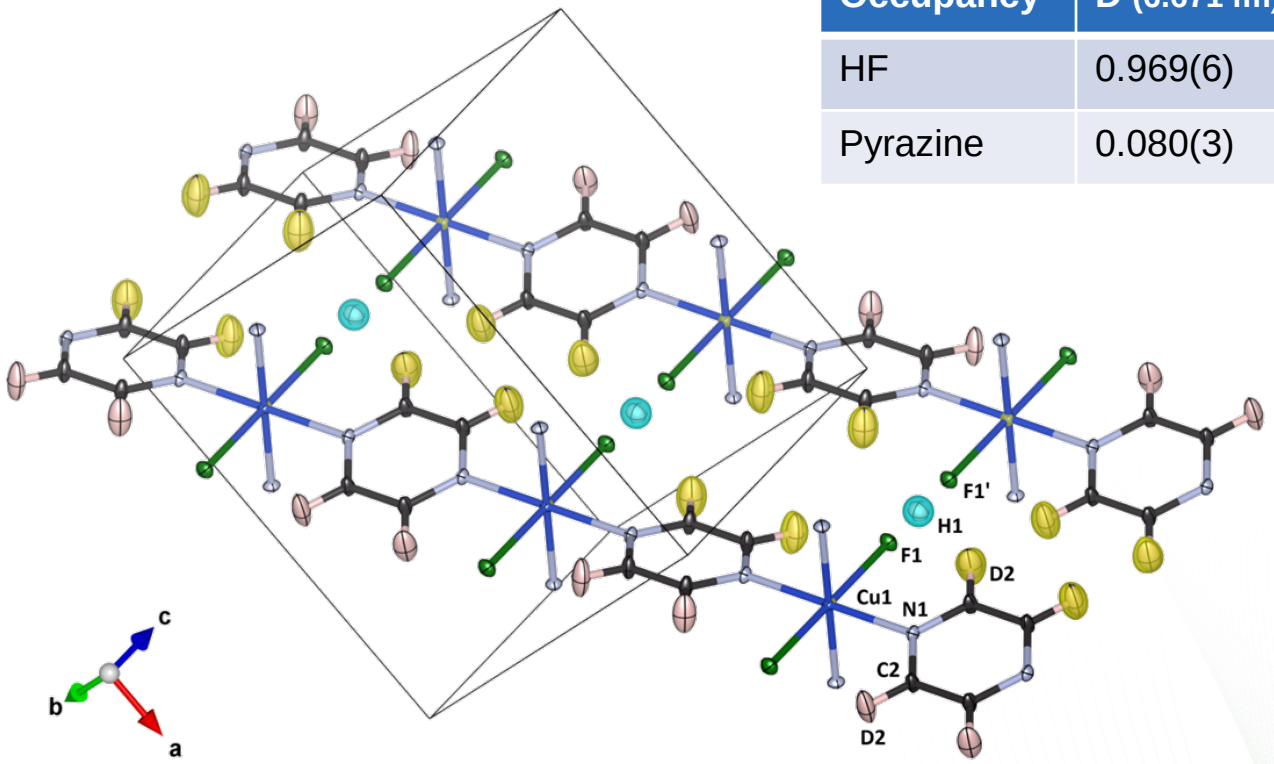

$[Cu(DF_2)(pyrazine\text{-}d_4)_2]PF_6$

J. A. Schlueter, *TOPAZ data*

Synthetic magnetoelectric multiferroics—means to control magnetism

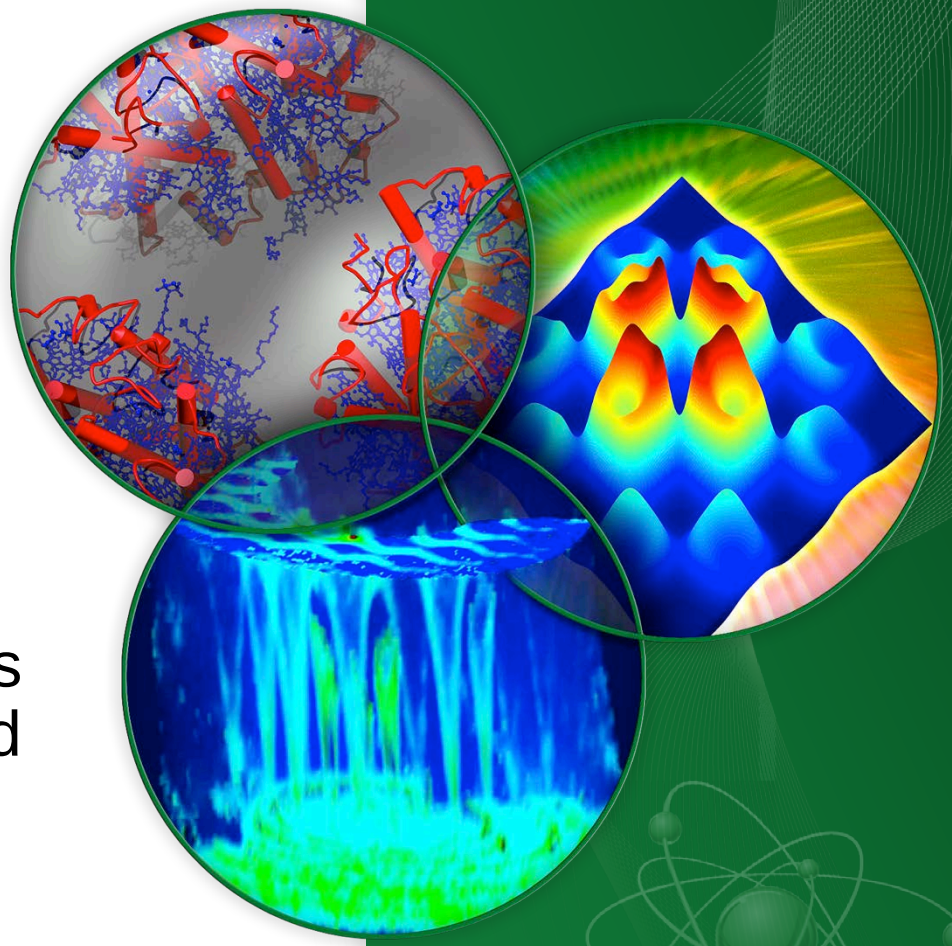

M.R. Fitzsimmons

Thin Films and Nanostructures Group in Quantum Condensed Matter Division

ORNL is managed by UT-Battelle
for the US Department of Energy

Outline

- Interfaces and mesoscale.
- Neutron scattering Wikisheet.
- Science examples
  - Advantage of bottoms-up synthesis
    - Overcoming magnetic dead layers
  - Magnetic impurities
    - Importance of Kondo effect in spintronics
  - Synthetic multiferroics
    - Superlattices
    - Pillar architecture

Why study interface science?

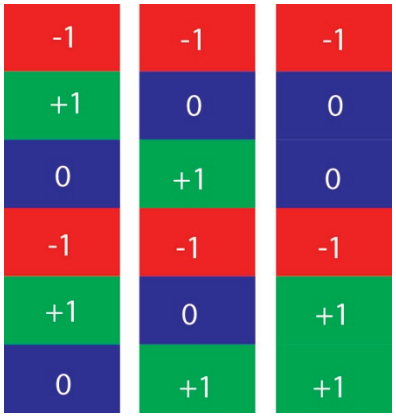

- Structure and properties of the interface differ from bulk.
- Opportunity to grow compositionally ordered structures.
  - Superconductivity in $La_{2-x}Sr_xCuO_4$ thin films, not bulk!
  - Harness electrostatic interactions, $(La,A)NiO_4$ A=Sr, Ca, Ba
- Interfaces automatically break P (parity or space) symmetry.
- Path forward to reconcile conflicts.
  - Robust insulators typically have empty d-bands
  - Magnetic materials typically have ½-filled d-bands
- Applications include:
  - Memory, computing, sensors
  - Permanent magnets
  - Lossless ferroelectrics
  - Thermoelectrics
  - Superconductivity

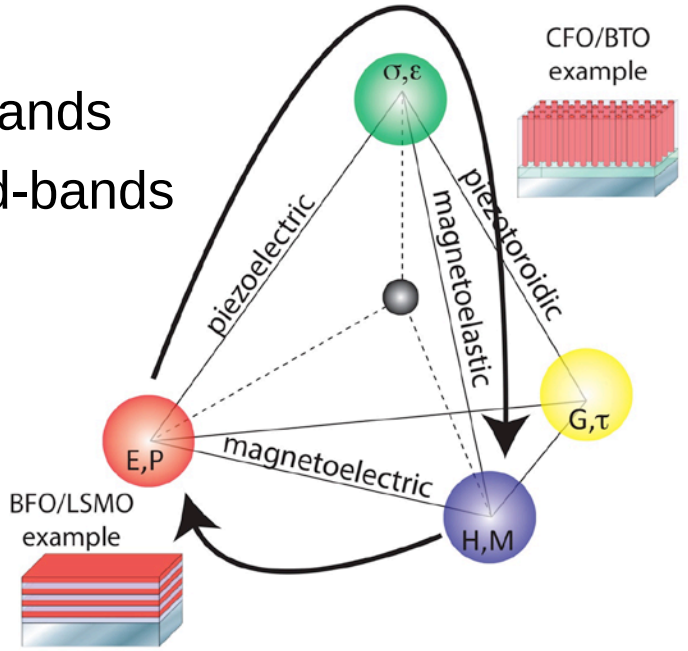

A neutron scattering Wikisheet

Reflectometry

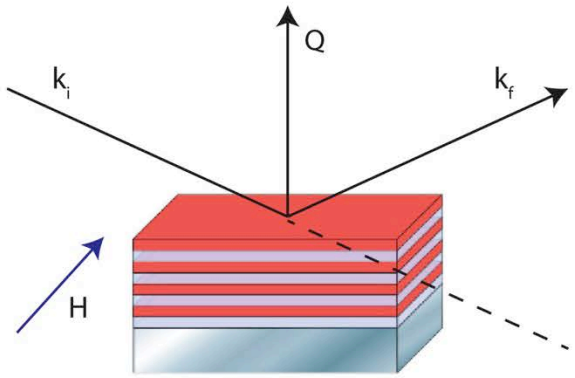

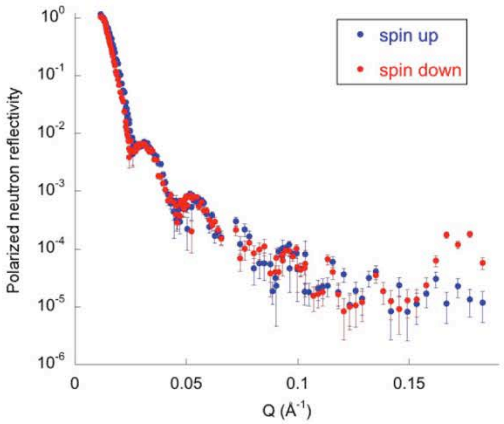

Sample requirements for thin films:
10 mm x 10 mm x 2-200 nm
Very smooth interfaces, σ < 1nm
Very uniform layer thicknesses, δ < 5%
M > 10 emu/cm^3 in sample plane

What do I learn?
Nuclear and (vector) M (parallel to sample plane) depth profile 1-2 nm resolution.
Variation of moment density in absolute units.

Small angle neutron scattering

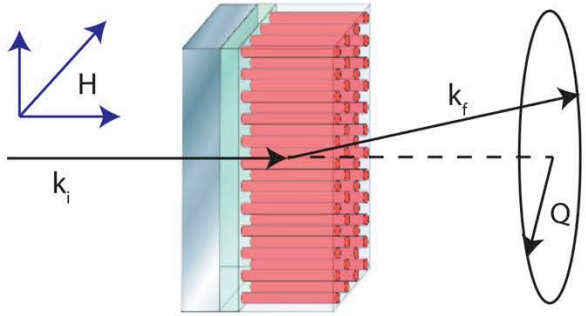

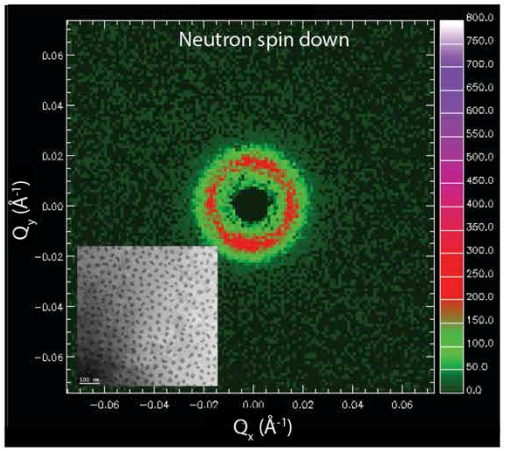

Sample requirements for thin films:
10 mm x 10 mm x ~20 nm
Samples can be stacked provided substrates are “transparent”.
M > 10 emu/cm^3

What do I learn?
Correlation between regions of different nuclear and vector M (in any direction) scattering length densities in range of 10-300 nm.
Variation of moment density in absolute units.

Magnetic dead layer problem

Polarization of spin current degraded by:

1) Spin flip scattering
2) Injection of wrong spins

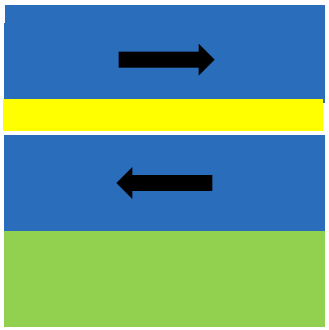

High R

Goal: <1 pJ per transition
(spin torque presently 5pJ/transition)

Magnetic dead layer problem

Polarization of spin current degraded by:

1) Spin flip scattering
2) Injection of wrong spins

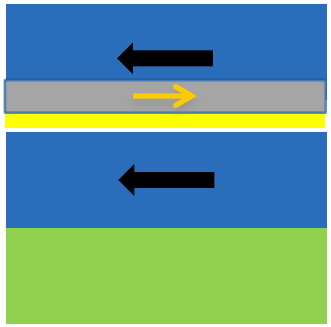

Goal: <1 pJ per transition
(spin torque presently 5pJ/transition)

Magnetic dead layer problem solved

- $La_{0.7}Sr_{0.3}MnO_3$ optimal composition for FM.
- (001) STO is non-polar.
- (001) $La_{0.7}Sr_{0.3}O$ has +2/3 charge.
- Polar discontinuity believed responsible for undesirable structure, e.g., magnetic dead layer and roughness.
- Hypothesis: Mitigate problem with layer-by-layer growth.
- (001) $La_{0.3}Sr_{0.7}O$ has +1/3 charge.

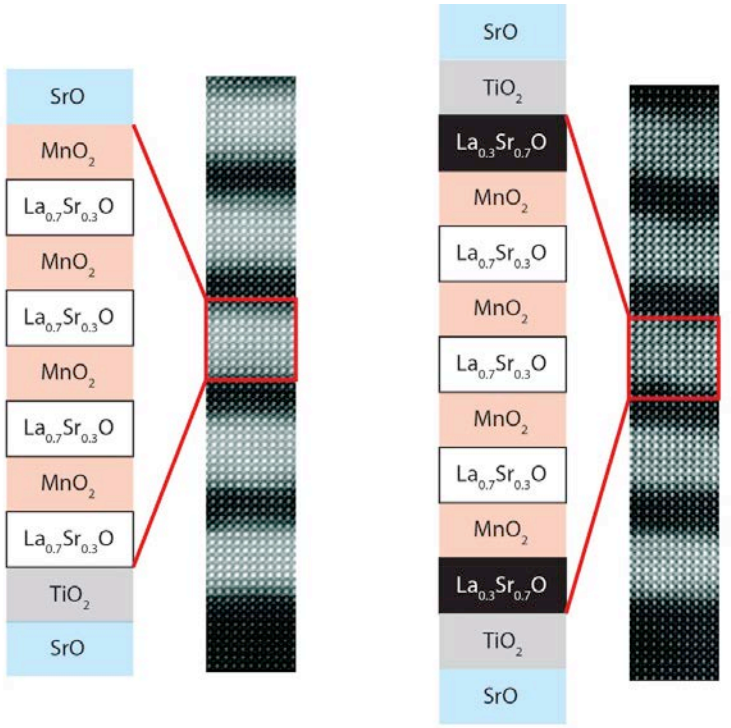

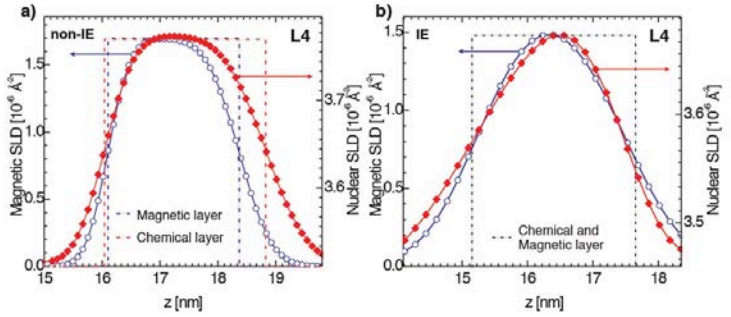

M. Huijben, Y. Liu, H. Boschker, V. Lauter, R. Egoavil, J. Verbeeck, S.G.E. te Velthuis. G. Rijinders, G. Koster, *Advanced Materials Interfaces*, **2**, 3, 1400416, (2015).

Synthetic multiferroic: We created a magnetic handle and then used it.

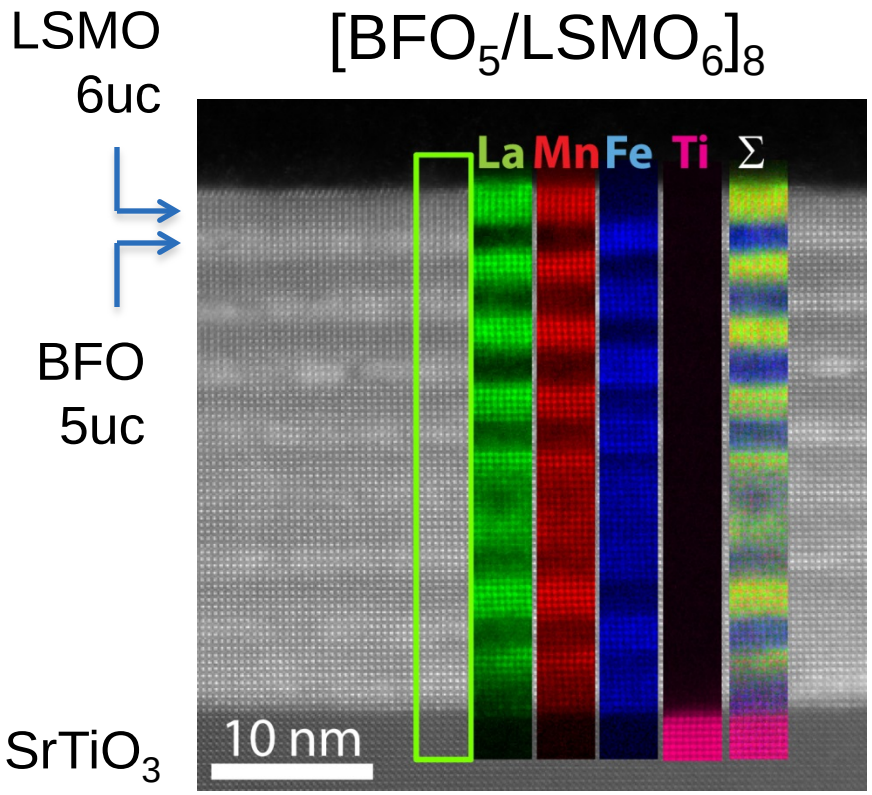

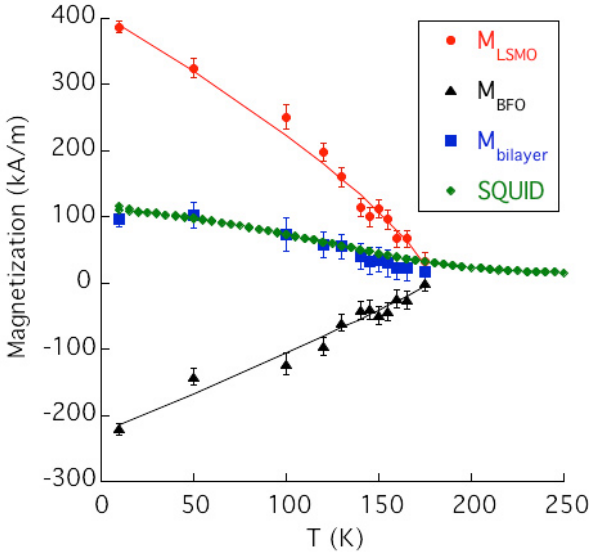

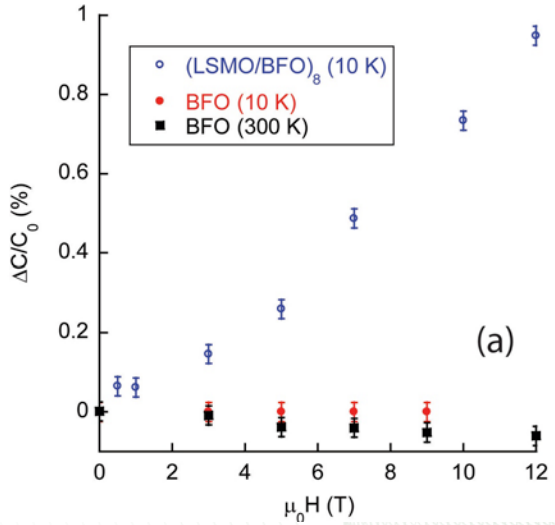

(1) Induced magnetization in BFO (sl), none found in BFO films.
(2) $1/C_0\, dC/dH = 0.1\%/Tesla.$

P. Jain *et al.*, Sci. Reports **5**, 9089 (2015)

Can a synthetic magnetoelectric multiferroic be realized at 300K?

- Fabricate $[BFO_5/LSMO_{20}]_9$ superlattice in Ho Nyung Lee's (MSTD) lab.
- T_c ~300+ K achieved.
- Neutron experiment completed 12/15.
- Electronic measurements beginning.

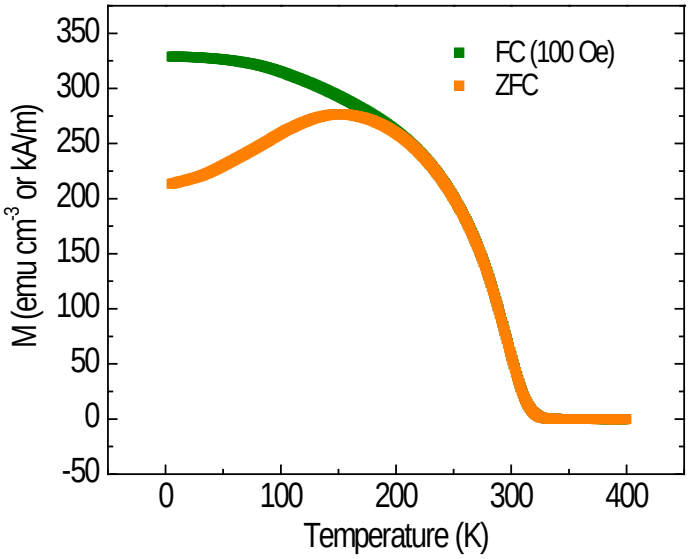

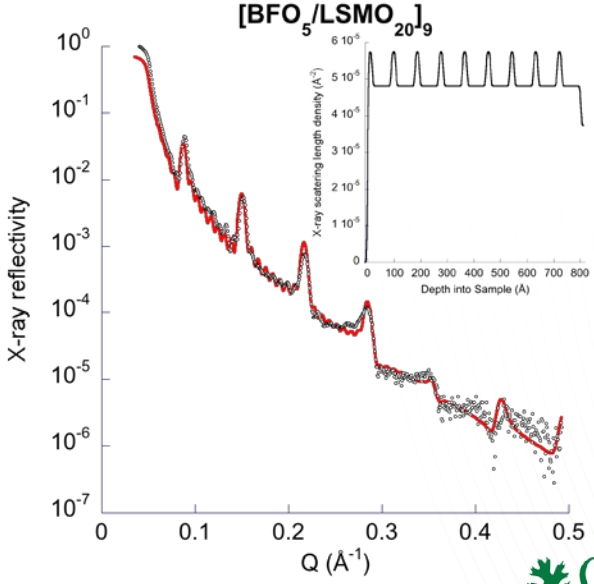

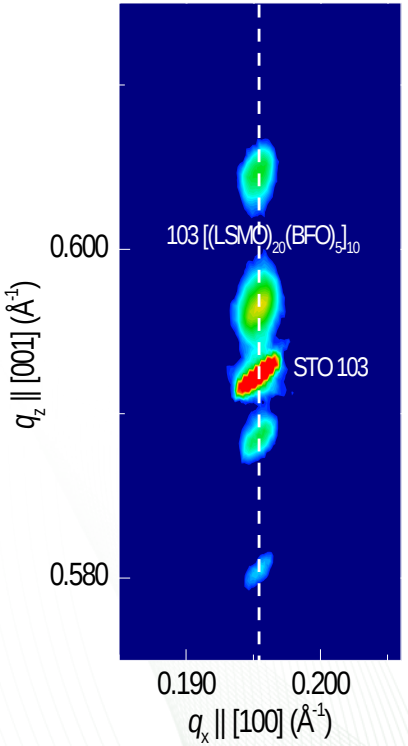

Small angle neutron scattering to probe E-field dependence of M

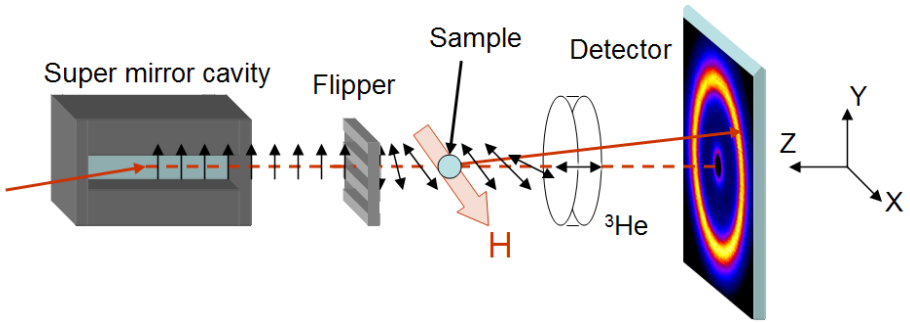

W.C. Chen *et al*, Physica B **404,** 2663 (2009); K.L. Krycka *et al*, Physica B **404,** 2561 (2009) and http://www.ncnr.nist.gov/equipment/he3nsf/index.html

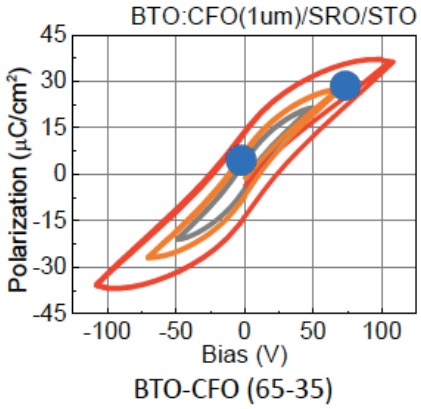

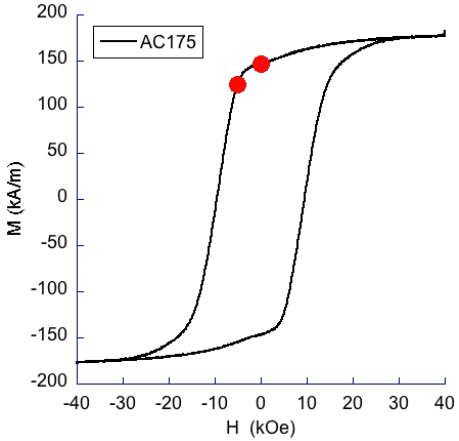

- Used polarized neutron beam
- H parallel to neutron beam (not as shown)
- Saturated at LANL, then measured at NIST
- 300 K
- H = +70 and-5000 Oe
- E = 0 and 700 kV/cm

Raw data pose a quandary—electric field *increases* magnetization.

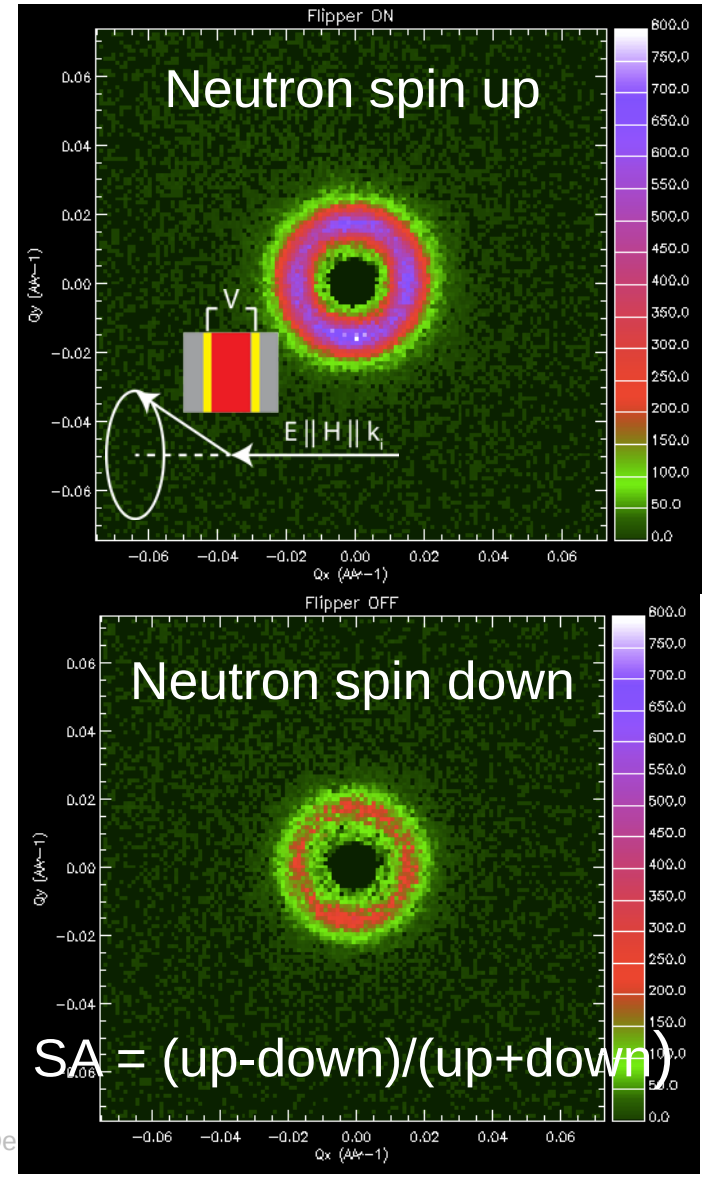

- Integrate region of interest
- Calculate spin asymmetry

B (G)	E (kV/cm)	SA
+70	0	0.484±0.004
+70	900	0.489±0.004
-5000	0	0.470±0.004
-5000	700	0.486±0.004

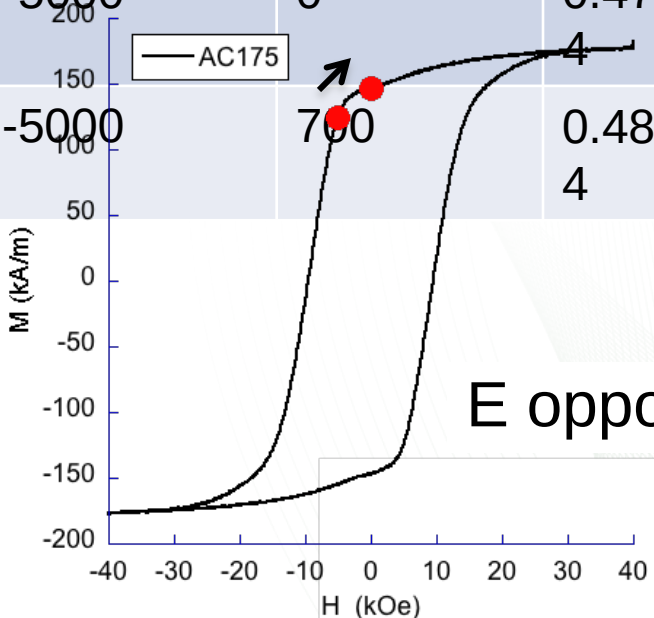

E opposes H

Combining techniques to extract M.

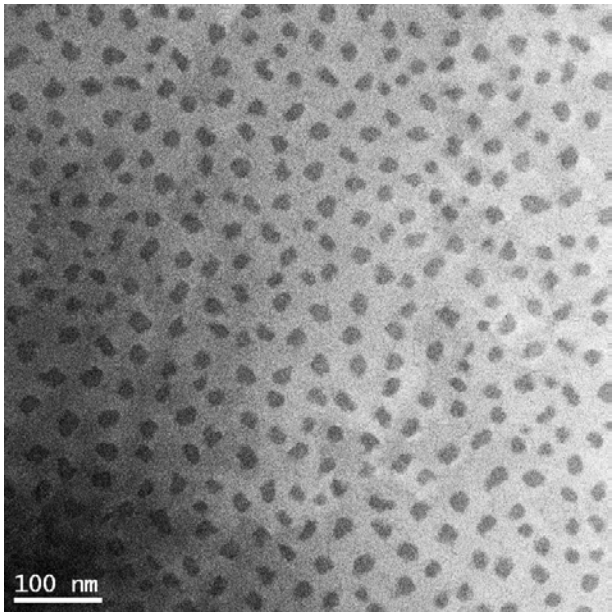

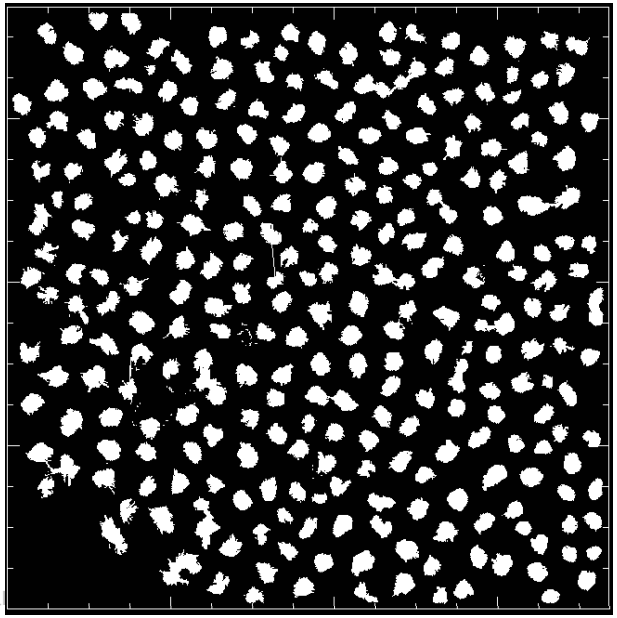

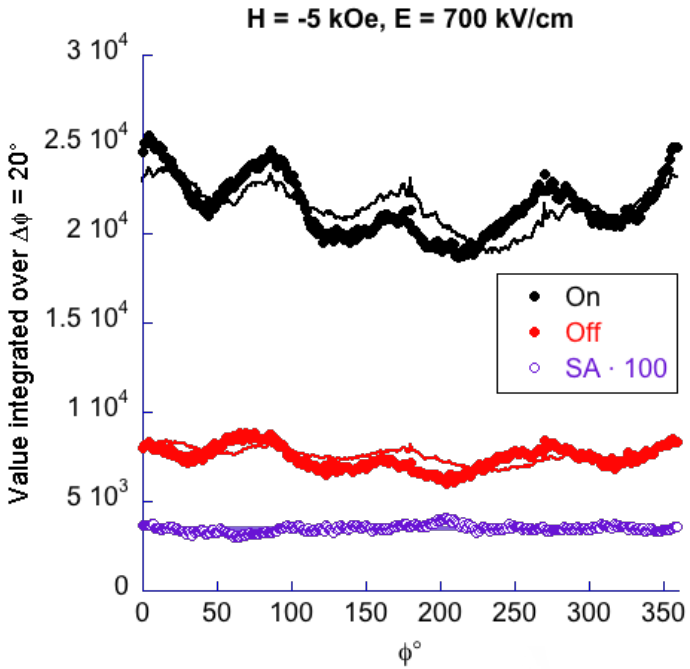

$|FFT|^2$

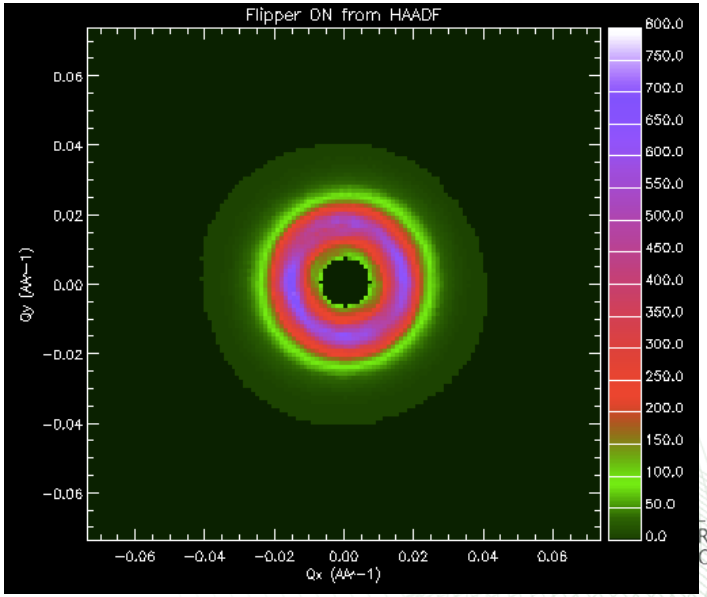

E-field affects magnetization reversal

- E-field increases M by ~4%
  - at H/H_c ~ 0.5
  - E = 700 kV/cm
  - M from 246±4 to 257±4 kA/m
- Reversal may start inside the pillar.
  - $M(H/H_c \sim 0.5) = 0.7M_s$
- Interface magnetism somewhat pinned.
- Weigand effect*

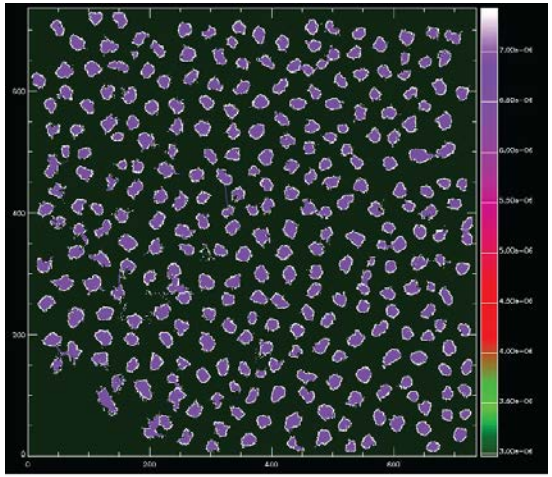

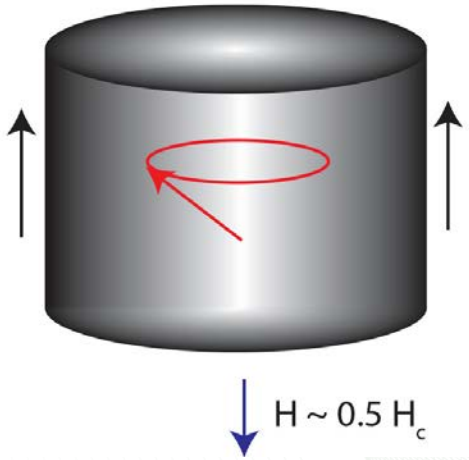

*H.E. Burke, Handbook of Magnetic Phenomena

Near future outlook for interface and mesoscale science

- Neutron scattering is a powerful tool to solve problems encountered in development of novel materials.
  - Or, applied to model systems representative of nanostructures in devices.
  - Especially true of magnetic materials.
- Pressure (1+ GPa) studies with reflectometry.
- 5 Tesla strong fields for reflectometry (11 Tesla for SANS).
- Combinations of E, H, P and T that are dynamic, *in operando*.

No-classical bonding of a side-on H_2 ligand

- **Open-shell Co-H2 moiety in (TPB)Co(H_2)**
  - Putative catalytic intermediates in Co-catalyzed proton reduction reactions
- **Single crystal neutron diffraction structure of Co−H_2**
  - A side-on H_2 ligand with H–H distance of 0.834(6) Å.

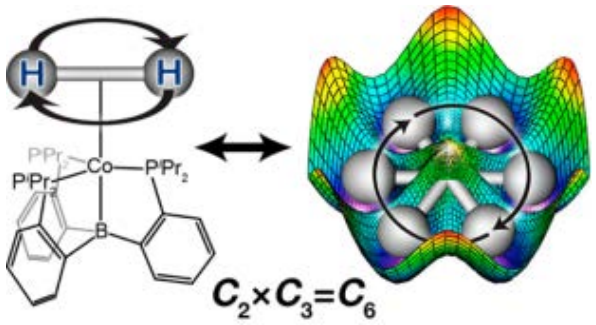

Neutron structure validates predictions that distortions of the complex in the solid state quenches free-rotor behavior of the H_2 ligand.

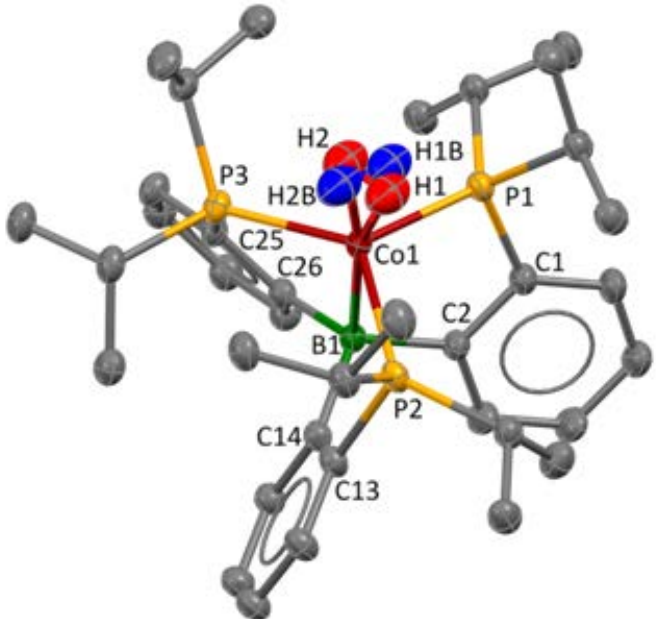

Neutron structure of **Co−H_2** showing the disordered H_2 ligand in the solid state

W. A. Gunderson, *et. al. J. Am. Chem. Soc.* **2014**, *136*, 14998−15009.

Polyhydrido Nanocluster with Intrinsic Chirality

The induction of chirality in metal hydrides is of added value because of the importance of such chiral complexes for asymmetric catalysis.

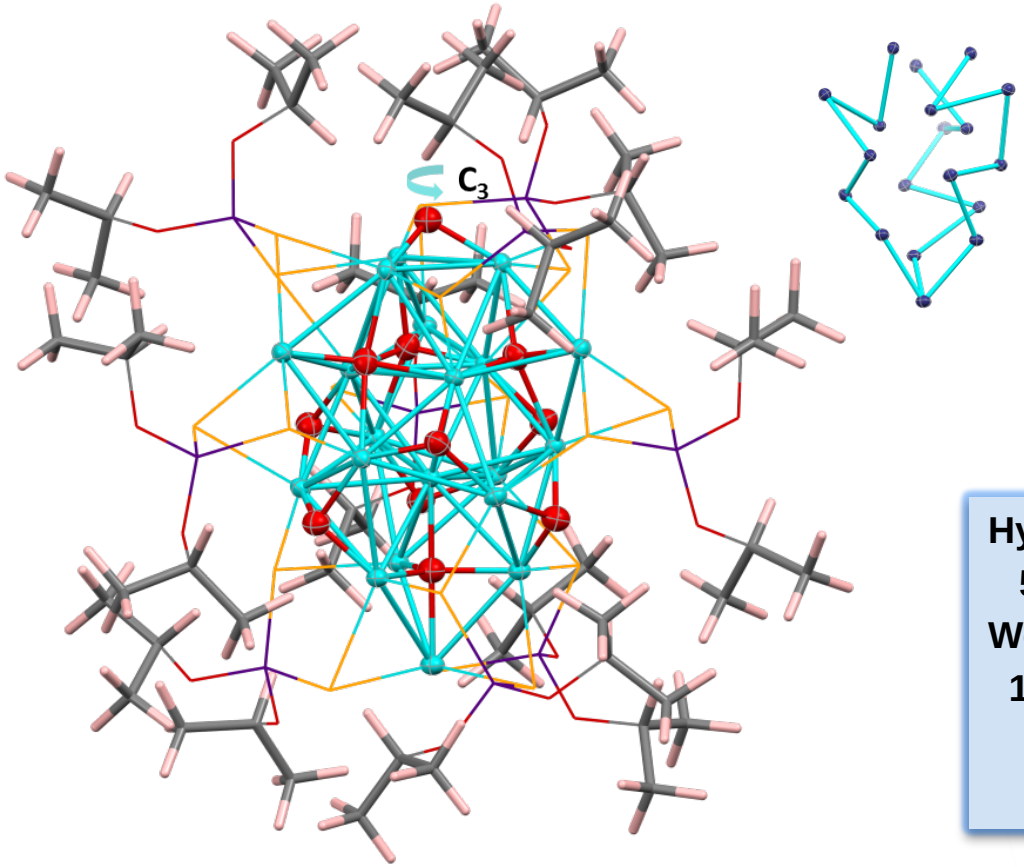

$C_{81}H_{172}Cu_{20}O_{18}P_9Se_{18}$
Space group *R*-3
a = 18.3282(2) Å
c = 74.7517(15) Å
V = 21746.6(6) Å^3
R_1 (obs) = 0.0672

Hydrogenated sample
54% Hydrogen contents by atom.
Well resolved hydrogen atom positions
10 Hydrides as capping μ_3-H ligands
1 Hydride as a μ_5-H ligand in trigonal-bipyramidal cavity

Crystal Structure of $Cu_{20}H_{11}\{Se_2P(O^iPr)_2\}_9$ (Cu cyan, Hydride red)

Dhayal, R. S., *et. al, Angew. Chem. Int. Ed.* **2015**, *54*, 13604.

Structural study of H-bond transformation

- **Hydrogen fuel cell** *Convert chemical bond to electricity*
  - Need a viable electrocatalyst (not Pt)
  - Iron-based molecular electrocatalyst

    Electrocatalyst from earth abundant elements
- **Neutron structural study of an iron-based electrocatalyst**
  - Hydrogen bonding related to H_2 oxidation

    Heterolytic cleavage of H−H bond
  - Hydrogen bonding related to H_2 production

    Heterocoupling of a proton and a hydride

High resolution neutron single crystal diffraction

Hydrogen Fuel Cell

Pt catalyst 0.125 – 0.30 mg/cm^2

Converts chemical energy into electricity

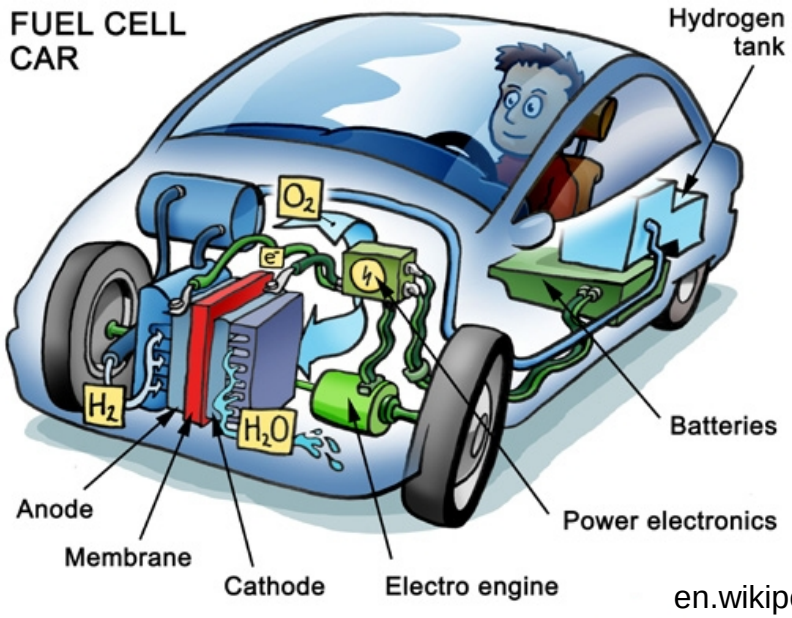

Energy stored in the form of H–H bond

en.wikipedia.org/wiki/Fuel_cell
transportevolved.com

Anode $2H_2 \rightarrow 4H^+ + 4e$

Cathode $O_2 + 4H^+ + 4e \rightarrow 2H_2O$

$2H_2 + O_2 \rightarrow 2H_2O$ + **Electricity**

Hydrogenase

Catalyzes the reversible oxidation of molecular hydrogen

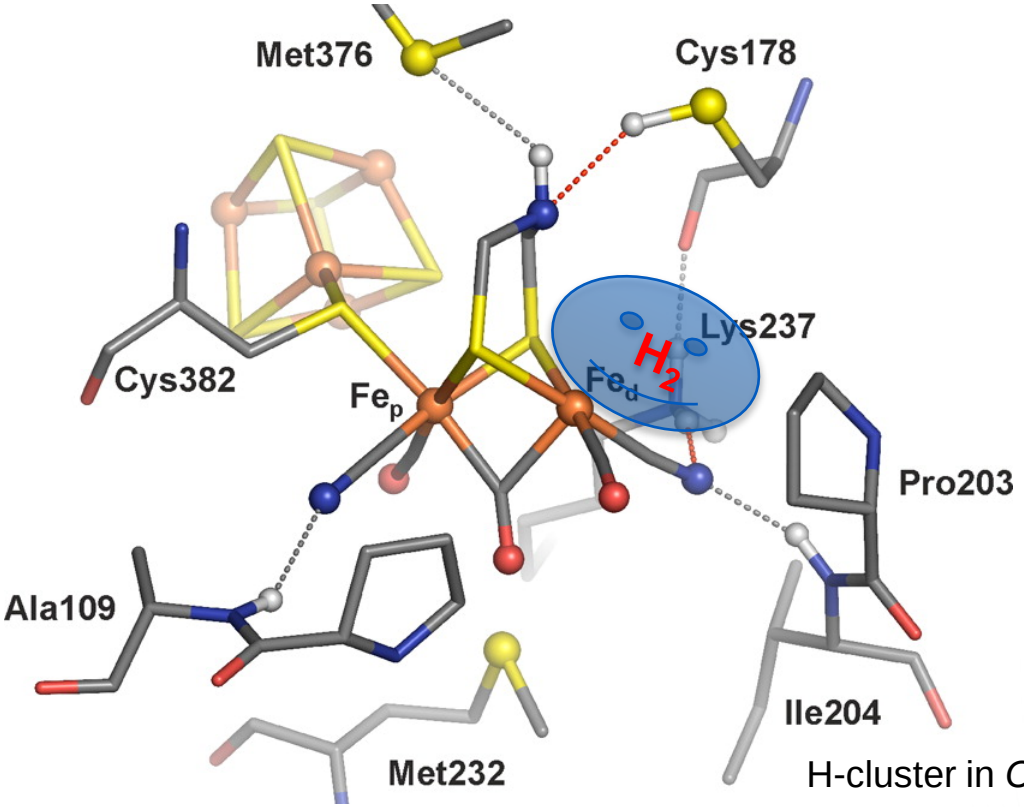

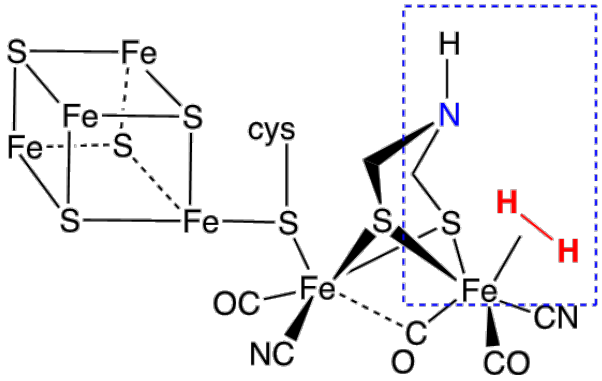

[FeFe] Hydrogenase

Using earth-abundant metals

H-cluster in *Cp*I (PDB 3C8Y)

The cleavage of **H–H** bonds cannot be readily observed by X-rays

Lubitz, W. *et. al. Chem. Rev.* **2014,** 114, 4081

Ogata, H.; Nishikawa, K.; Lubitz, W. *Nature* **2015**, *520*, 571

Electrocatalysts Using Earth Abundant Elements

The Elements According to Relative Abundance

A Periodic Chart by Prof. Wm. F. Sheehan, University of Santa Clara, CA 95053
Ref. Chemistry, Vol. 49, No. 3, p 17–18, 1976

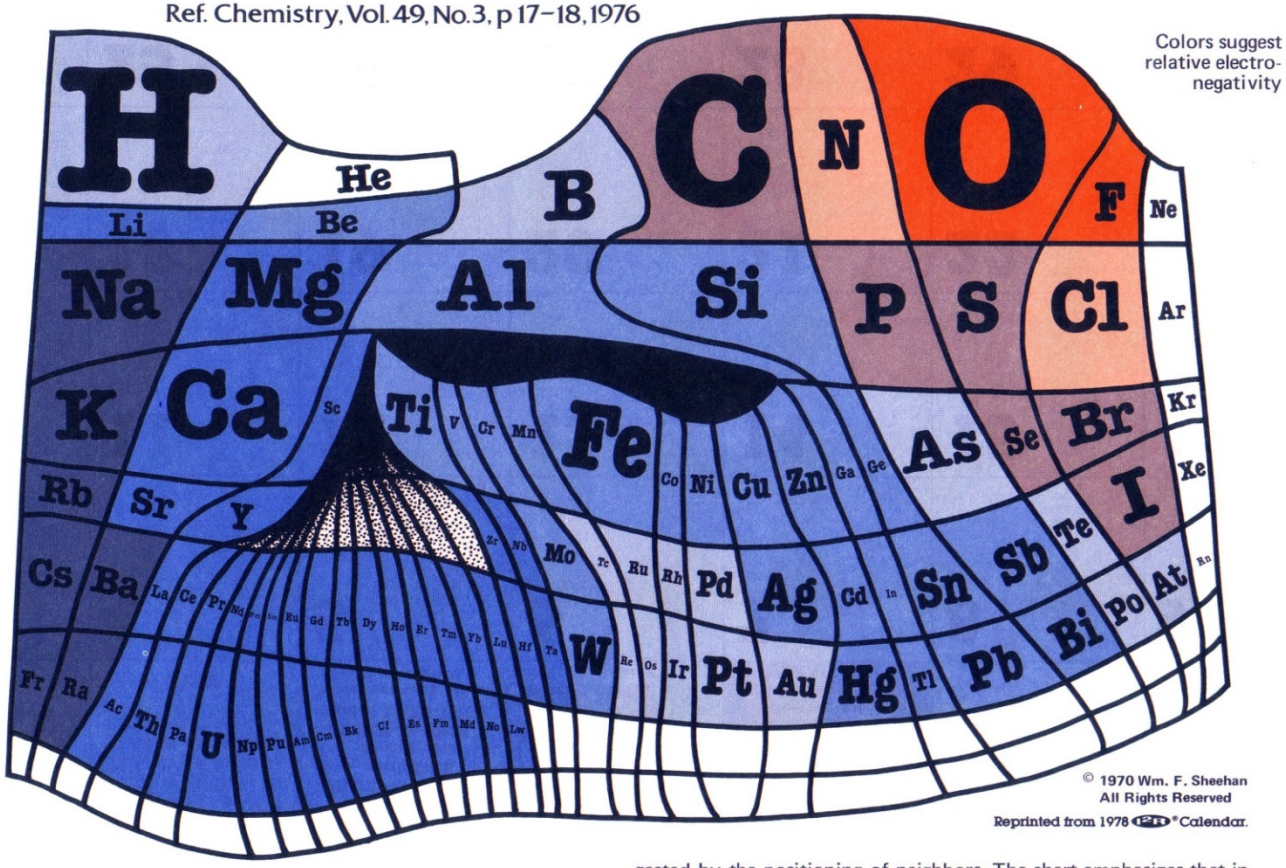

Roughly, the size of an element's own niche ("I almost wrote square") is proportioned to its abundance on Earth's surface, and in addition, certain chemical similarities (e.g., Be and Al, or B and Si) are suggested by the positioning of neighbors. The chart emphasizes that in real life a chemist will probably meet O, Si, Al, . . . and that he better do something about it. Periodic tables based upon elemental abundance would, of course, vary from planet to planet. . . W.F.S.

NOTE: TO ACCOMMODATE ALL ELEMENTS SOME DISTORTIONS WERE NECESSARY, FOR EXAMPLE SOME ELEMENTS DO NOT OCCUR NATURALLY.

Hydrogen Oxidation Reaction

- **Three steps**
  - Reaction of H_2 with the metal complex
  - Heterolytic cleavage of H_2 into a proton and a hydride ion
  - Release of the two protons and two electrons

$$H_2 \rightarrow (H^+ + H^-) \rightarrow 2H^+ + 2e$$

Hydrogen Oxidation
(Heterolytic Cleavage of H−H Bond)

Pendant amine as proton relay

Mimic the second coordination sphere at the enzyme active site

[*Cp*FeN_2P_2)](BArF) (**1**)

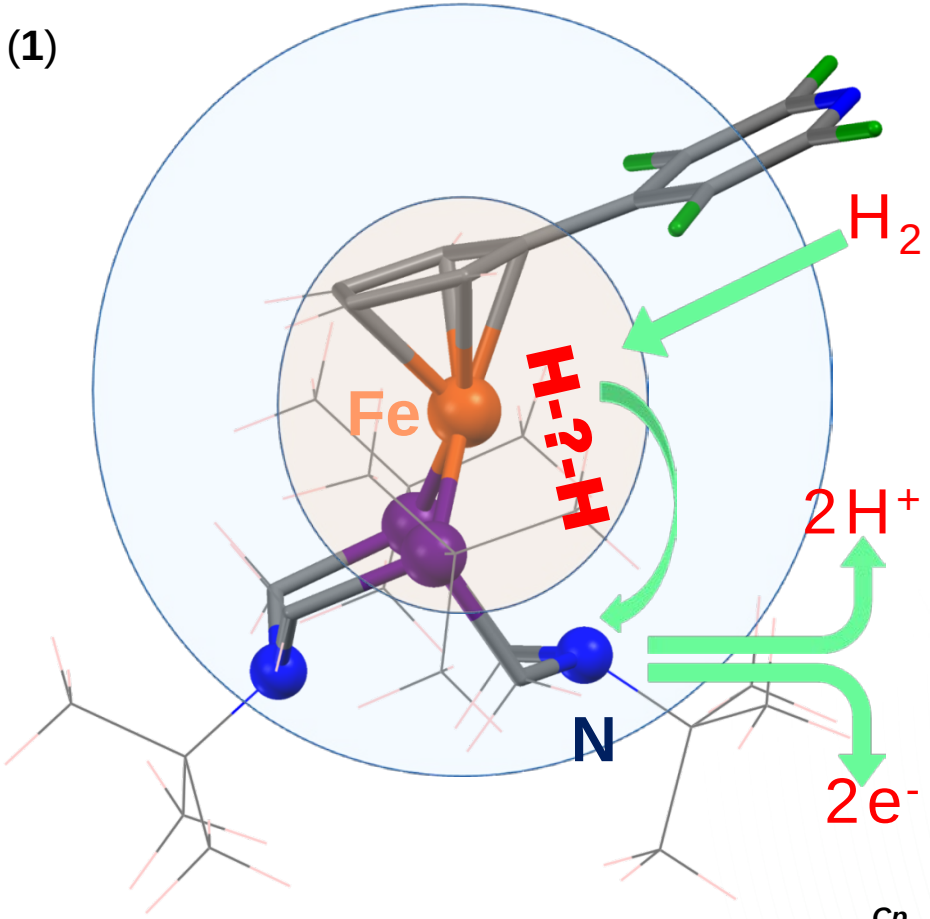

Cp = pentafluoro-pyridylcyclopentadienide,
N_2P_2 = 1, 5-di(*tert*-butyl)-3,7-di(*tert*-butyl)-1,5-diaza-3,7-diphospha-cyclooctane
BArF = $[B[3,5\text{-}(CF_3)_2C_6H_3]_4]^-$

Bullock, R. M.; Helm, M. L. *Acc. Chem. Res.* **2015**, *48*, 2017.

Design a Functional Electrocatalyst

Facilitate proton-coupled electron transfer

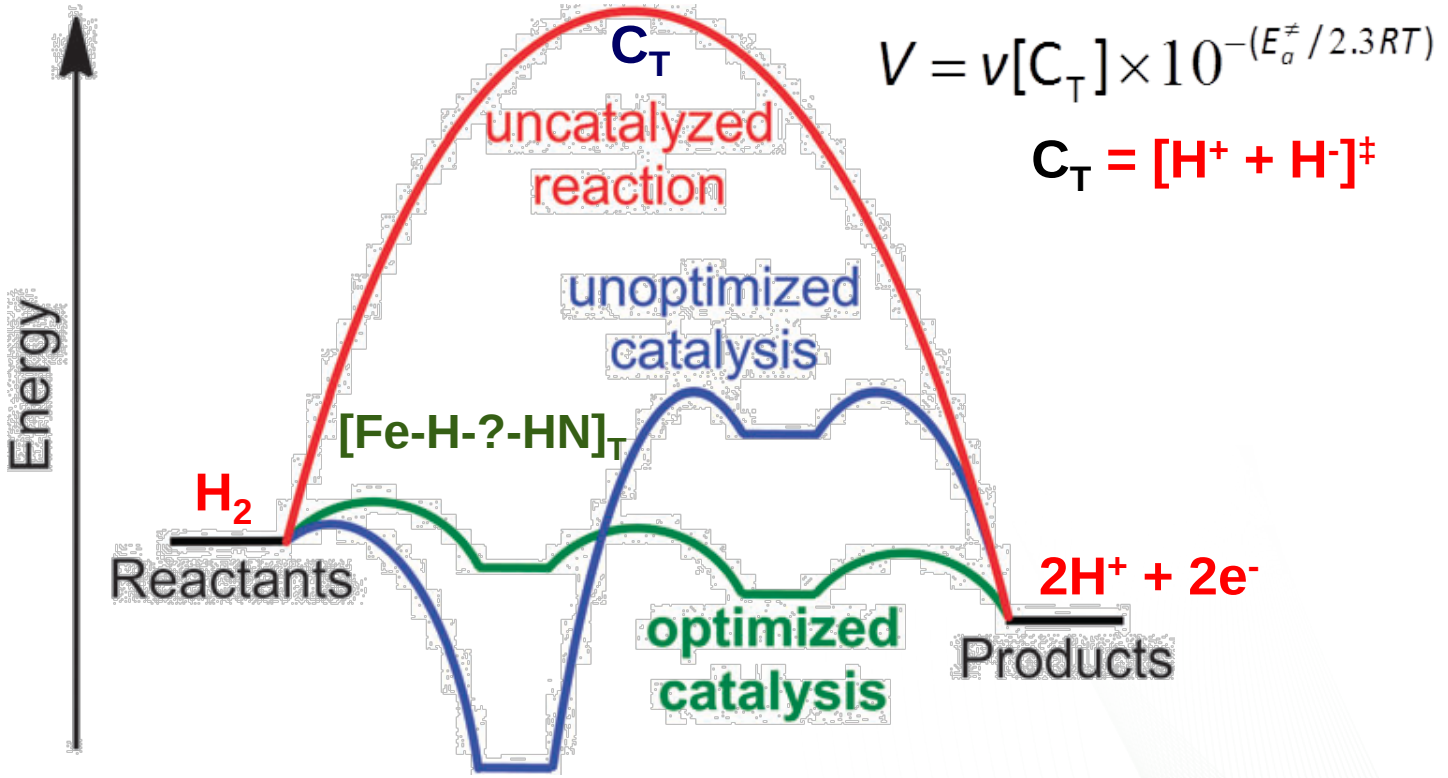

Bullock, R. M.; Appel, A. M.; Helm, M. L. *Chem. Commun.* **2014**, *50*, 3125

DFT Energy landscape

Model electrocatalyst for H_2 oxidation

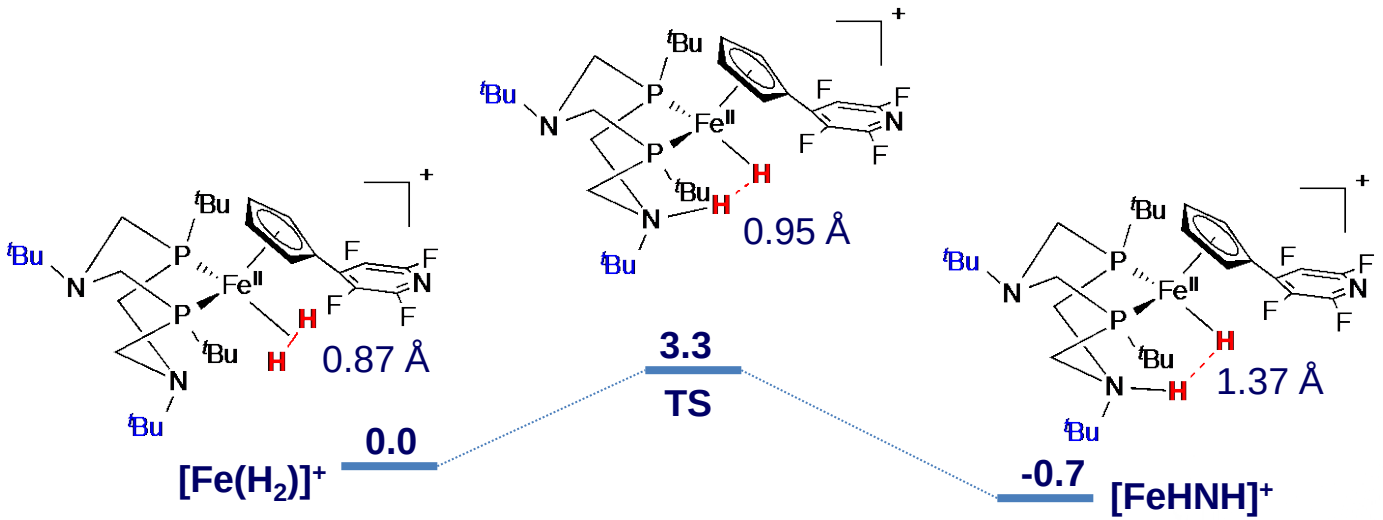

Lower the activation barrier:

Promote **Heterolytic** cleavage of the H—H bond into a proton and a hydride

Liu, T. B.; DuBois, D. L.; Bullock, R. M. *Nat. Chem.* **2013**, *5*, 228

The postulated “dihydrogen” bond

- **Non-covalent interaction between hydrogen atoms with partial negative and positive charges**

$$M–H^{\delta-}\cdots\cdots H^{\delta+}–X$$

- **Hydride as proton acceptor**

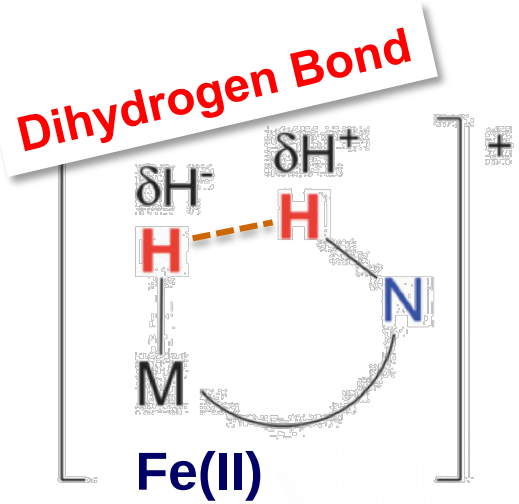

Custelcean, R.; Jackson, J. E. *Chem. Rev*. **2001**, *101*, 1963

Neutron single crystal diffraction

- **Capture the structure details of the electrocatalyst in action**
  - The electrocatalyst is at its intermediate state
  - Hydrogenated sample (39% H by atom)
  - Locate hydrogen atoms at ***sub-atomic resolution***

Locate hydrides and protons from single-crystal neutron diffraction

Sub-atomic resolution

$H^{\delta+}\cdots H^{\delta-}$ **1.489(10) Å**

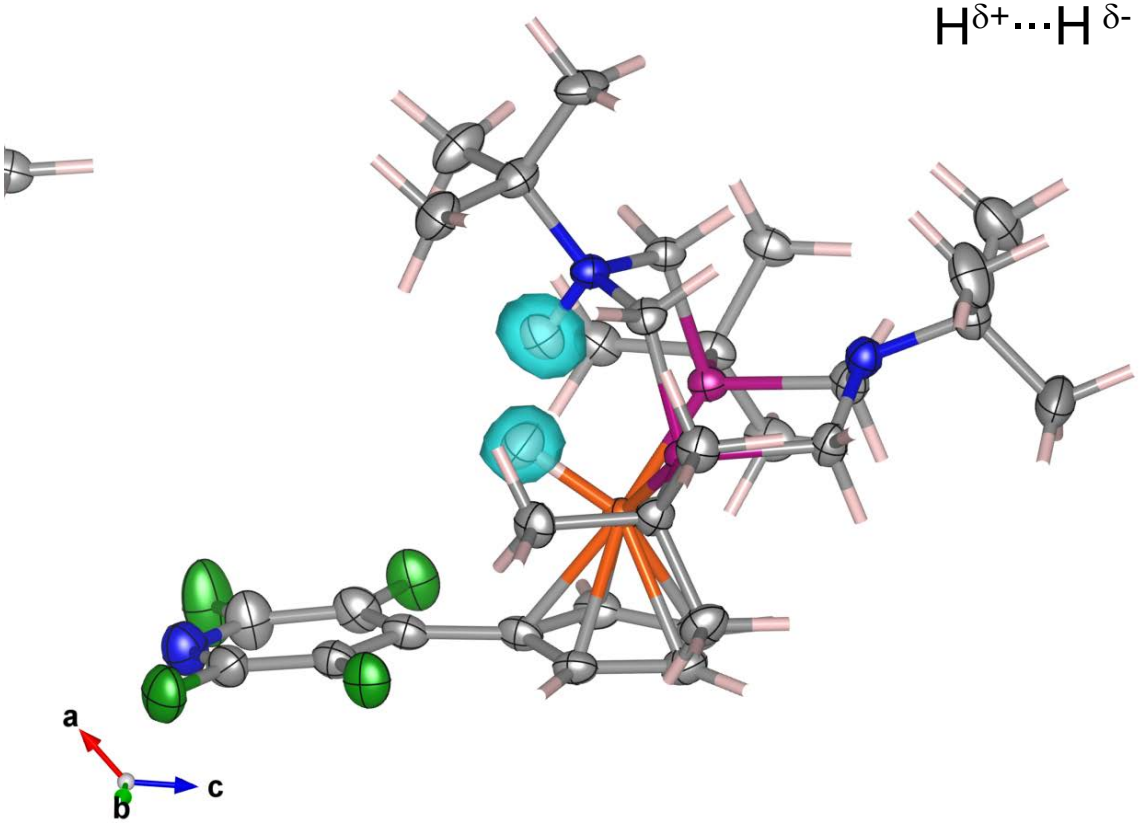

Neutron structure – Dihydrogen bond

Distance, Å	[FeH---HN]+
Fe1–H1B	1.544(7)
N1–H1A	1.079(6)
Fe1–P1	2.157(3)
Fe1–P2	2.160(3)

$H^{\delta+}\cdots H^{\delta-}$

1.489(10) Å

0.32 x 0.90 x 1.95

1 mm

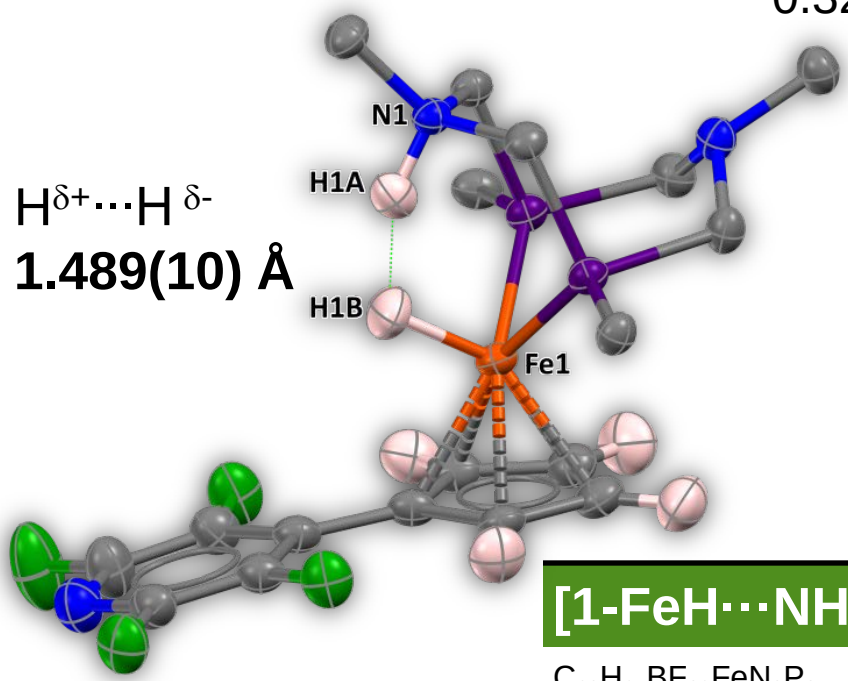

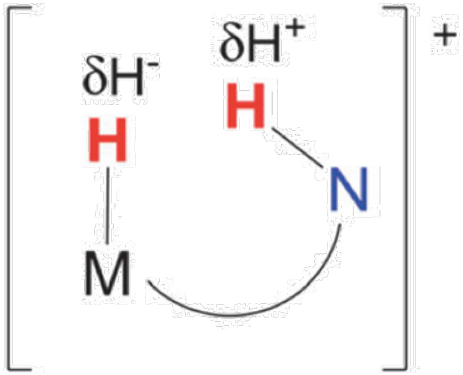

{Fe(II)–$H^{\delta-}$} acts as the H-bond acceptor
The shortest H···H distance observed
between the hydridic Fe−$H^{\delta-}$ and protic N−$H^{\delta+}$ site

[1-FeH···NH](BARF)·PhF

$C_{68}H_{67}BF_{29}FeN_3P_2$

Monoclinic, $P2_1/c$

a = 13.9202 (3) Å	$R[F^2 > 2\sigma(F^2)]$ = 0.067
b = 36.0546 (13) Å	$wR(F^2)$ = 0.150
c = 19.5234 (4) Å	S = 1.07
β = 133.6892 (13)°	25230 reflections
V = 7085.3 (3) Å^3	1628 parameters
Z = 4	110 restraints

$$H_2 \rightarrow (H^+ + H^-) \rightarrow 2H^+ + 2e$$

Hydrogen Oxidation
(Heterolytic Cleavage of H−H Bond)

$$2H^+ + 2e \rightarrow (H^+ + H^-) \rightarrow H_2$$

Hydrogen Production
(Heterocoupling of a proton and a hydride)

Bullock, R. M.; Helm, M. L. *Acc. Chem. Res.* **2015**, *48*, 2017

Transfer of H atoms in the solid state

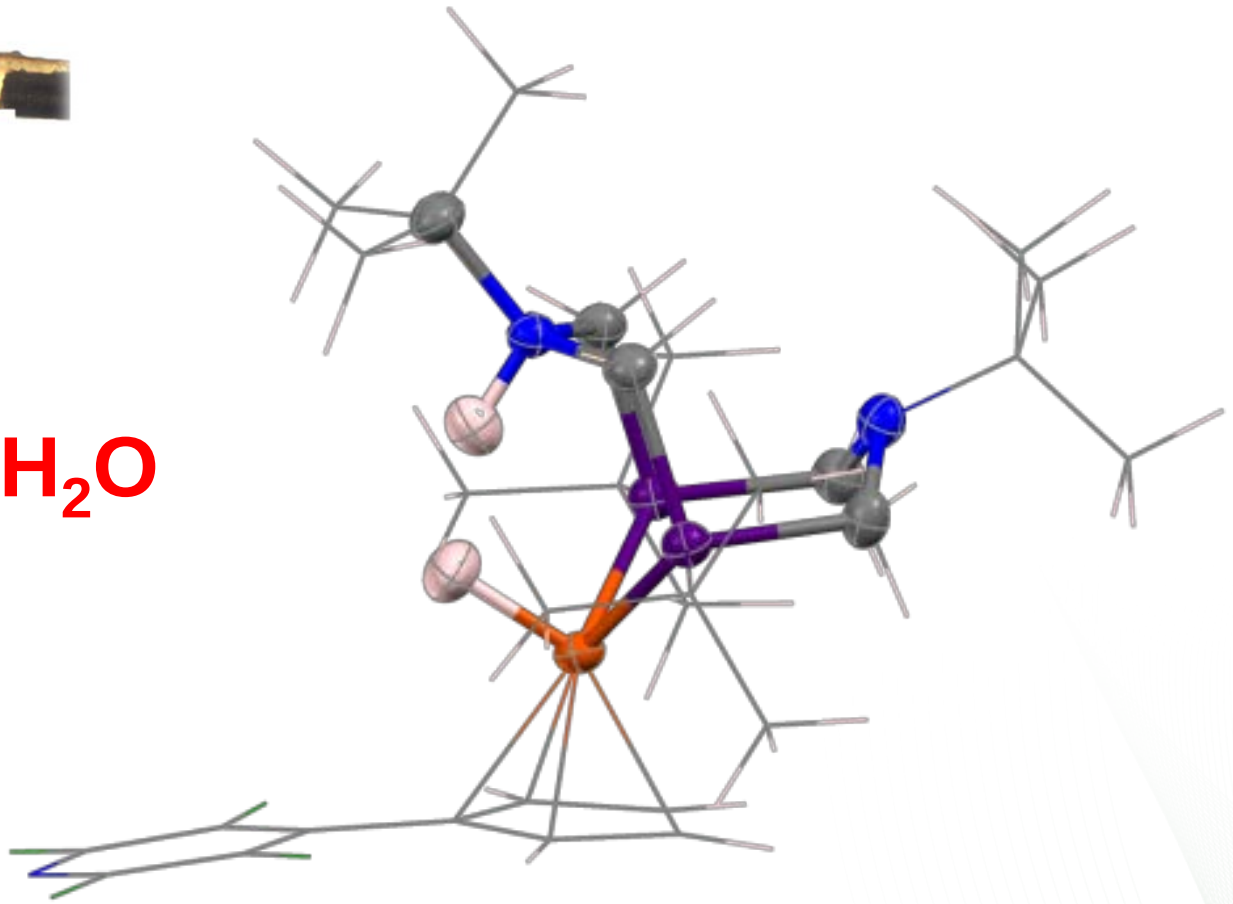

H_2O

Transfer of H atoms in SCS reaction

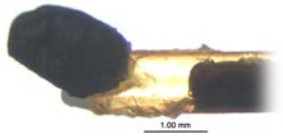

H_2

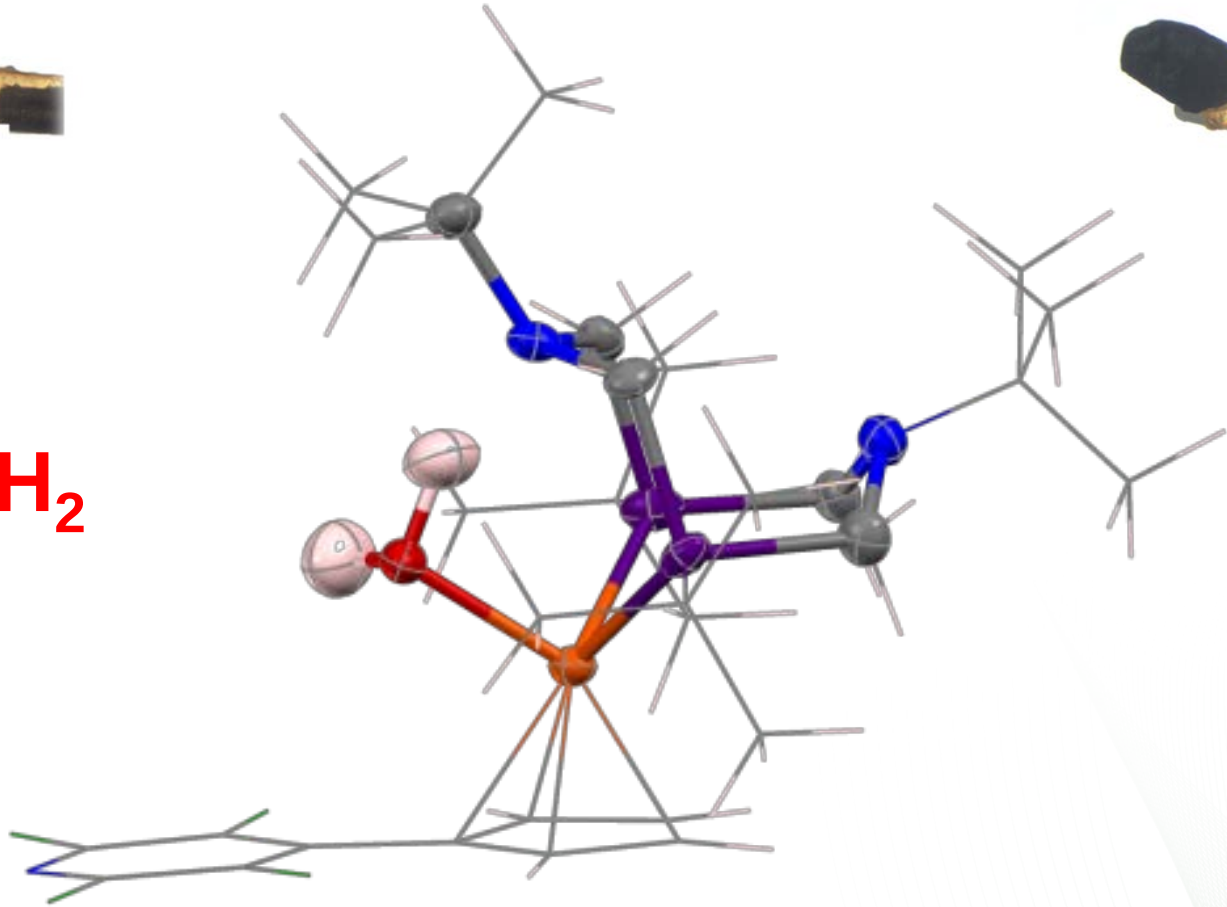

Locating Hydrogen atoms in [1-Fe(OH_2)N]$^+$

```
wR2 =  0.1479 before cycle   1 for  13638 data and     0 /  1569 parameters
GooF = S =     1.212;     Restrained GooF =      1.214  for    109 restraints
R1 =  0.0831 for  11858 Fo > 4sig(Fo)  and  0.0900 for all  13638 data
wR2 =  0.1479,  GooF = S =   1.212,  Restrained GooF =    1.214  for all data
R1 =  0.0868 for   5831 unique reflections after merging for Fourier
Highest peak    0.79  at  0.2544  0.8462  0.1203
Deepest hole   -5.21  at  0.2805  0.8731  0.1482
```

Difference map
Showing **nuclear densities**
from missing **H** atoms

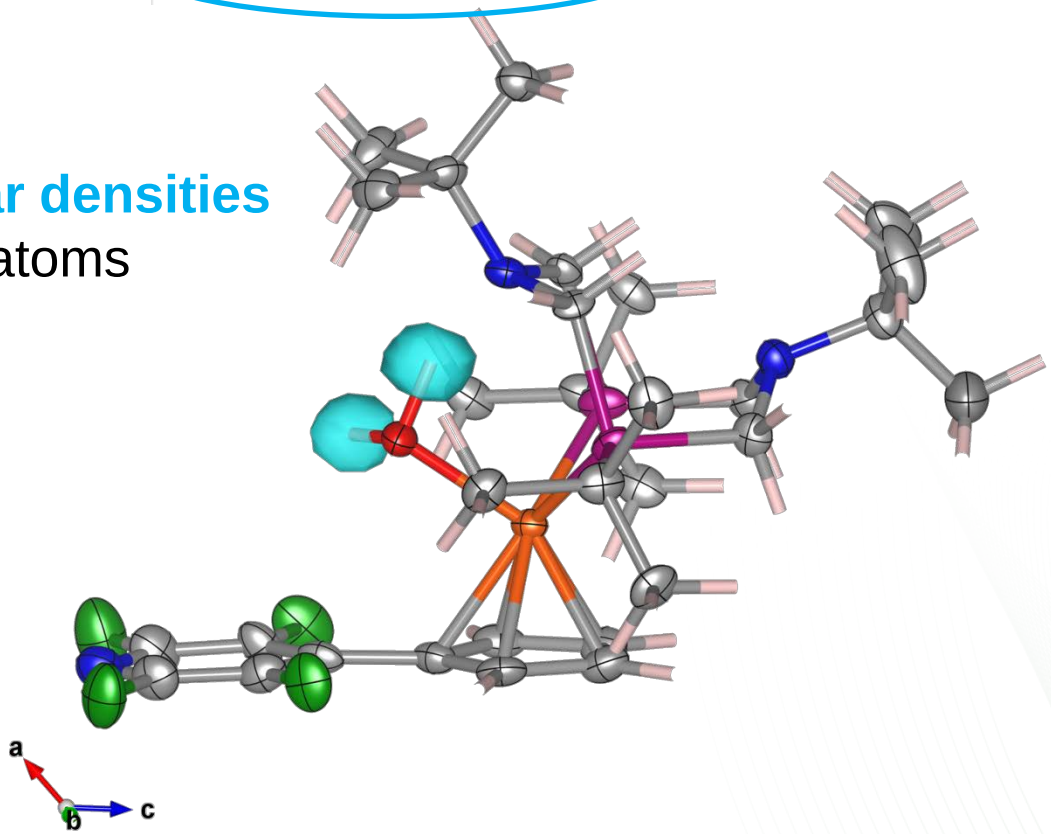

Locating Hydrogen atoms in [1-Fe(OH_2)N]$^+$

```
wR2 =  0.1245 before cycle   8 for  13638 data and     0 /  1569 parameters
GooF = S =     1.022;     Restrained GooF =      1.024  for    109 restraints
R1 =  0.0721 for  11858 Fo > 4sig(Fo)  and  0.0777 for all  13638 data
wR2 =  0.1245,  GooF = S =   1.022,  Restrained GooF =    1.024  for all data
R1 =  0.0717 for   5831 unique reflections after merging for Fourier
Highest peak    0.71  at  0.3693  0.8773  0.4887  [  0.14 A from C10 ]
Deepest hole   -0.71  at  0.1124  0.8352  0.2988  [  0.42 A from H9A ]
```

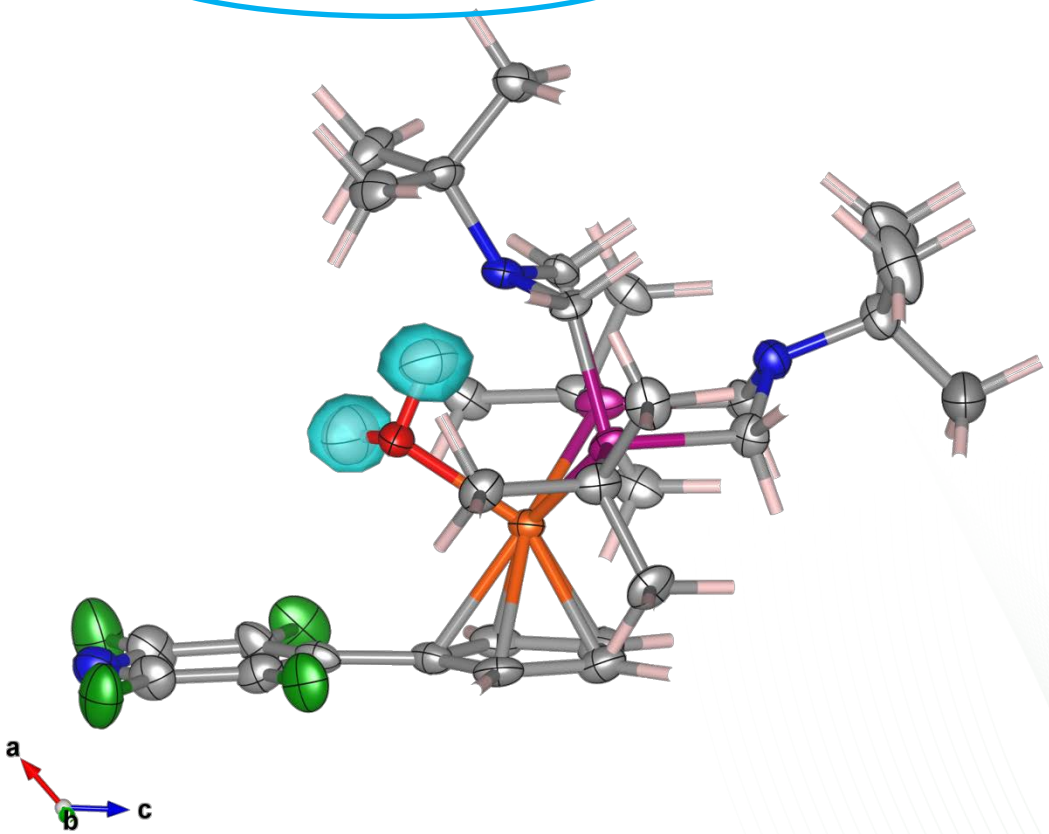

Comparison of Neutron & X-ray structures

	X-ray	Neutron
Fe-O1	2.022	2.032
H1a-O1	0.852	0.995
H1b-O1	1.693	**1.096**
Hb-N1	0.930	**1.503**
Fe-P	2.208	2.208
O1-Hb-N1	162.74	162.3
P1-Fe-P2	81.88	82.25

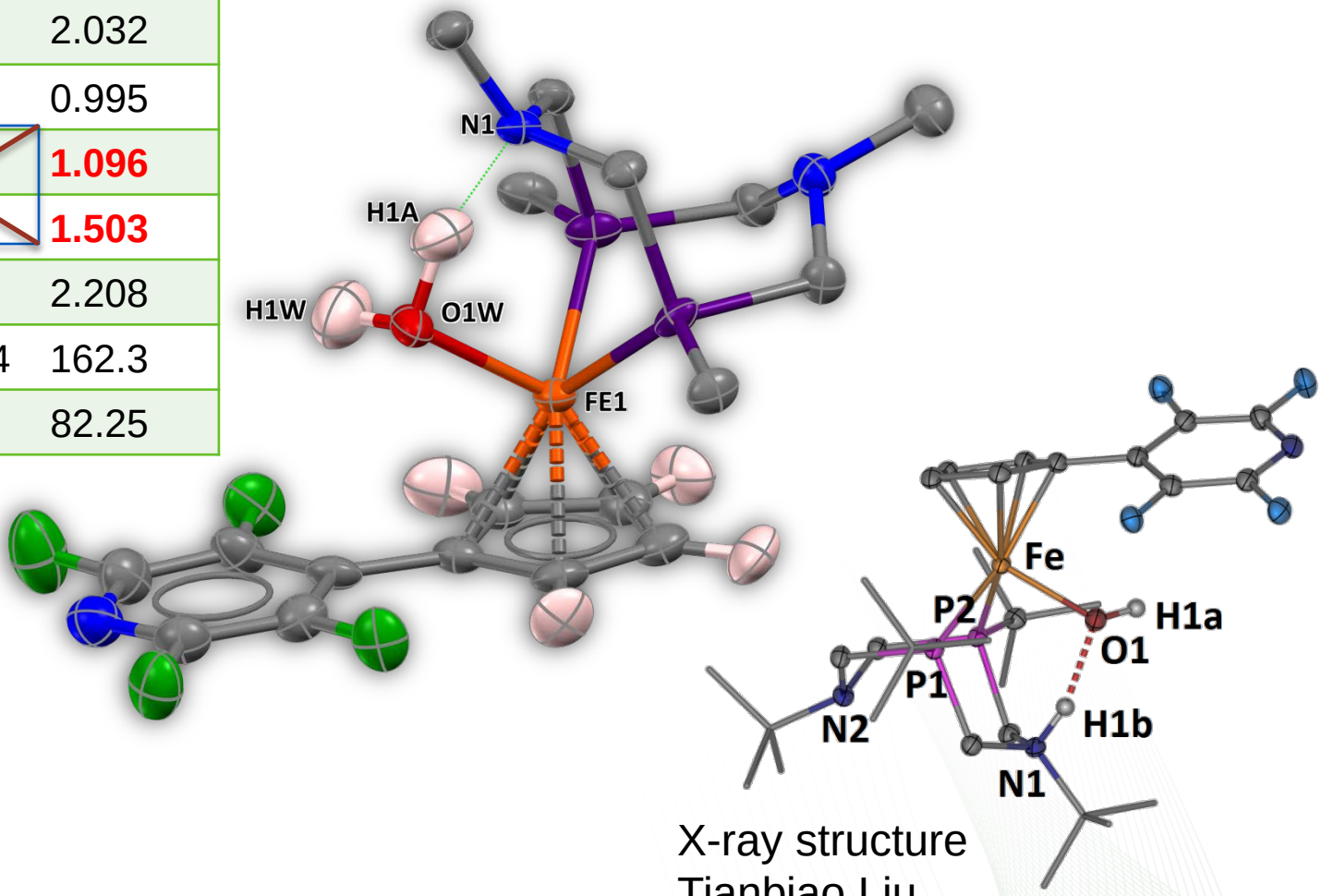

X-ray structure
Tianbiao Liu

Reaction pathway for H_2 production

Spontaneous combination of a proton with a hydride

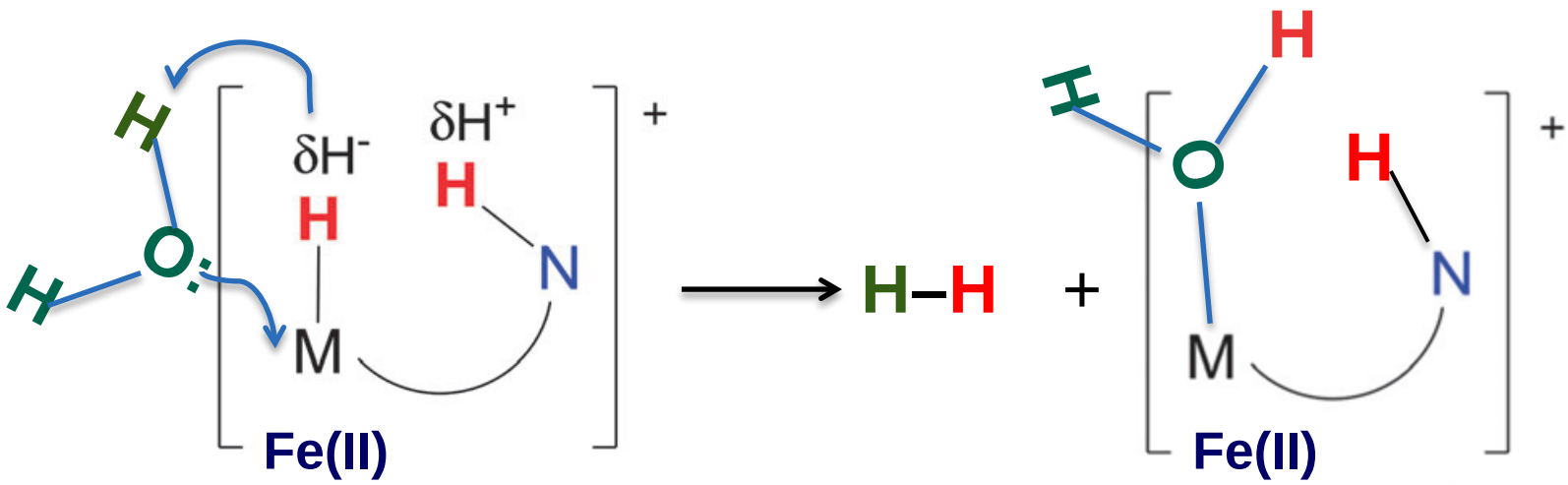

H_2O + [**1**-FeH---HN]$^+$ ⟶ H_2 + [**1**-Fe(OH_2)N]$^+$

$H^+ + H^- \longrightarrow H_2$

Hetero-coupling of a proton and a hydride

Conclusions

Neutron single crystal diffraction confirmed:

A strong Fe–$H^{\delta-}\cdots^{\delta+}$H–N “dihydrogen bond” exists in the intermediate state of an iron-based molecular electrocatalyst.

Water assisted hetero-coupling of a proton and a hydride leads to hydrogen production.

The water adduct of the iron complex is stabilized by a conventional hydrogen bond.

Angewandte Communications

Angew. Chem. Int. Ed. **2014**, *53*, 5300 –5304

DOI: 10.1002/anie.201402090

VIP Heterolytic H_2 Cleavage | Very Important Paper

Heterolytic Cleavage of Hydrogen by an Iron Hydrogenase Model: An Fe-H···H-N Dihydrogen Bond Characterized by Neutron Diffraction**

Tianbiao Liu, Xiaoping Wang, Christina Hoffmann, Daniel L. DuBois, and R. Morris Bullock**

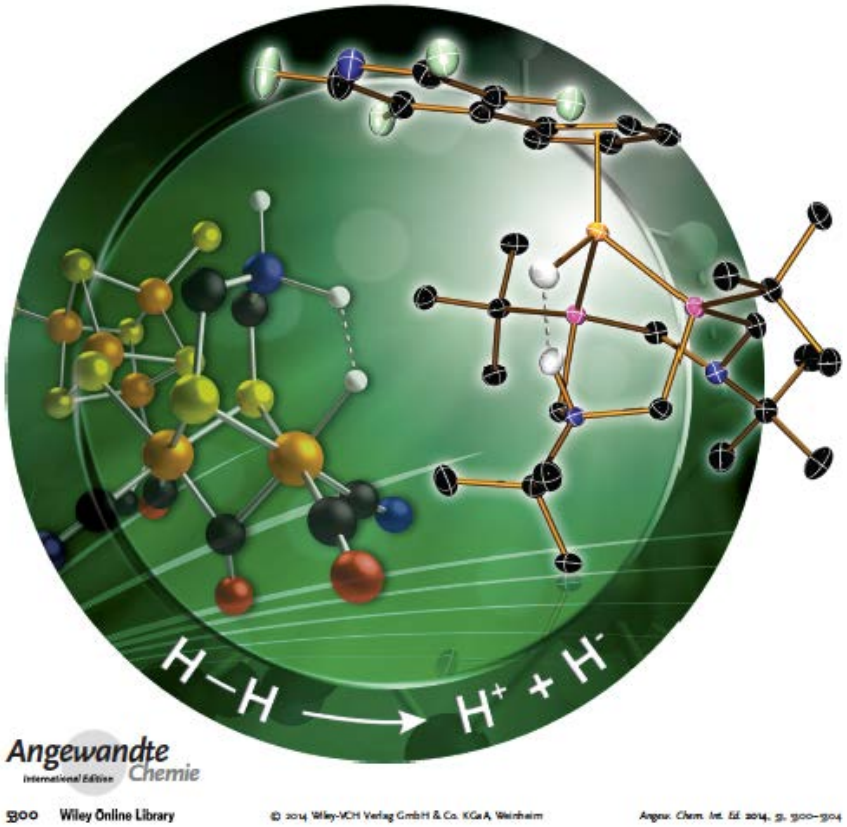

Summary

The SNS TOPAZ instrument opened a new horizon for high resolution structural study of materials that would not be possible with X-rays.

Potential applications of TOPAZ

Study the chemical structure and bonding of molecules and ions with their surroundings involving light elements;

Resolve the site occupancy associated with neighboring elements;

Solve and refine magnetic structures;

Probe structural modulation originated from nuclear/magnetic phase transitions;

3D Q space mapping and parametric studies using neutron event data …

www.neutrons.ornl.gov/topaz/

Acknowledgements

Dr. Tianbiao Liu

Dr. R. Morris Bullock

Pacific Northwest NATIONAL LABORATORY
Proudly Operated by Battelle Since 1965

Center for MOLECULAR ELECTROCATALYSIS

Dr. Christina Hoffmann

Helen He

Matthew Frost

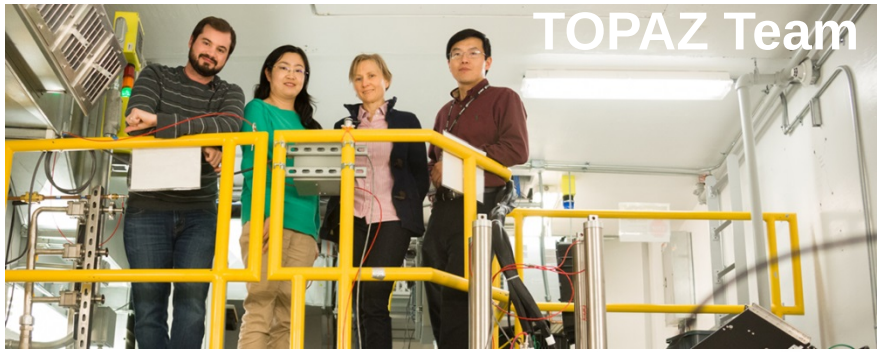

U.S. DEPARTMENT OF ENERGY | Office of Science

The neutron single crystal study at ORNL's Spallation Neutron Source TOPAZ instrument was sponsored by the Scientific User Facilities Division, Office of Basic Energy Sciences, US Department of Energy.

Universal characteristics of water dynamics in restricted geometries investigated with neutron scattering

Souleymane O. Diallo

Chemical & Engineering Materials Division

Oak Ridge National Laboratory

ORNL/Georgia Tech Workshop 2016
January 27, 2016

U.S. DEPARTMENT OF ENERGY

OAK RIDGE NATIONAL LABORATORY
MANAGED BY UT-BATTELLE FOR THE DEPARTMENT OF ENERGY

Motivations: recent MD simulations

ARTICLE

Received 11 Sep 2013 | Accepted 5 Mar 2014 | Published 3 Apr 2014

DOI: 10.1038/ncomms4565 OPEN

Scaling behaviour for the water transport in nanoconfined geometries

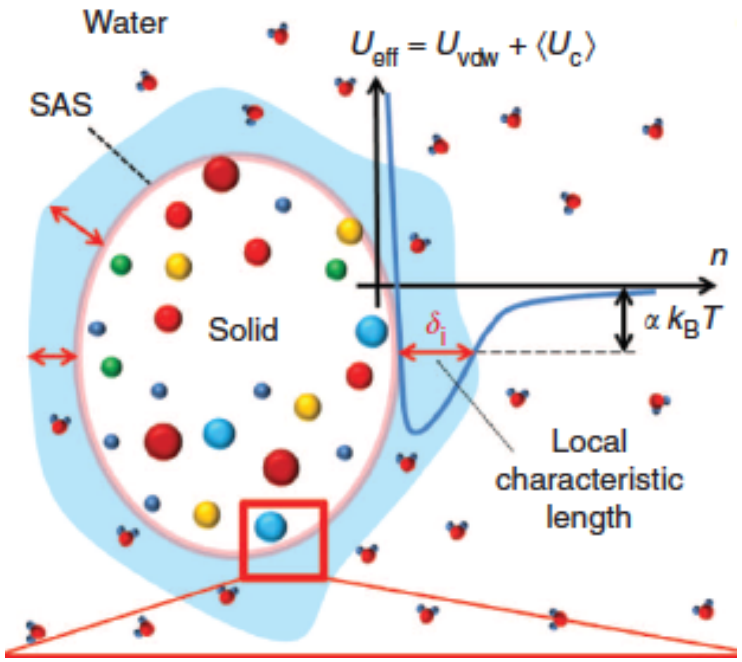

$$\delta = \frac{\sum_{i=1}^{N} \delta_i S_{loc,i}}{S_{tot}}$$

Simplifying

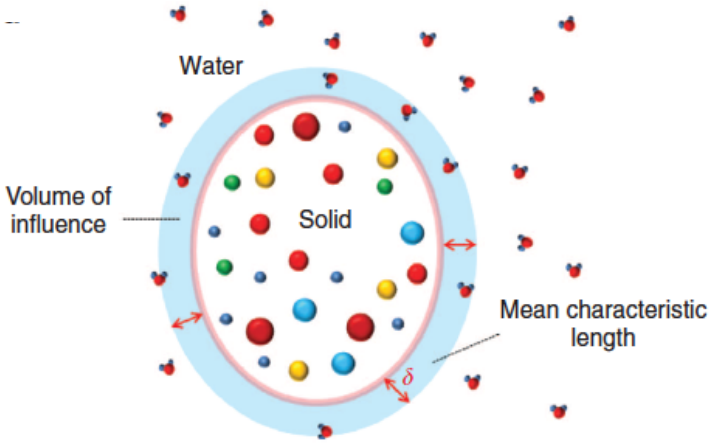

Significance →

$$D_r(T) = \theta D_c + (1-\theta) D_{bulk}(T)$$

Objectives

- **Verify/test proposed law – *against exp'ts***
- **Identify common characteristics/trends**
- **Develop predictive models**
- **Validate models using recent measurements**

Challenge: Disentangling variables???

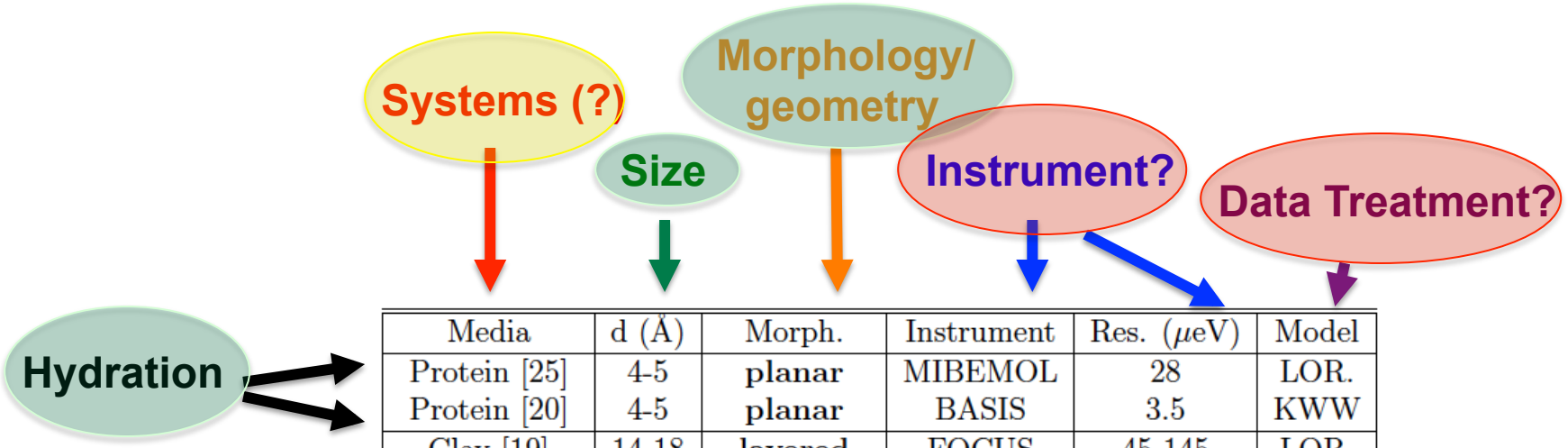

Media	d (Å)	Morph.	Instrument	Res. (μeV)	Model
Protein [25]	4-5	planar	MIBEMOL	28	LOR.
Protein [20]	4-5	planar	BASIS	3.5	KWW
Clay [19]	14-18	layered	FOCUS	45-145	LOR.
Clay [28]	10-16	layered	FOCUS	45-145	LOR.
AOT [33]	7-12	shell	IN5,BASIS IN16	3.5-25	LOR.
Vycor [17]	50	rand. arr.	MIBEMOL	28	LOR.
C-S-H [34]	10-30	rand. arr.	BASIS	3.5	KWW
Nafion [32]	14	rand. arr.	HFBS	0.8	LOR.
Zeolite [18]	11-14	rand. arr.	IN5	11	KWW
MCM-41 [21]	28	ord. cyl.	MIBEMOL	28	KWW
MCM-41 [21]	21	ord. cyl.	MIBEMOL	28	KWW
SWNT [30]	14	ord. cyl.	HFBS	0.8	LOR.
FSM-12	16	ord. cyl.	BASIS	3.5	KWW
FSM-22	39	ord. cyl.	BASIS	3.5	KWW
Cu Rub. [35]	7	ord. rect.	HFBS AGNES	1-120	KWW
ACF-10 [22]	12	rand. slit	BASIS	3.5	KWW
ACF-20 [22]	18	rand. slit	BASIS	3.5	KWW

LEGEND:
- Trivial
- Unclear
- Difficult

N.C. Osti *et al*. J. Chem. Phys. **465-466**, 1-8 (2016)

Hydration

A. Vycor glass (pore size = 5nm)

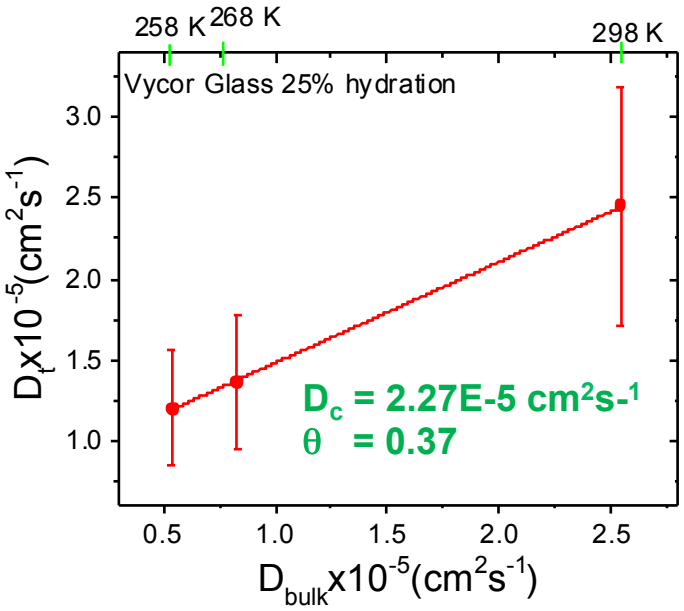

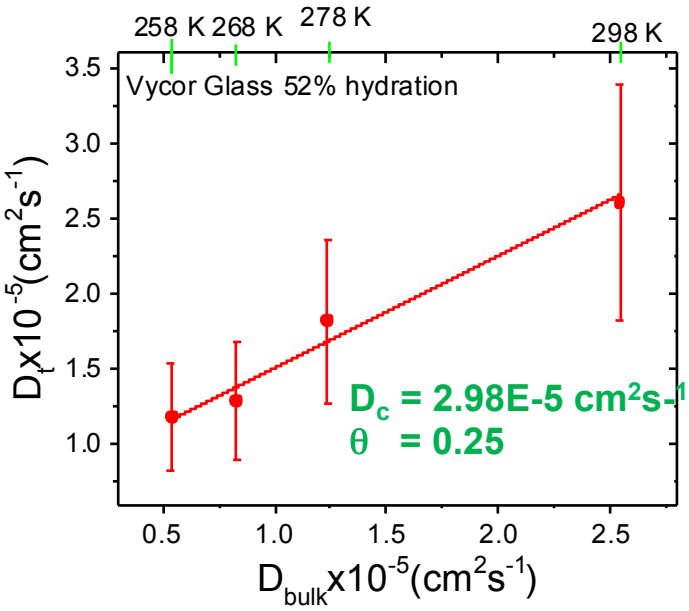

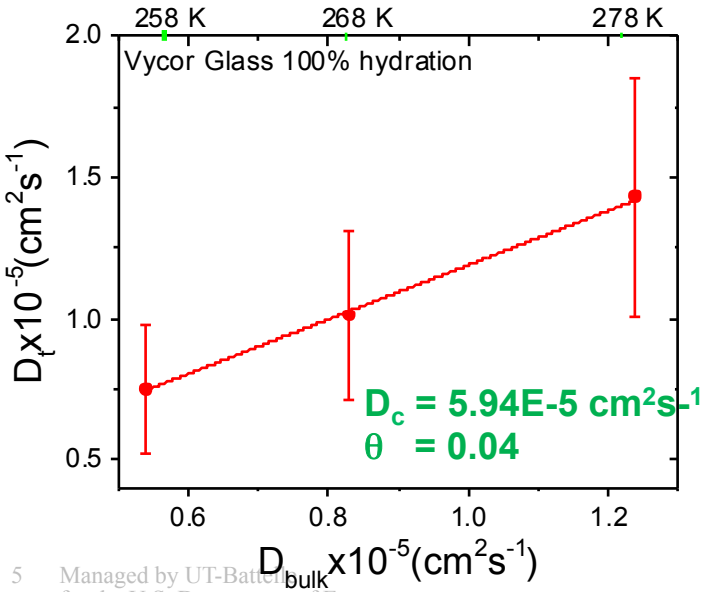

Sample	$h = m_{water}/m_{sample}$	θ	D_c (10^{-6}cm^2/s)
Vycor [17]	25%	37%	22.7
	52%	25%	29.8
	100%	4%	59.4
Zeolite [18]	22%	86%	0.09
	28%	85%	0.95
Hydrotalcite clay [19]	10%	78%	2.36
	30%	4%	75.3
Lysozyme [20]	35%	77%	-
	45%	54%	-

TREND: When h ↗ Θ ↘

M.-C. Bellissent-FuneL, S. H. Chen, and J.-M. Zanotti, Physical Review E, **1995**, Volume 51, Number 5

Confinement Size

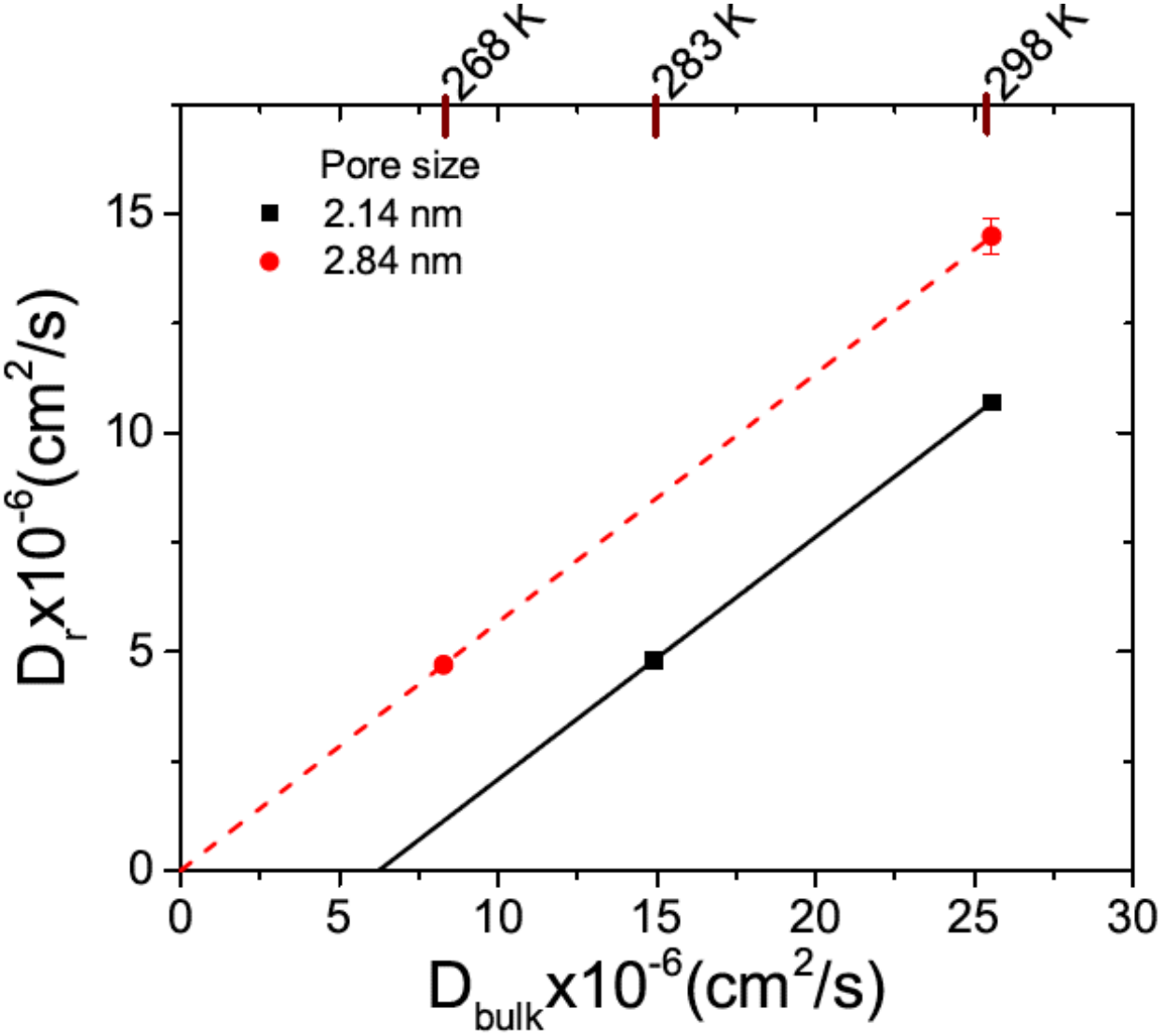

TREND: When size ↗ Θ ↘

Takahara et al., *J. Phys. Chem. B, Vol. 109, No. 22,* ***2005***

Varying Confinement Size?

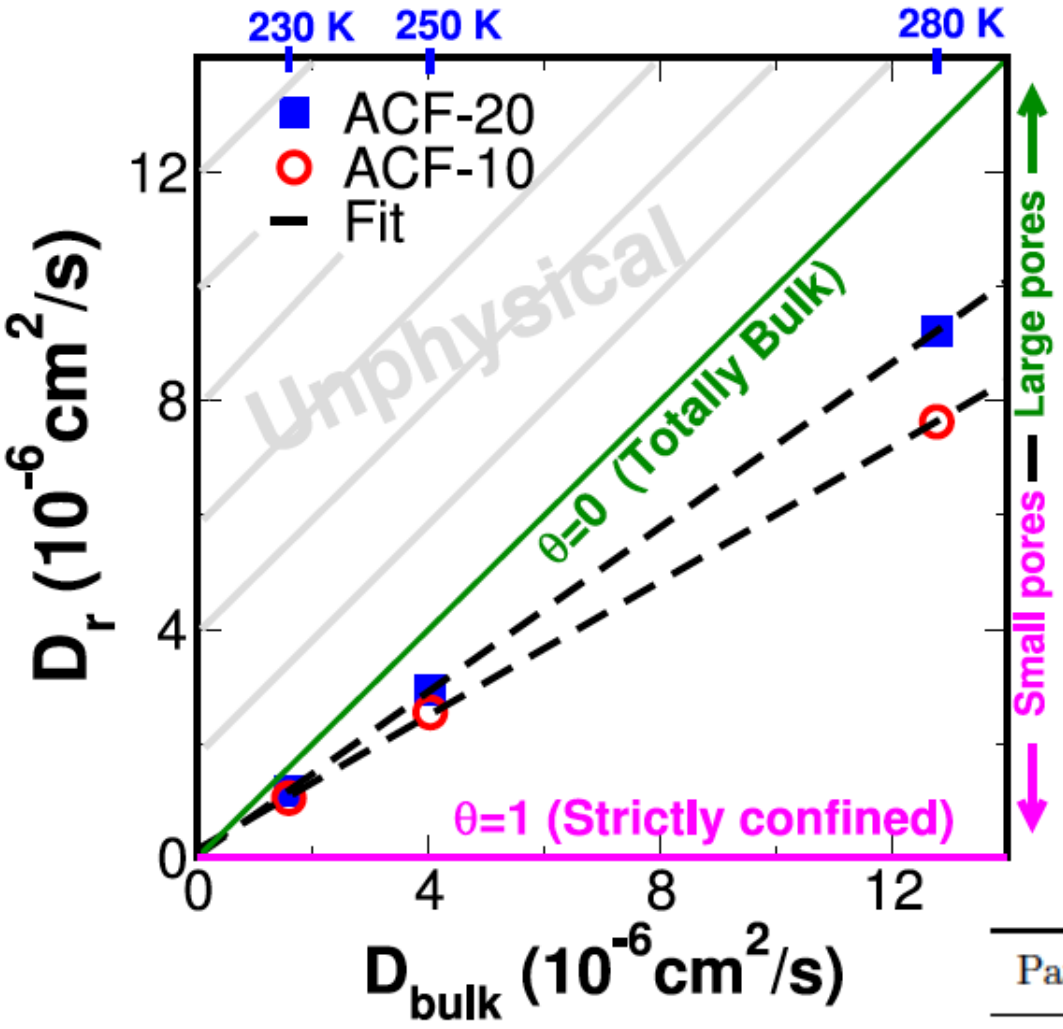

ACF-10 (ATC)

Scientist's hair
(Quiz: Guess whose?)

$$D_r(T) = \theta D_c + (1-\theta) D_{bulk}(T)$$

Parameters	$\theta = \frac{N_{bound}}{N_{total}}$	D_c (10^{-6}cm^2/s)
ACF-10	0.41	0.35
ACF-20	0.28	0.14

S. O. Diallo *et al*. Physical Review E **91**, 022124 (2015)

Confinement Geometry/Morphology

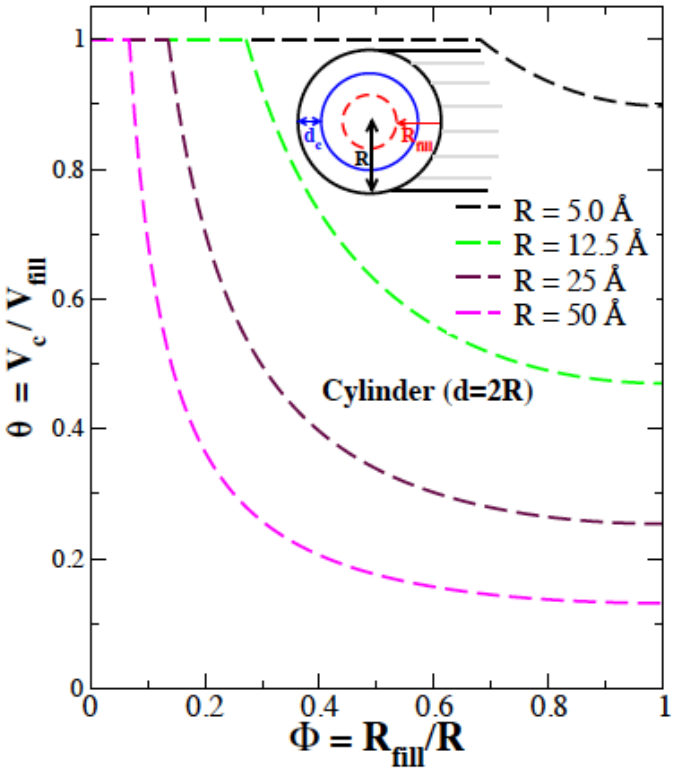

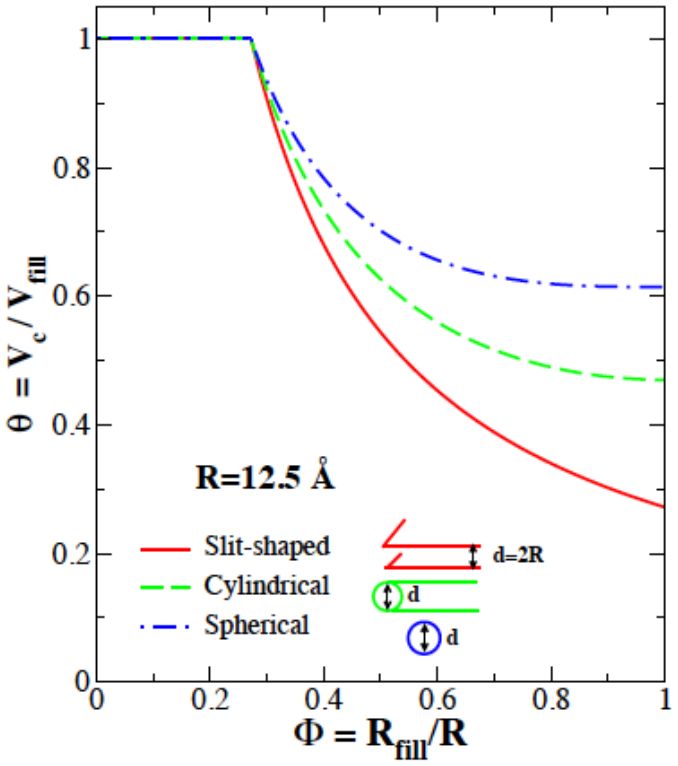

$$\Phi = (R_{fill}/R)$$

$$\Phi_c = d_c/R$$

Geometry	$0 < \Phi_{fill} \leq \Phi_c$	$\Phi_c \leq \Phi_{fill} \leq 1$
Slit	1	$\Phi_c \Phi^{-1}$
Cylinder	1	$(2\Phi_c - \Phi_c^2)\,(2\Phi - \Phi^2)^{-1}$
Sphere	1	$(3\Phi_c - 3\Phi_c^2 + \Phi_c^3)\,(3\Phi - 3\Phi^2 + \Phi^3)^{-1}$

Predictive models consistent with observations

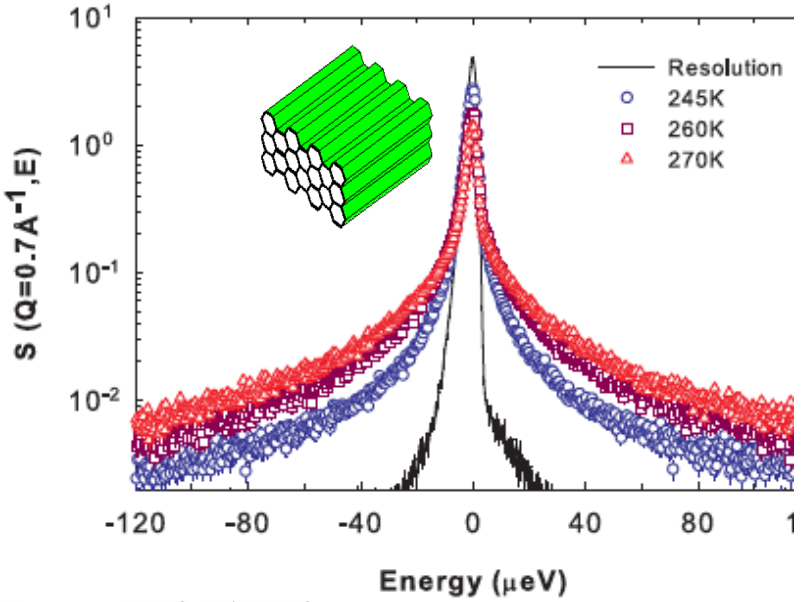

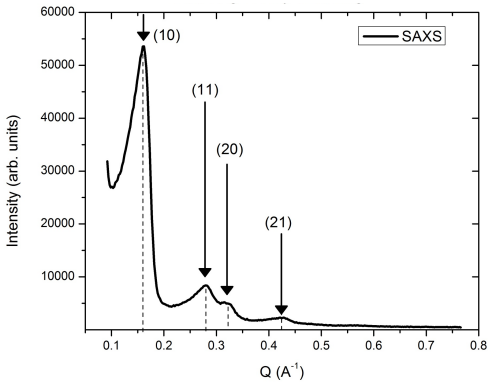

SAXS (FSM-12)

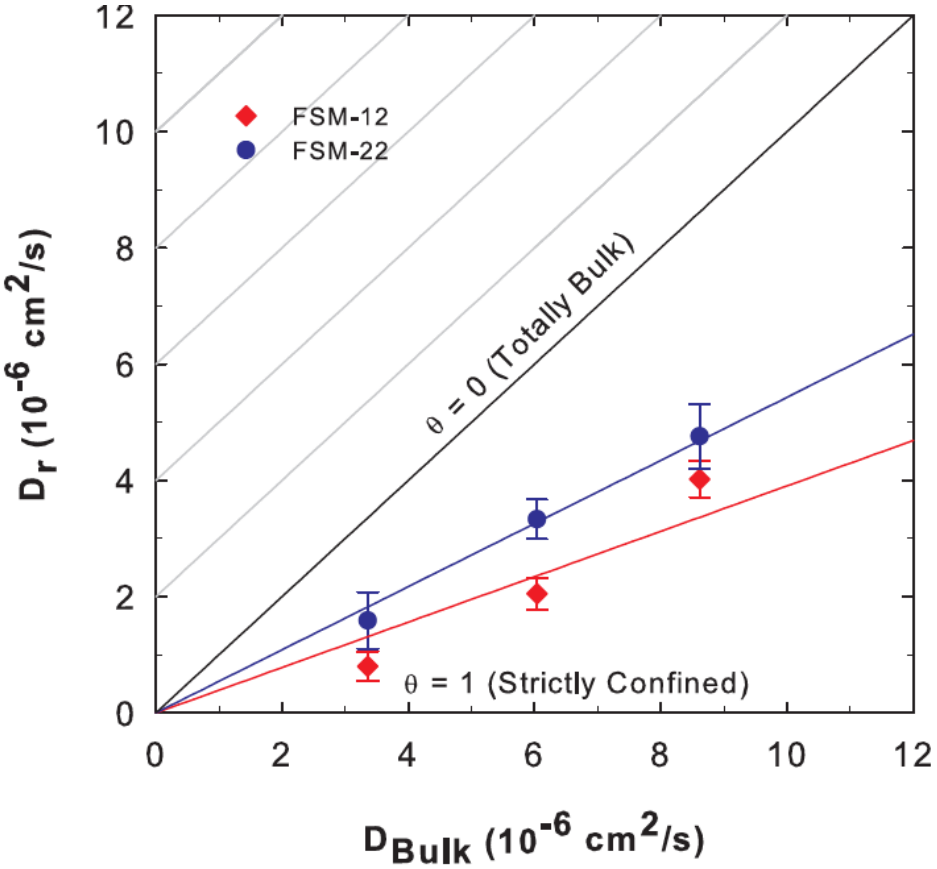

Sample	diameter (Å) (BJH)	$\theta = \frac{N_{bound}}{N_{total}}$	θ_{model}
FSM-12	16	61%	67%
FSM-22	39	46%	32%

In summary …

- **Scaling law verified for water in a wide range of systems**
- **Common attributes**
  - *Increasing hydration, θ decreases*
  - *Conf. size increases, θ decreases*
  - *3D confinement → larger θ*
  - *Hydrophilic systems, D_c~0*
- **Parameters for FSM silica determined**

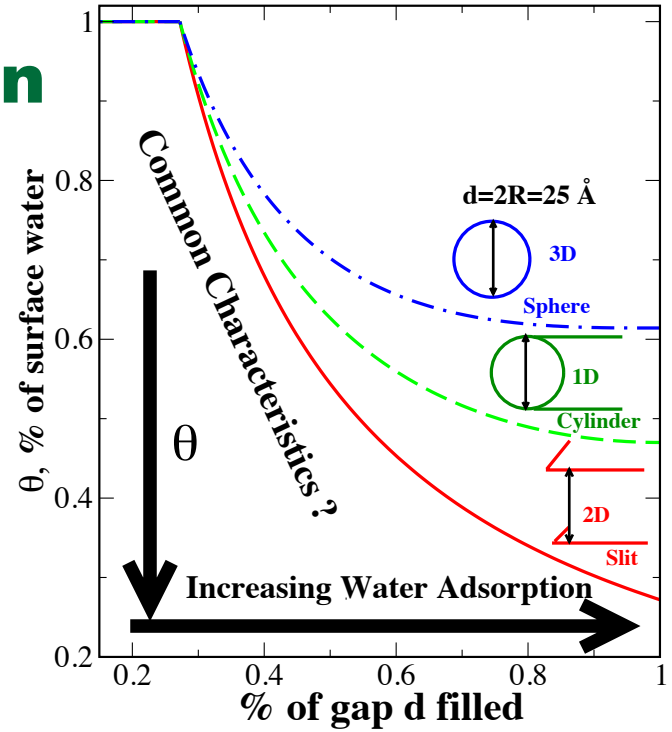

Back to Quasi-Elastic Neutron Scattering (QENS)

QENS probes dynamics ~ 1ns to 1ps

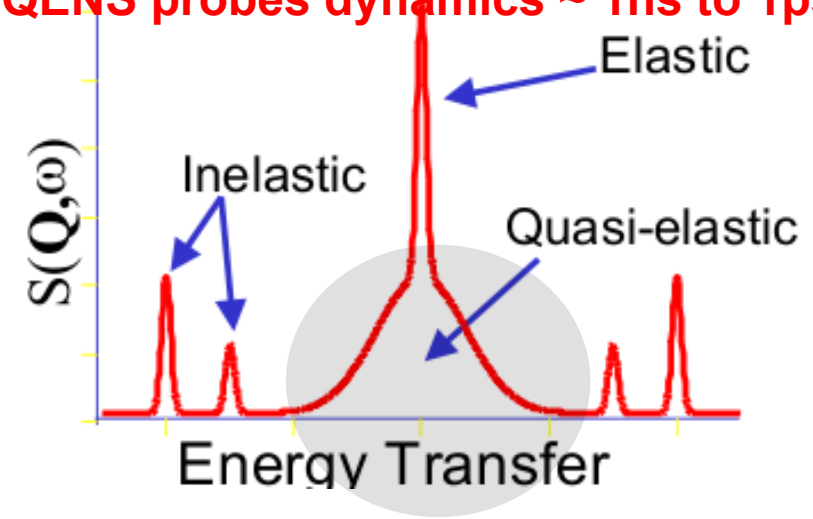

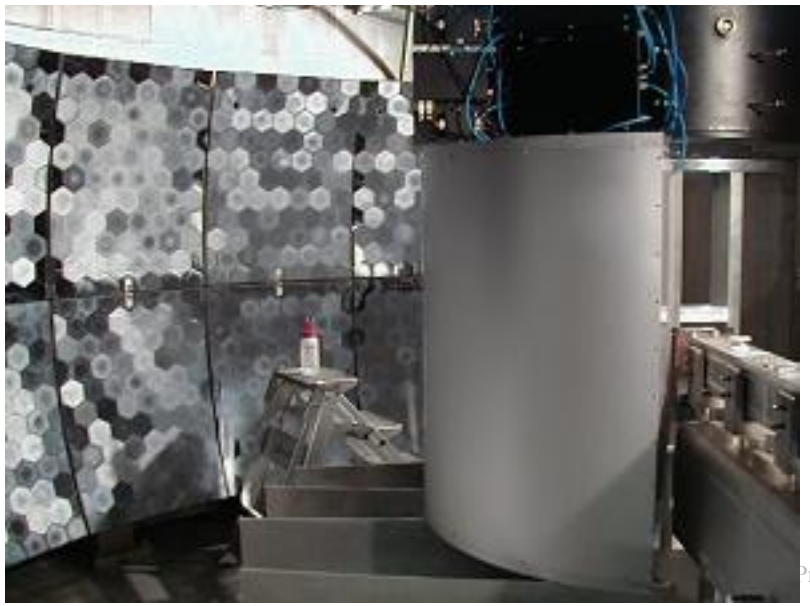

- **Biology** –proteins, hydration water..
- **Chemistry** – catalysis, polymers, complex fluids, ionic liquids ..
- **Condensed Matter & Materials science** –quantum fluids, spin ice...

QENS – *unique* probe for proton dynamics

Scattering event

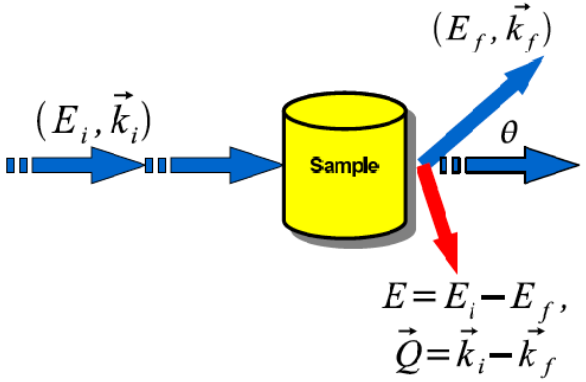

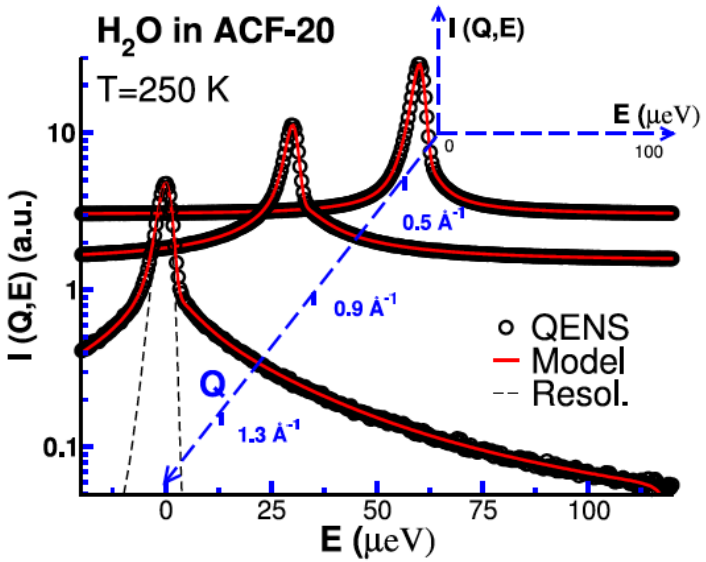

- **Momentum transfer** $Q \Rightarrow$ $\vec{Q}^2 = \vec{k_i}^2 + \vec{k_f}^2 - 2\vec{k_i}\vec{k_f}\cos\theta$
- **Energy transfer** $E = \hbar\omega \Rightarrow$ $E = E_i - E_f$
- $S(\mathbf{Q}, \omega)$, **Scattering function**

Advantages of QENS

- **Takes advantage of H/D exchange**
- **Diffusion Type (e.g. translational or rotational)**
- **Length scale (localized or long ranged)**
- **Relaxation Times**
- **Activation Energies …**

Recent upgrades to BASIS – *to enable new science*

Si 111	
Elastic energy	2.08 meV
Bandwidth	±250 μeV
Resolution (elastic)	3.5 μeV
Q range (elastic)	0.2 $Å^{-1}$ < Q < 2.0 $Å^{-1}$

Si 311 (upgrade)	
Elastic energy	7.64 meV
Bandwidth	±1700 μeV
Resolution (elastic)	10 μeV
Q range (elastic)	0.38 $Å^{-1}$ < Q < 3.8 $Å^{-1}$

Added capabilities will enable

- **New experimental studies (Non-hydrogenous, magnetic materials etc..)**
- **Simultaneous measurements of faster and slower dynamics (broadband spectroscopy)**
- **Higher Q => accurate geometrical information**

Examples: INS/Quantum fluids studies

Observed P-R dispersion in Liquid ^{4}He

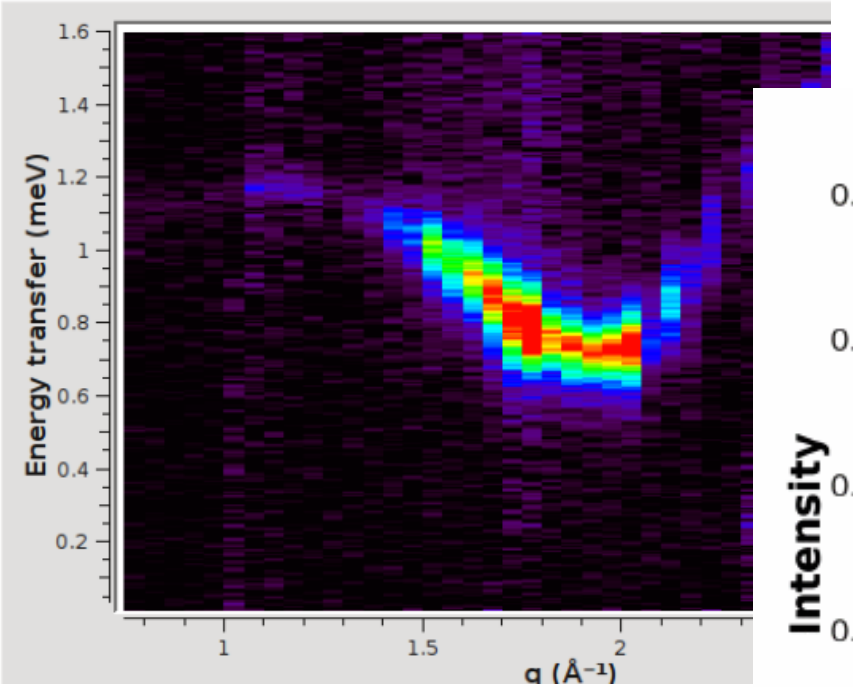

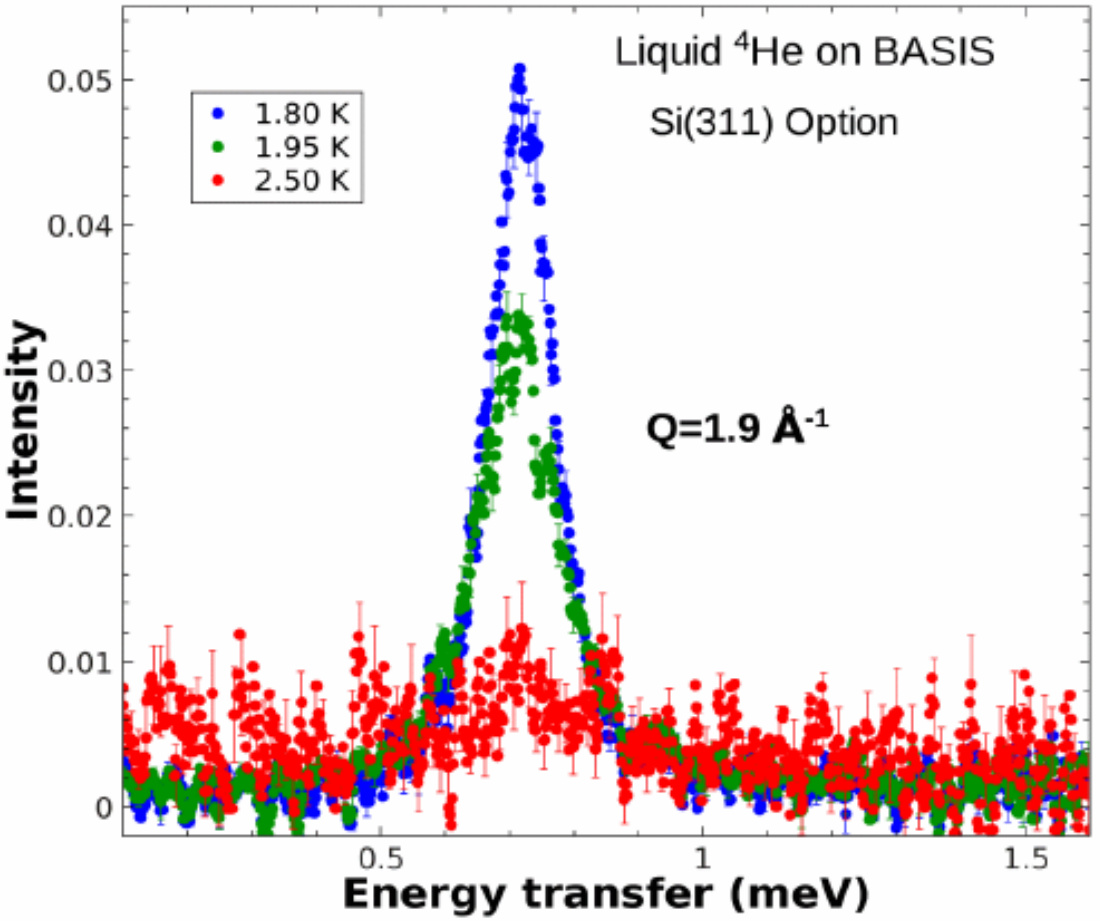

Examples: INS / Rotational tunneling

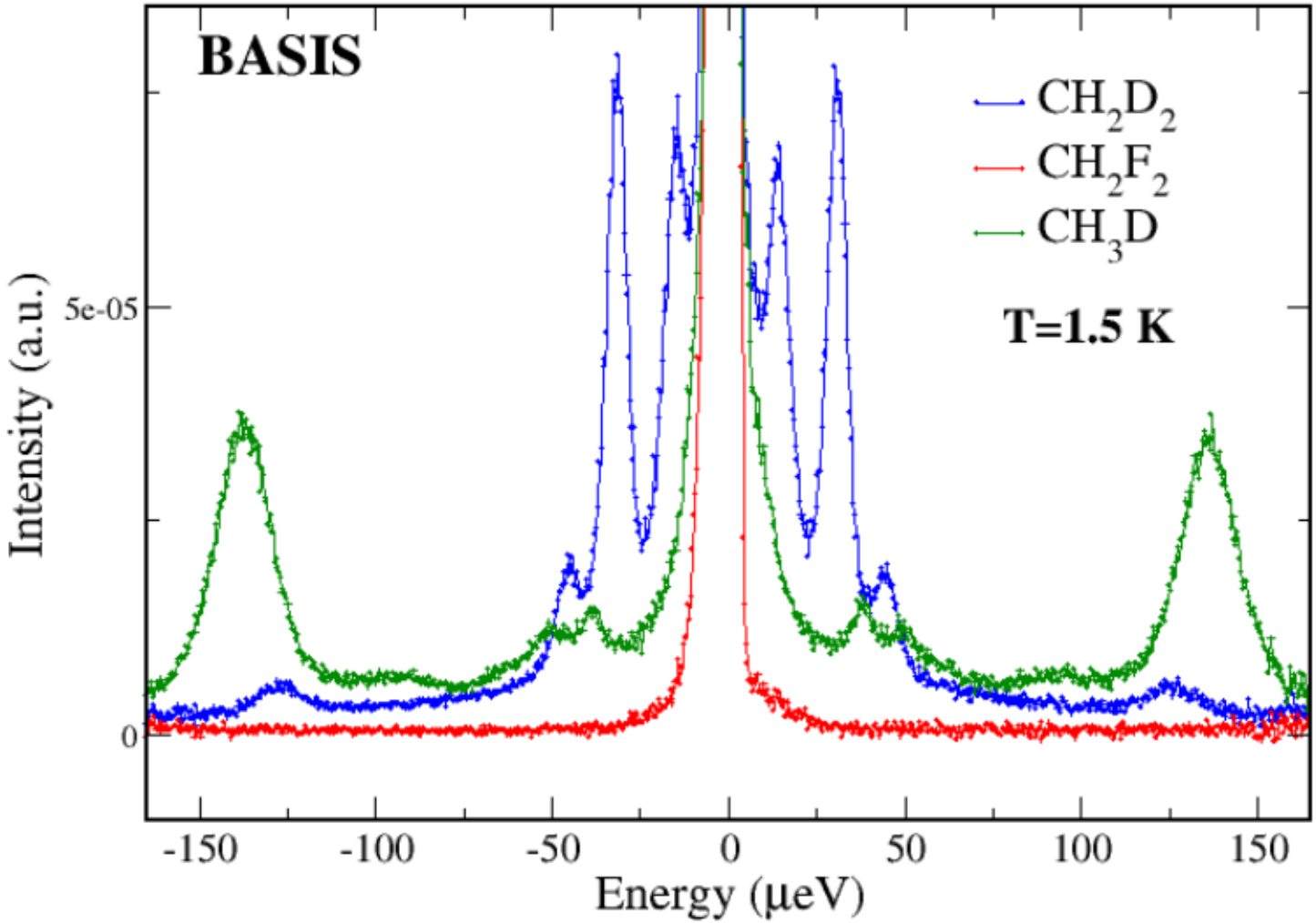

A. Hicks and J.Z. Larese . *Chem. Phys.*, **427**, 71 (2013).

PI: J.Z. Larese (UTK)

Examples: Ferroelectric materials

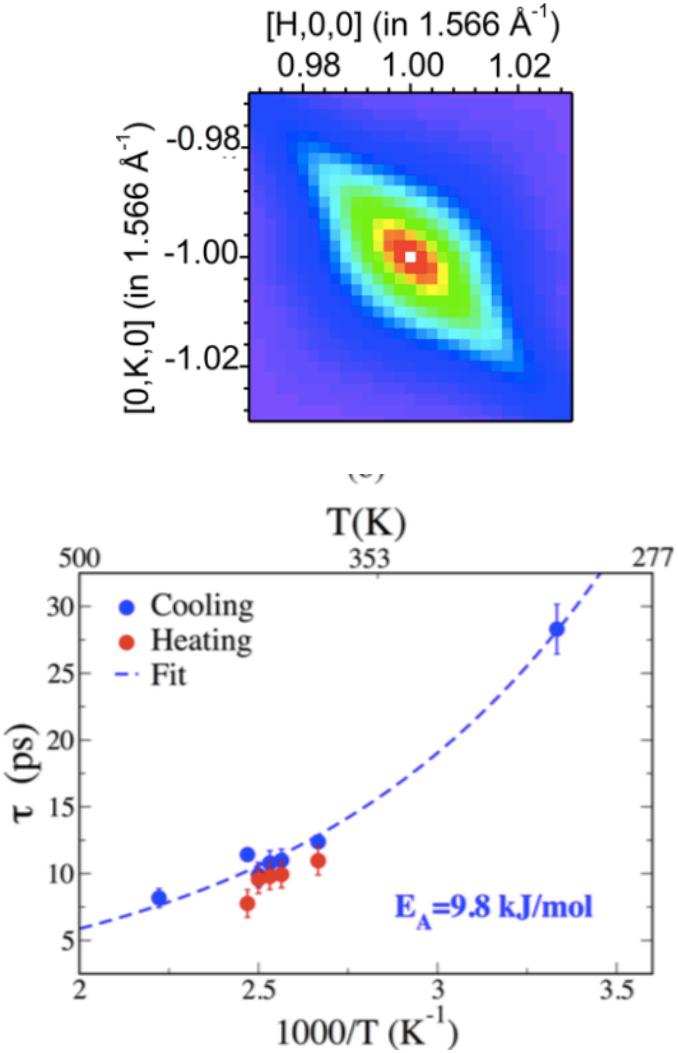

Pramanick *et al*., *Phys. Rev. B.* **92**, 174103 (2015).

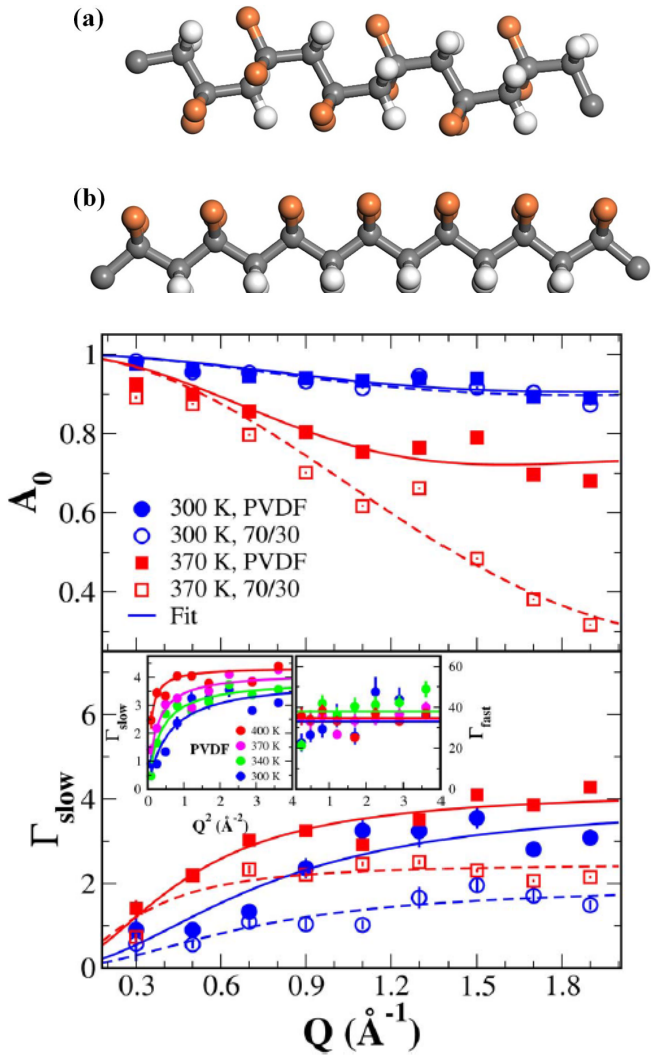

Jalarvo et al., *App. Phys. Lett.* **107**, 082907 (2015)

Examples: QENS/Protein dynamics

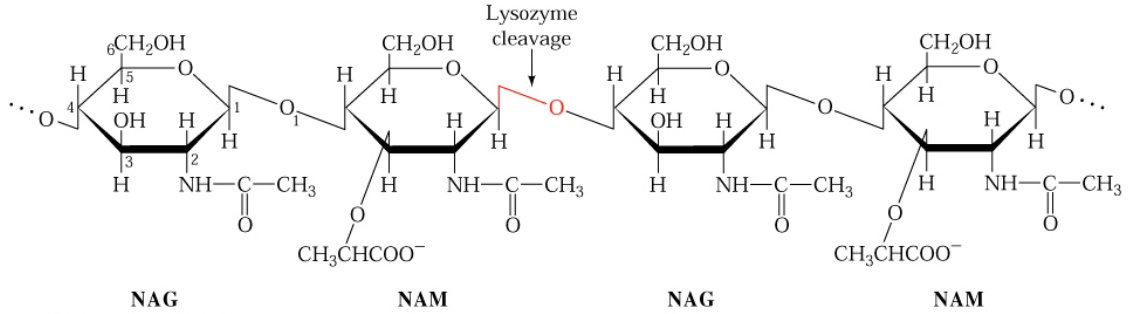

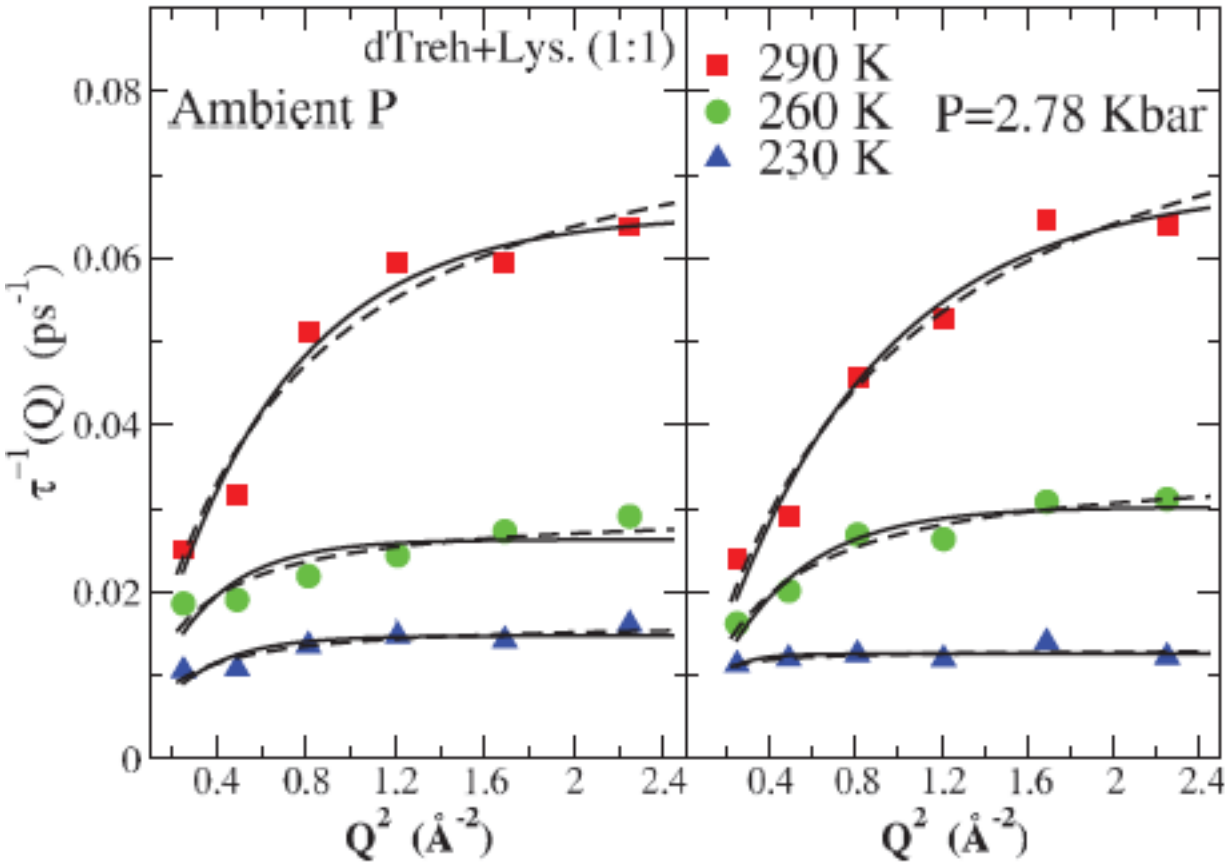

S. O. Diallo *et al*. Physical Review E **90**, 042725 (2014)

Examples: QENS/Hydration water studies

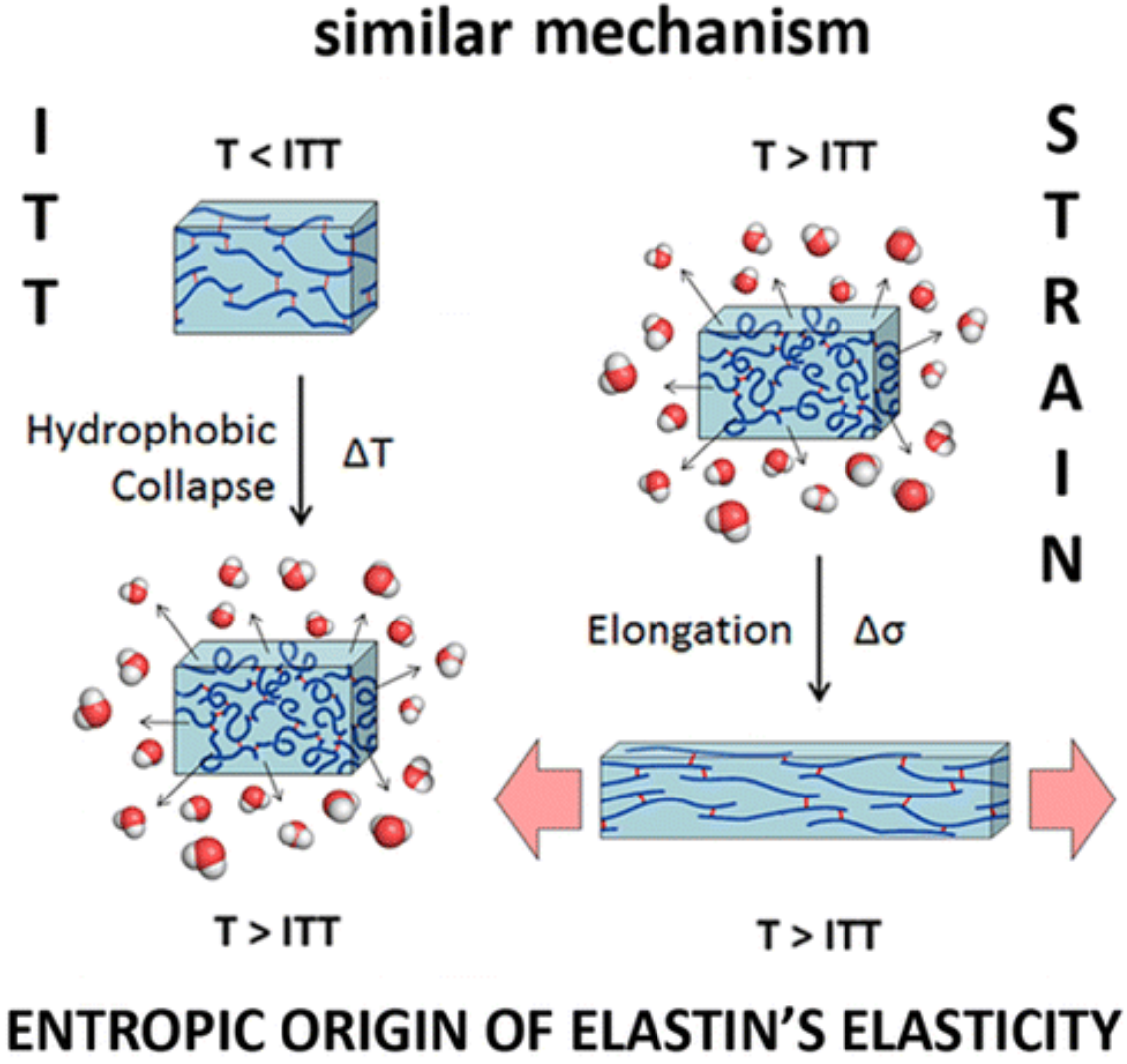

S. Perticaroli *et al. J. Phys. Chem. Lett.*, **6**, 4018 (2015).

Acknowledgments

Alexandra Cote (Summer intern)

Naresh Osti (Postdoc)

Eugene Mamontov

T. Ramirez-Cuesta

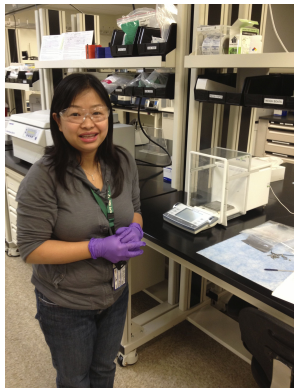

Qiu Zhang

Hugh O'Neill

Abhijit Pramanick

Many others at ORNL…

Funding:
Work at **BASIS** is supported by DOE BES
Partial support from FIRST EFRC, DOE BES

Macromolecular Neutron Crystallography

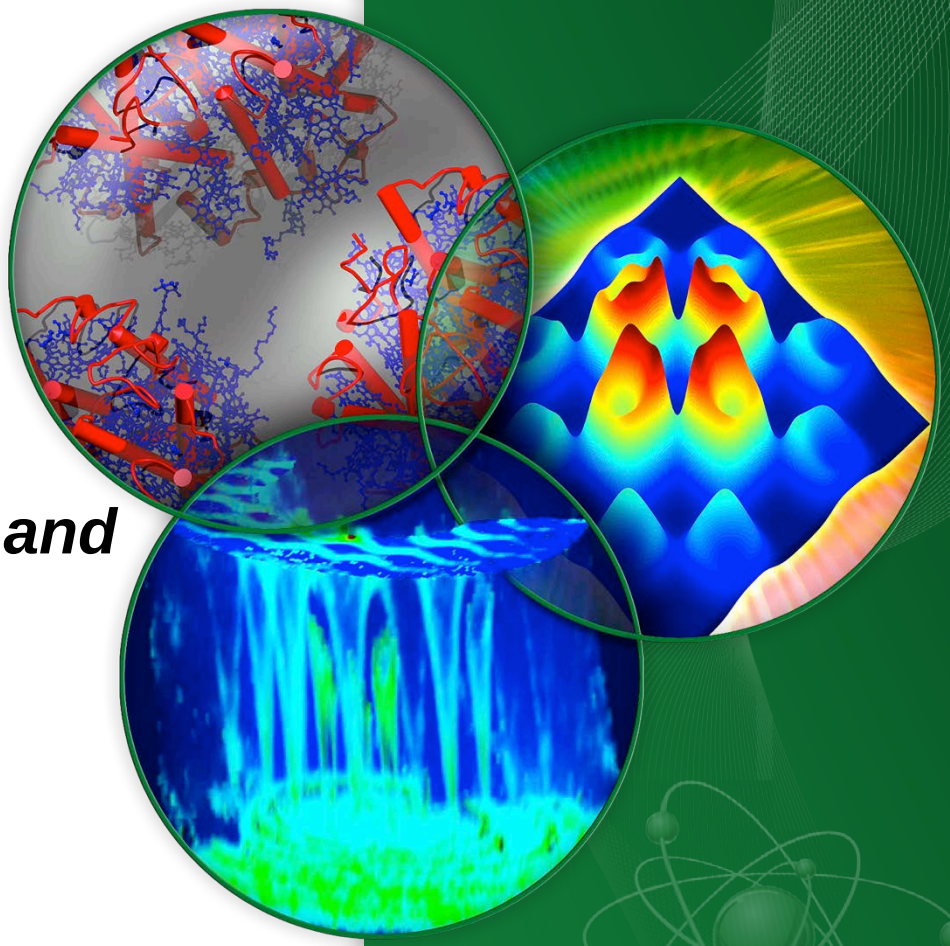

Elusive species, protonation states, and proton transfer

Andrey Kovalevsky
R&D Scientist
Biology and Soft Matter Division
Oak Ridge National Laboratory
Oak Ridge, TN

ORNL is managed by UT-Battelle
for the US Department of Energy

OAK RIDGE National Laboratory | HIGH FLUX ISOTOPE REACTOR | SPALLATION NEUTRON SOURCE

X-rays reveal structural details

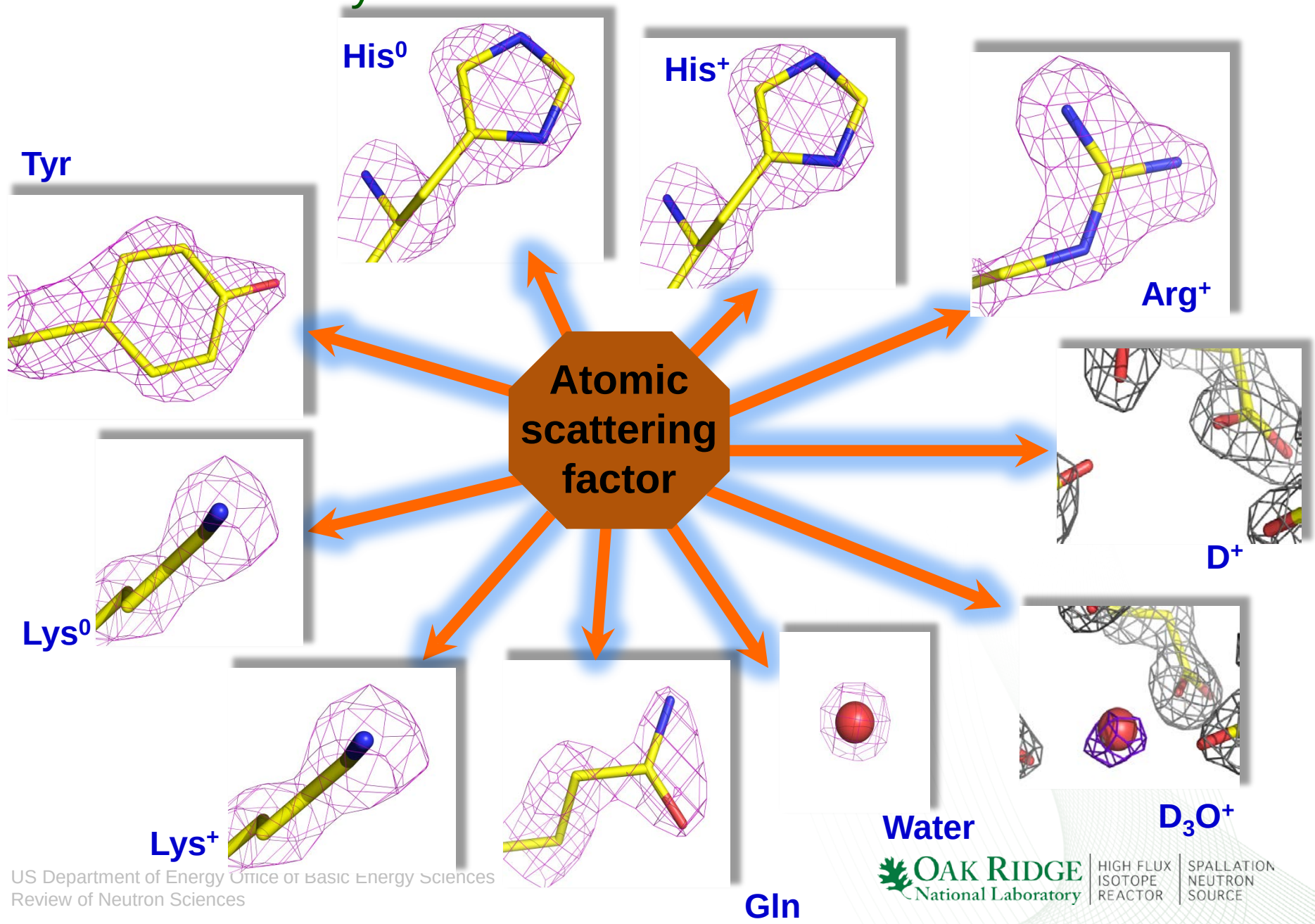

Neutrons reveal atomic details

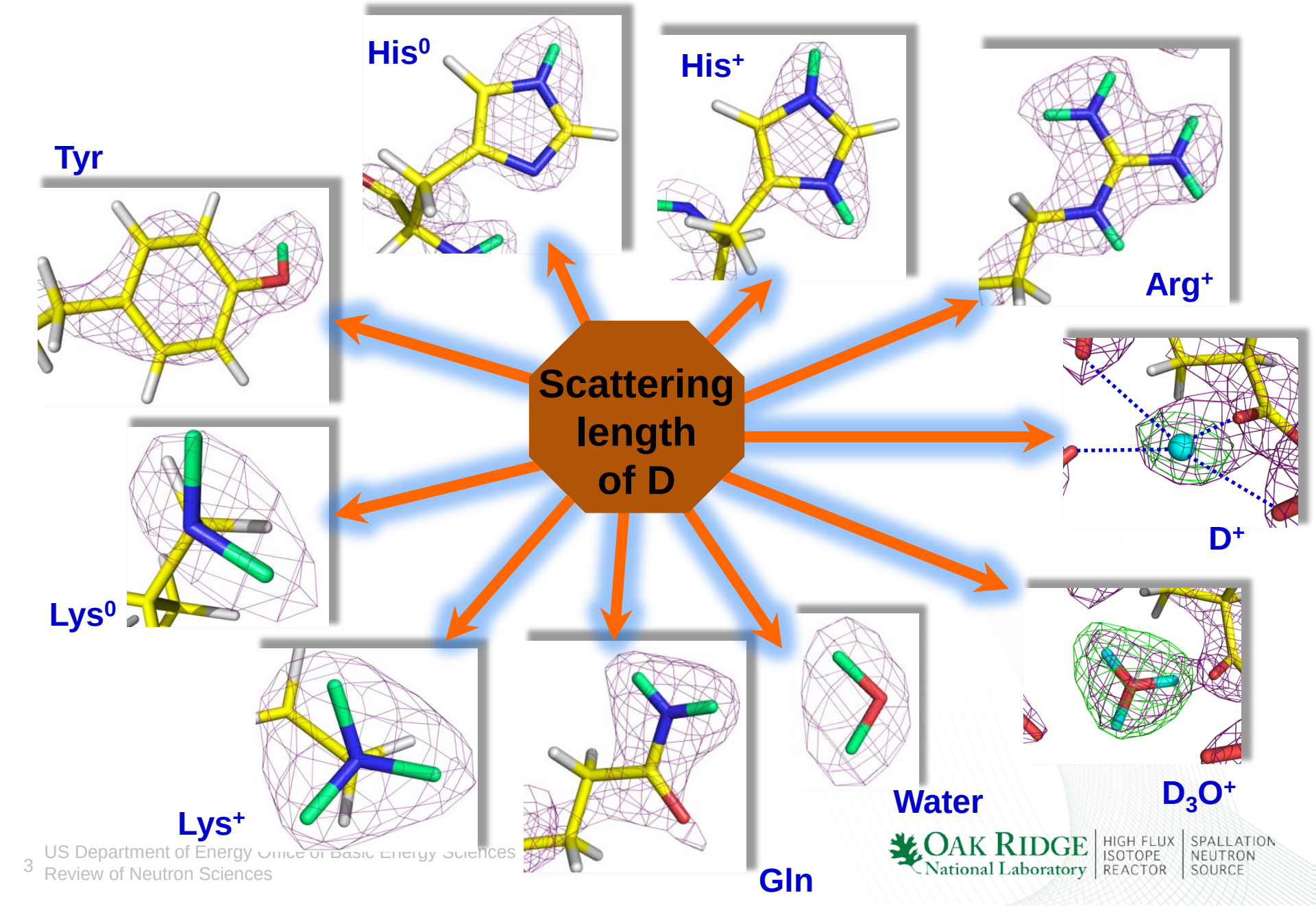

50 mm³
first instrument at BNL
D19 at ILL

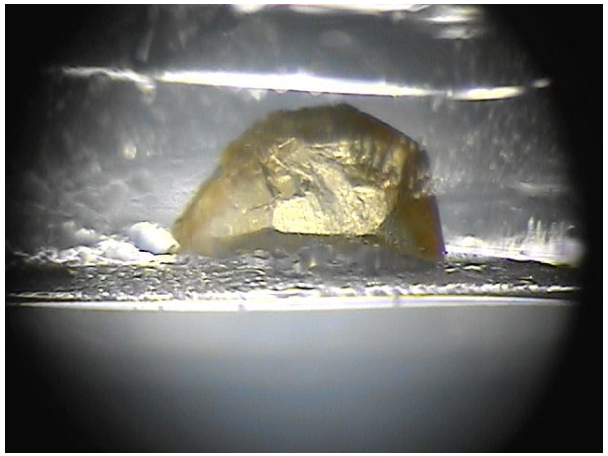

>1 mm³
PCS at LANSCE
LADI at ILL

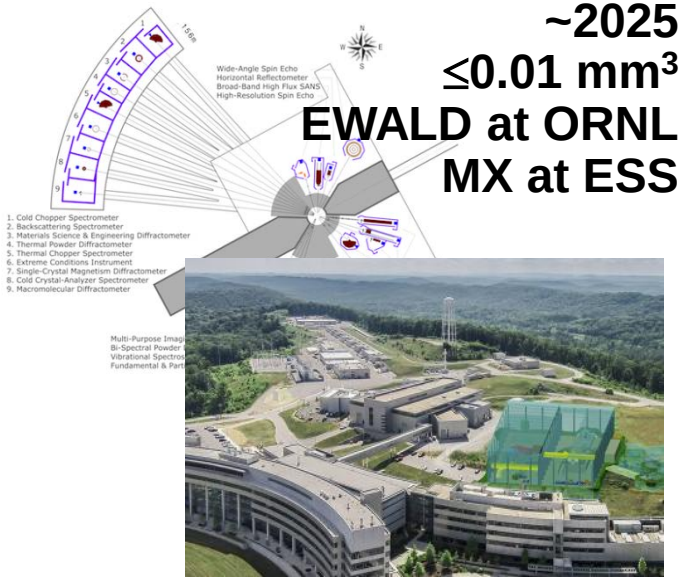

~2025
≤0.01 mm³
EWALD at ORNL
MX at ESS

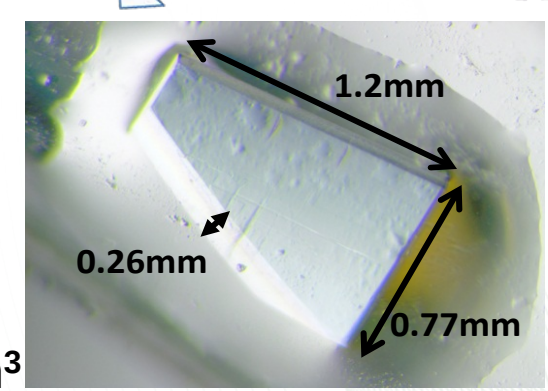

≤0.2 mm³
IMAGINE, MaNDi at ORNL
LADI-III at ILL
iBIX at JPARC

IMAGINE Beamline - Quasi-Laue single crystal neutron diffractometer

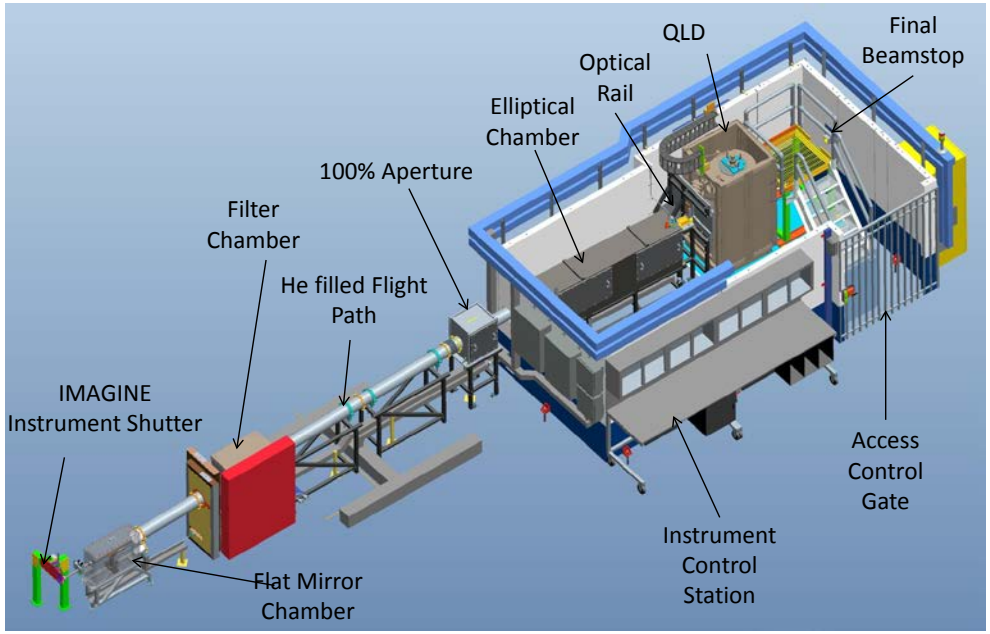

Wavelength range:

2.0 Å - 3.0 Å	2.78 Å - 3.0 Å	3.33 Å - 4.0 Å
2.0 Å - 4.0 Å	2.78 Å - 4.0 Å	3.33 Å - 4.5 Å
2.0 Å - 4.5 Å	2.78 Å - 4.5 Å	

Flux: ~3 x 10^6 n s^{-1} cm^{-2}

Beam size: 2 x 3.5 mm^2

Applications

- **Macromolecular structure-function**
- **Supramolecular crystallography**
- **Materials chemistry**

MaNDi beamline - The Macromolecular Neutron Diffractometer

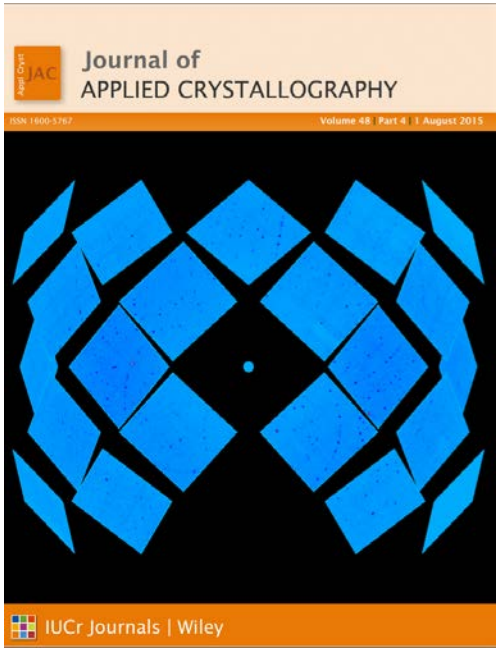

38 SNS Anger Cameras now surround the sample position giving 4sr detector coverage

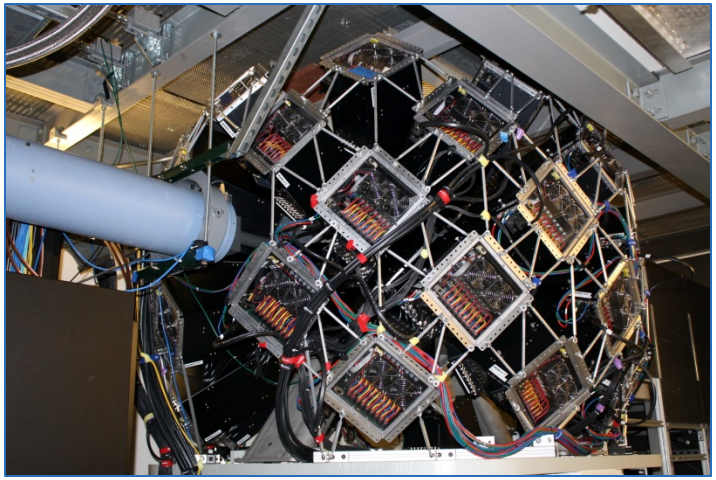

The MaNDi Team

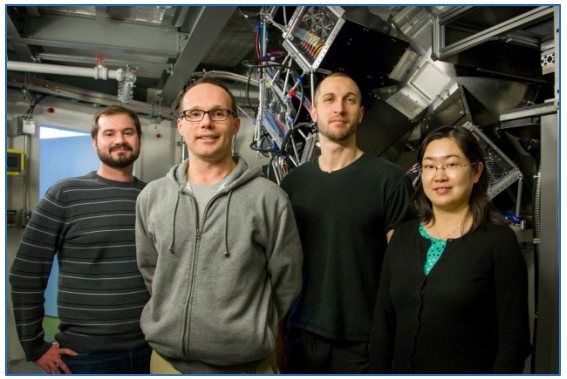

MaNDi is a Time of Flight wavelength resolved Laue diffractometer designed for flexibility and high signal to noise data collection. Several Key instrumental parameters can be adjusted to match the parameters of the sample.

D-Xylose Isomerase – aldo-keto sugar conversion

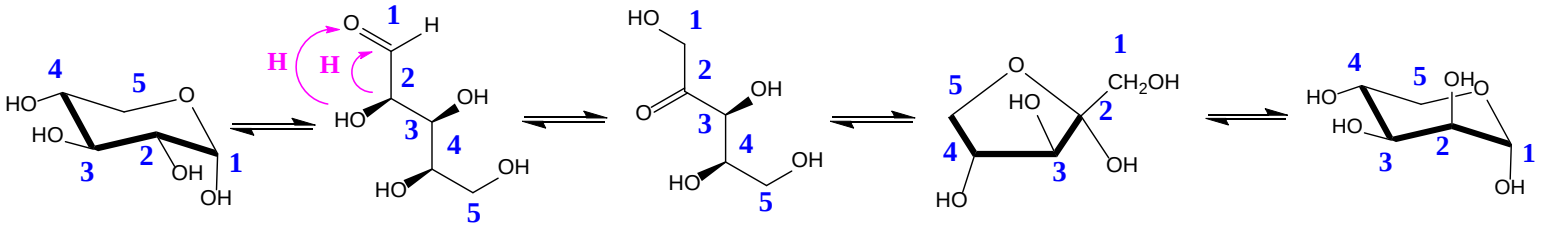

α-D-xylose (xylopyranose) | D-xylose (linear form) | D-xylulose (linear form) | α–D-xylulose (xylulofuranose) | β-D-lyxose

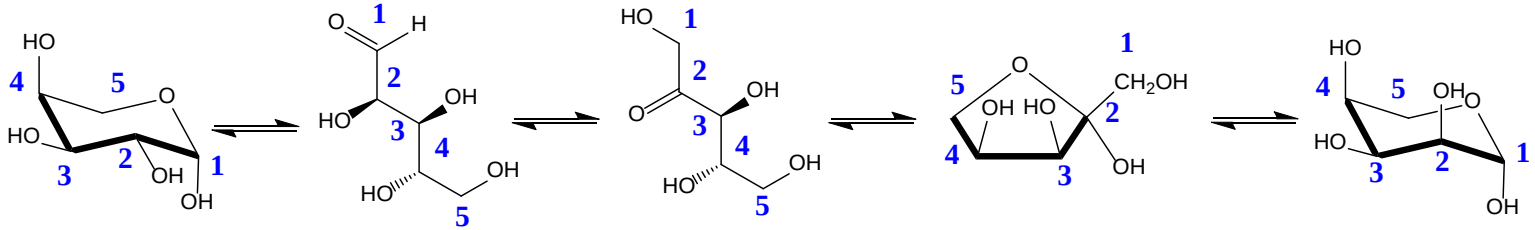

β-L-arabinose (arabinopyranose) | L-arabinose (linear form) | L-ribulose (linear form) | β–L-ribulose (ribulofuranose) | β-L-ribose ribopyranose)

isomerization

epimerization

In total, 9 neutron structures have been obtained.

D-xylose isomerase

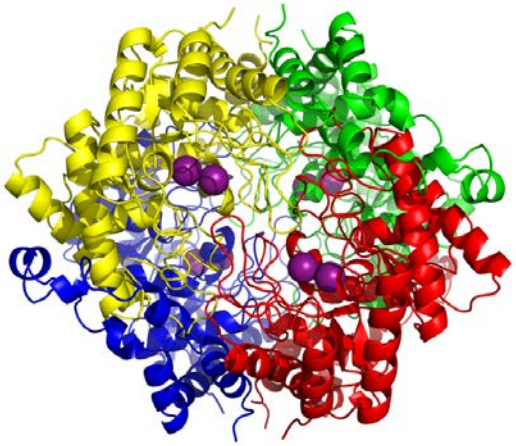

Active homotetramer

k_{cat} = 5 s^{-1}
K_M = 3 mM (D-xylose)
200mM (D-glucose)

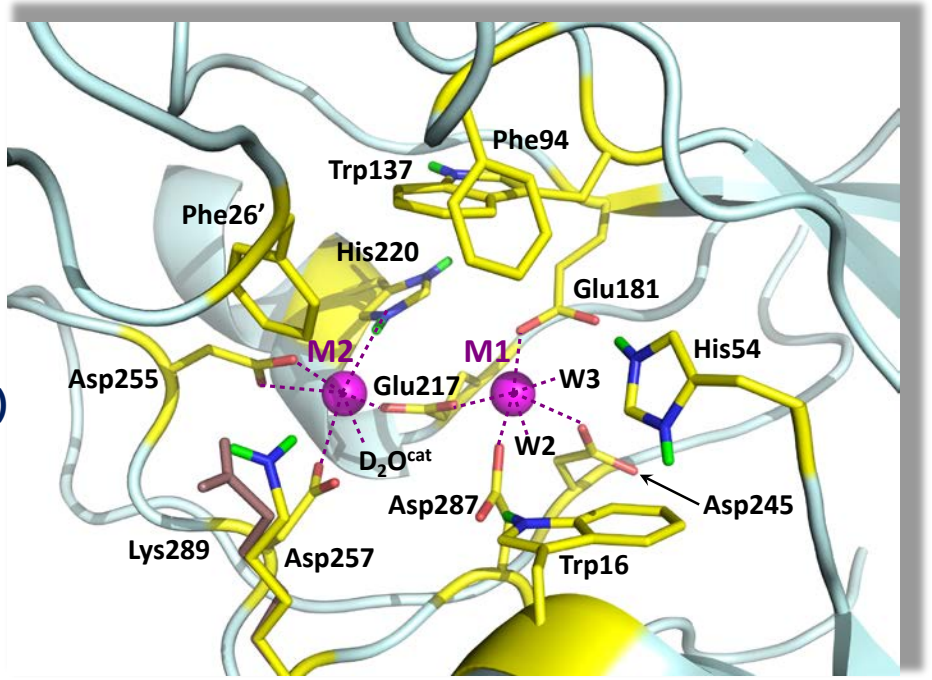

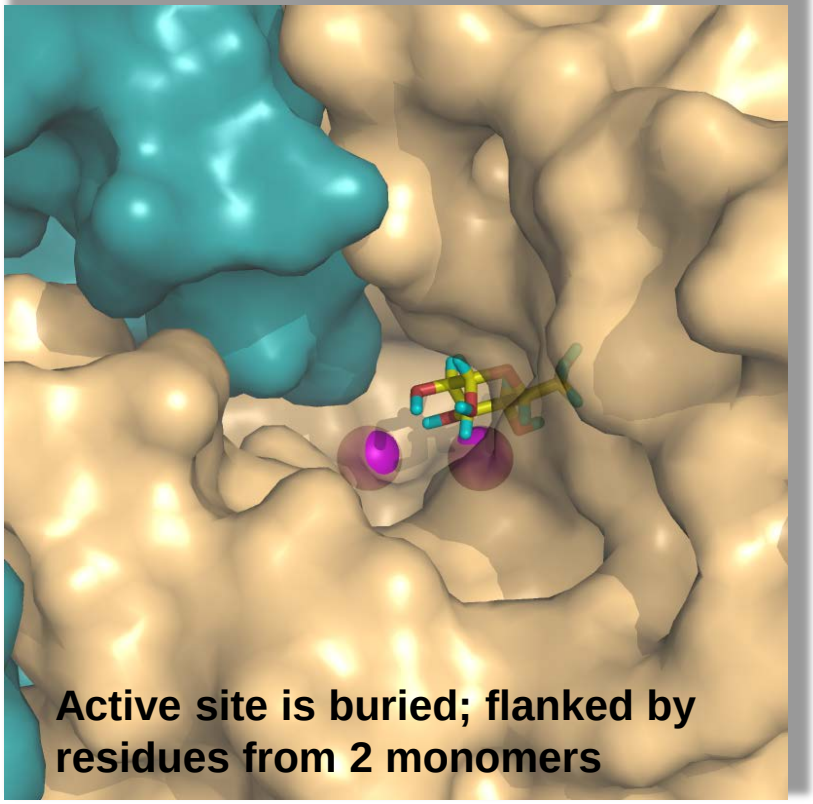

Highly stereospecific: O1 in axial position of a sugar ring

Catalized reactions:
xylose-to-xylulose
glucose-to-fructose
arabinose-to-ribulose
...

Activators: Mg^{2+}, Co^{2+}, Mn^{2+}
Inhibitors: most transition metals, polyalcohols, acidic pH (< 6)

Joint X-ray/Neutron crystallography:

Snapshots of D-xylose isomerase-catalyzed isomerization reaction

Catalytic water stays as H_2O

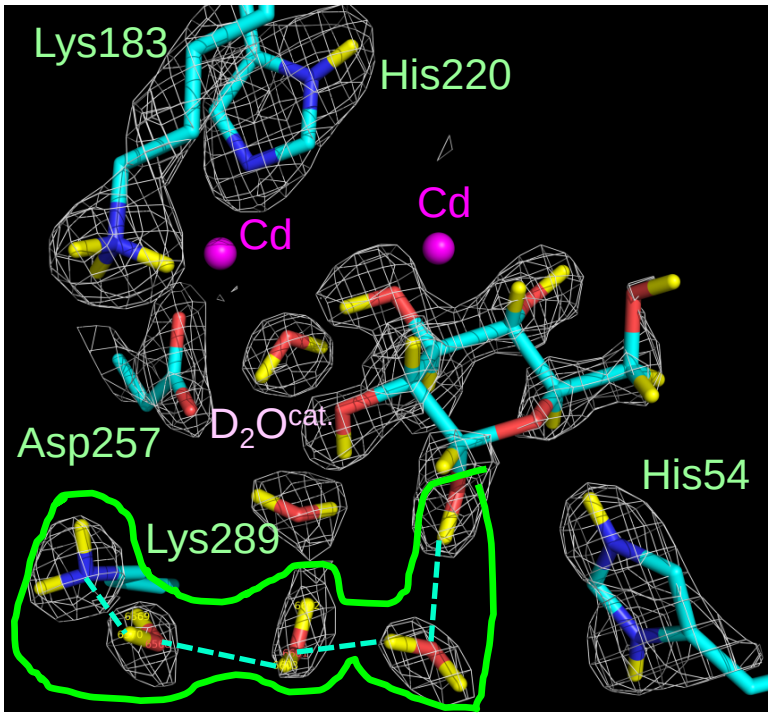

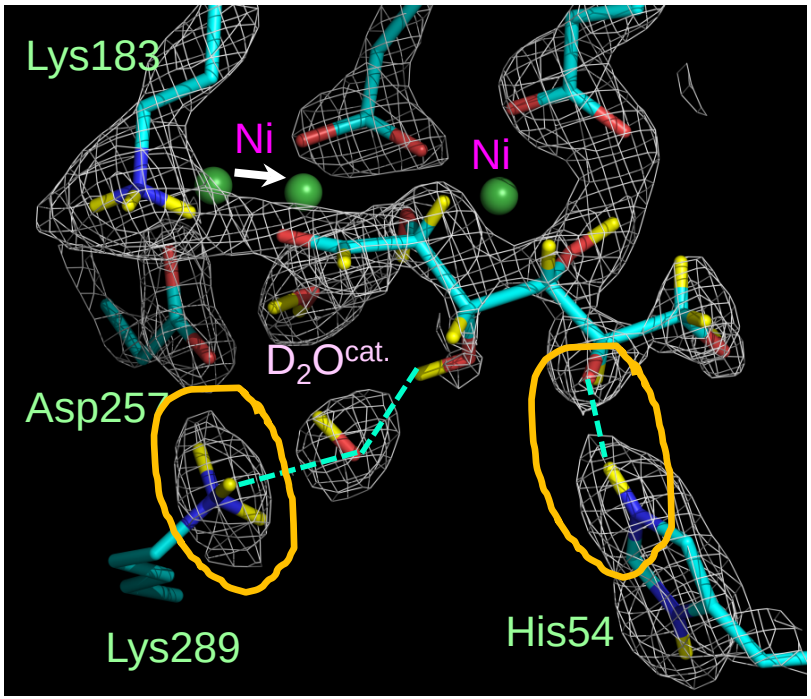

Ring opening:

what deprotonates O1? – O1 is deprotonated by a water molecule and H is transferred to Lys289

what protonates O5? – O5 remains deprotonated in the crystal, His54 keeps both H atoms

XI variant	pH = 7.7		
	k_{cat}, s^{-1}	K_M, mM	k_{cat}/K_M, $M^{-1}s^{-1}$
rWT-His_6	1.22 ± 0.02	5.0 ± 0.2	240
Lys289His	1.38 ± 0.07	4.3 ± 0.3	321
Lys289Glu	0.51 ± 0.04	8 ± 1	64

Kovalevsky et al. (2010) *Structure* **18**, 688-699.

Waltman et al., *PEDS* **27**, 59-64 (2014)

Joint X-ray/Neutron crystallography:
Snapshots of D-xylose isomerase-catalyzed isomerization reaction

Catalytic water is deprotonated
Metal movement towards substrate may be crucial

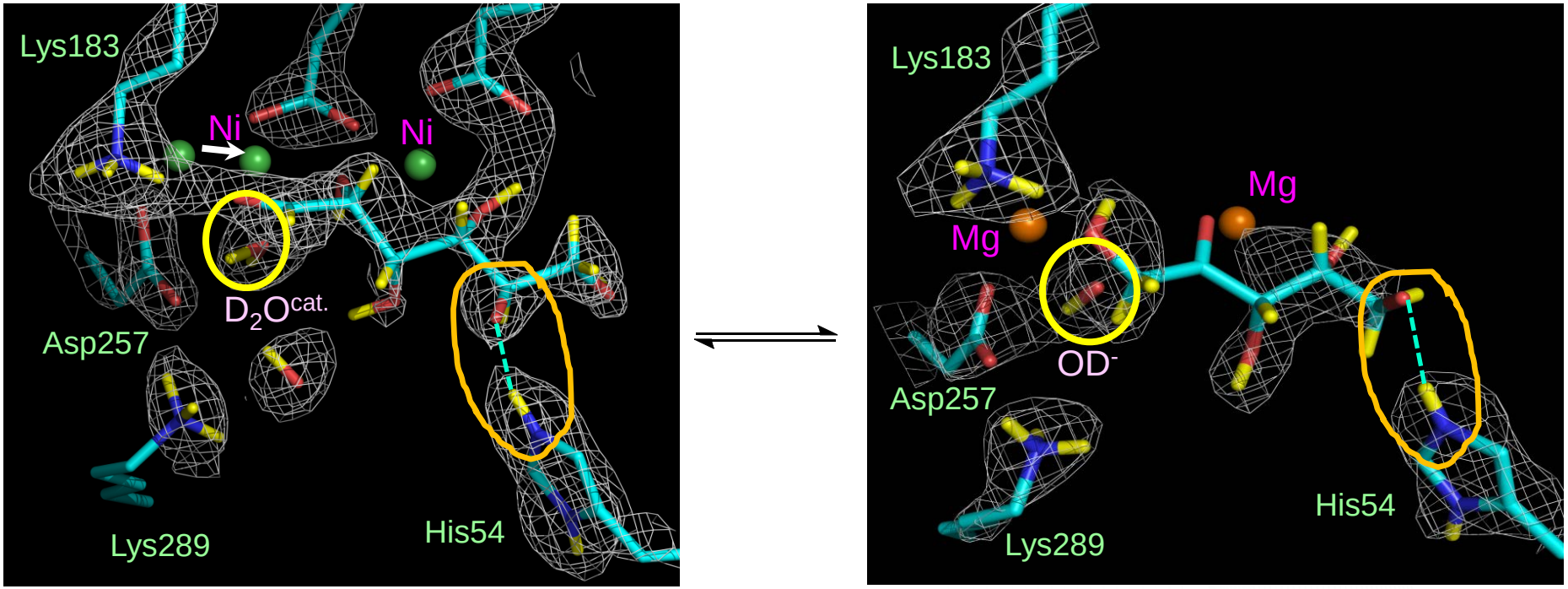

Isomerization:

what deprotonates O2? – unclear
what protonates O1? – catalytic H_2O may be the proton donor; it is converted to OH^-
which protonation event occurs first? – unclear
is it a base or acid hydrolysis? – unclear

Kovalevsky et al. (2008) *Biochemistry* **47**, 7595-7597.

Joint X-ray/Neutron crystallography:

D_3O^+ exchanges roles with D^+ at metal site M1

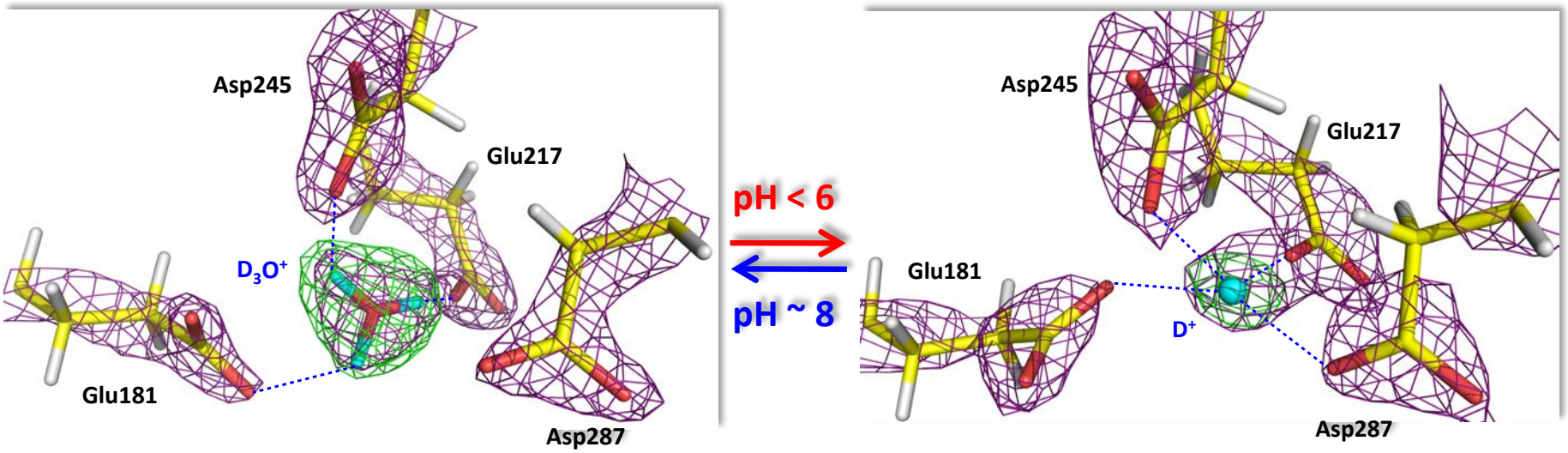

XI variant	pH = 7.7			pH = 5.8		
	k_{cat}, s^{-1}	K_M, mM	k_{cat}/K_M, $M^{-1}s^{-1}$	k_{cat}, s^{-1}	K_M, mM	k_{cat}/K_M, $M^{-1}s^{-1}$
Native WT	5.52 ± 0.05	3.0 ± 0.1	1840	0.41 ± 0.02	83 ± 10	4.9
rWT-His_6	1.22 ± 0.02	5.0 ± 0.2	240	0.31 ± 0.01	33 ± 3	9.4
rWT-His_{12}	**0.80 ± 0.01**	**3.8 ± 0.3**	**211**	**0.140 ± 0.003**	**14 ± 1**	**10**
Asn215Asp	**2.3 ± 0.1**	**3.4 ± 0.1**	**676**	**0.19 ± 0.01**	**10 ± 1**	**19**
Lys289His	1.38 ± 0.07	4.3 ± 0.3	321	0.064 ± 0.007	27 ± 2	2.4
Lys289Glu	0.51 ± 0.04	8 ± 1	64	0.070 ± 0.002	37 ± 4	1.9
Asp287Asn	no activity			no activity		

Kovalevsky *et al.*, *Angew. Chem. –Int. Ed.* **50**, 7520-7523 (2011)

Waltman et al., *PEDS* **27**, 59-64 (2014)

Xylanase – glycoside hydrolysis

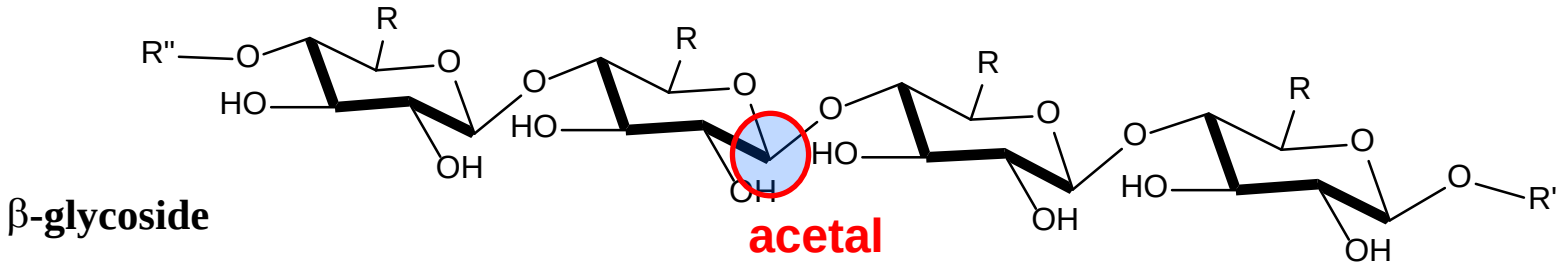

uncatalyzed	*catalyzed by* H_3O^+	*catalyze by* **glycosidase**
$k_{cat} \sim 10^{-15}\ s^{-1}$	$k_{cat} \sim 10^{-8}\ s^{-1}$	k_{cat} up to $10^{3}\ s^{-1}$

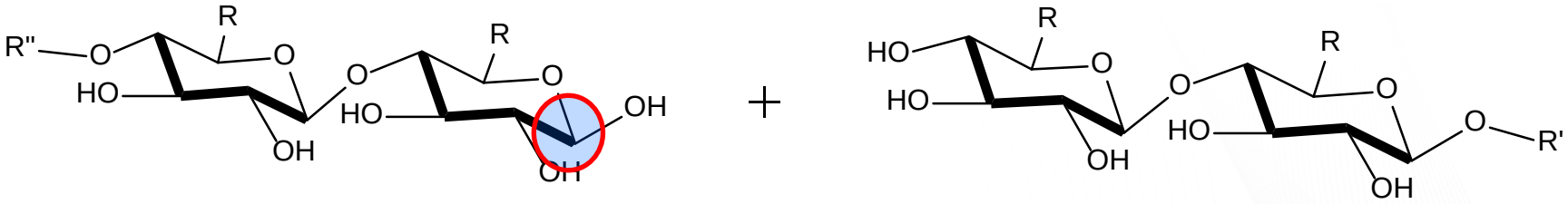

hemiacetal

glycone **non-reducing end**

aglycone **reducing end**

Retaining glycoside hydrolase:
Family 11 xylanase with a “jelly roll” fold

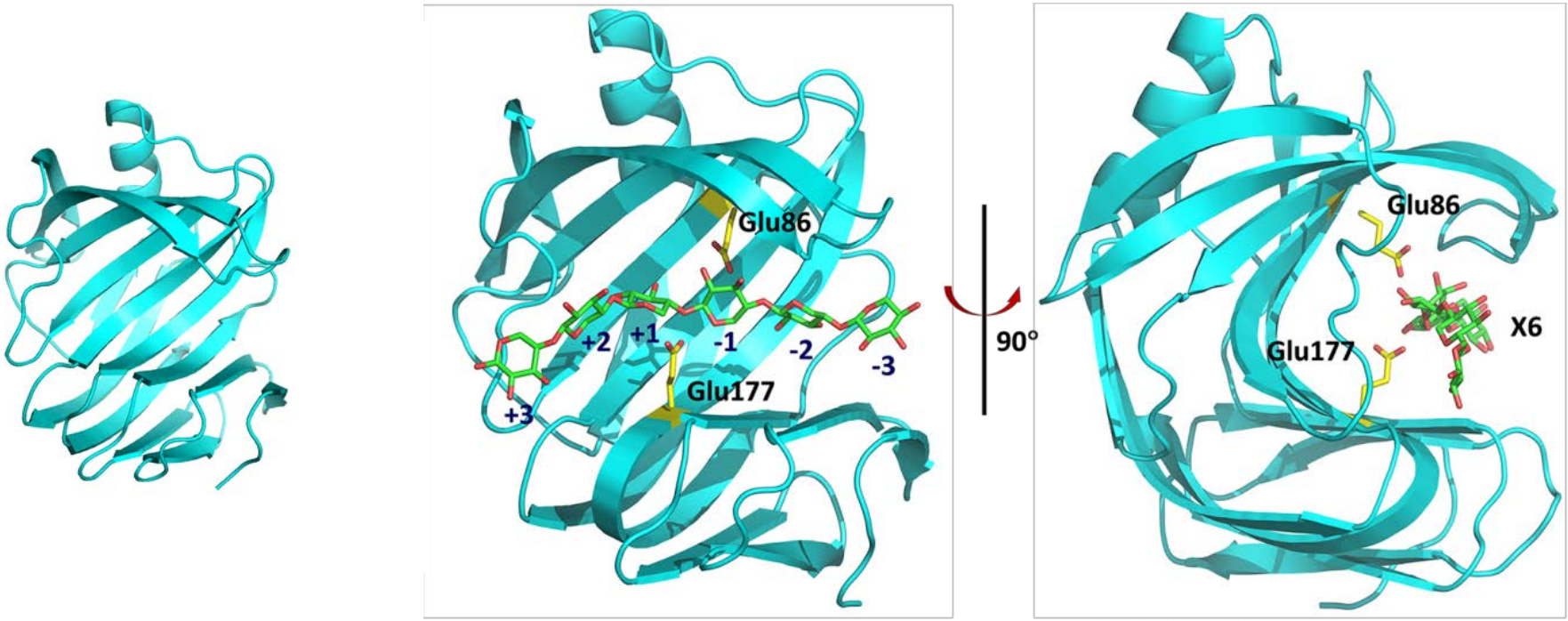

Glu177 – general acid/base catalyst;
Glu86 – nucleophile.

Wan, et al., *Acta Crystallogr.* 2014, **D70**, 11-23.

We are studying a retaining β-GH endo-1,4-β-xylanase (*XynII*) from filamentous fungus *Trichoderma reseei* in an effort to understand its catalytic mechanism in depth *as a paradigm for all retaining β-GH enzymes*.

XynII at pH 5.8: No Glu177 protonation, normal hydrogen bonding around the catalytic residues

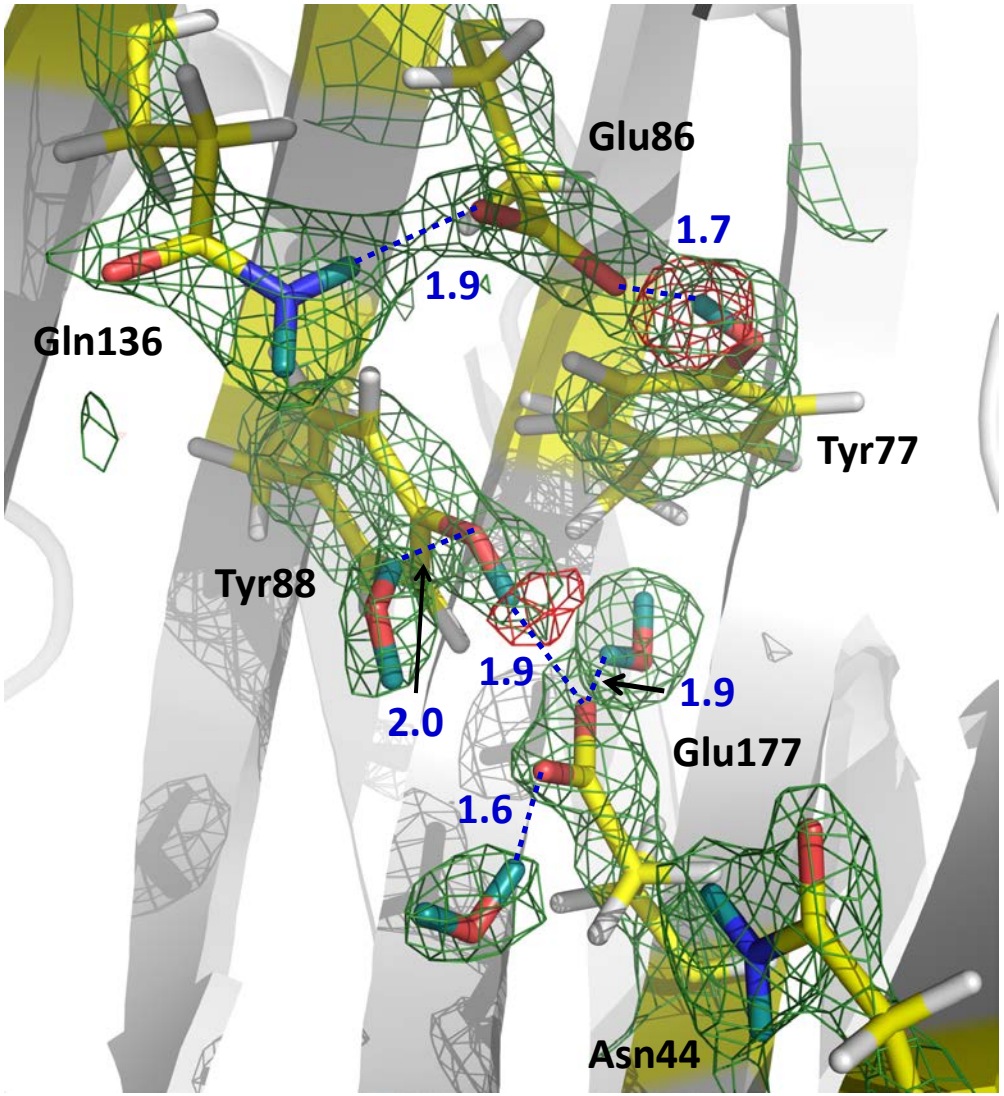

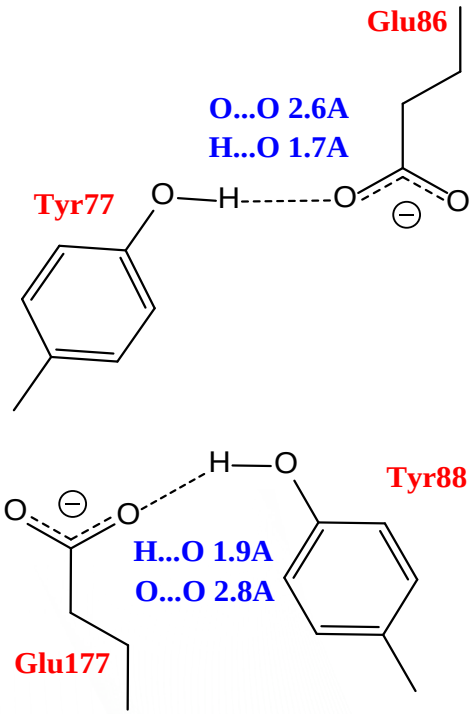

Similar hydrogen bonding patternwas observed in the neutron structure of N44D variant at pH 6.0.

A.Y. Kovalevsky et al. (2011) *Acta Crystallogr.* **F67**, 283-286.

Family 11 xylanases: Early X-ray work showed Glu177's side chain can adopt two conformations near the physiological pH for the enzyme

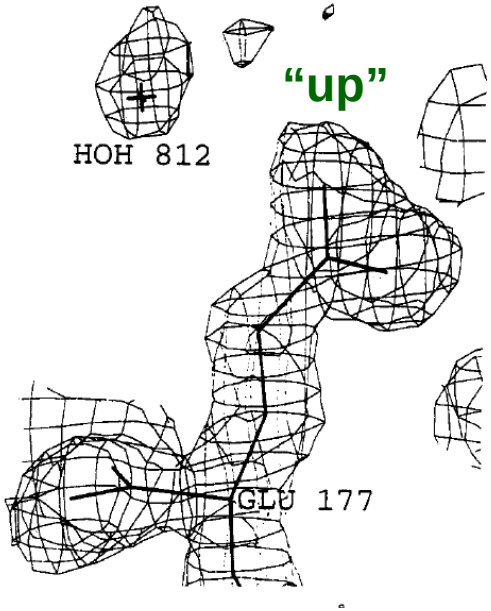

pH = 6.5

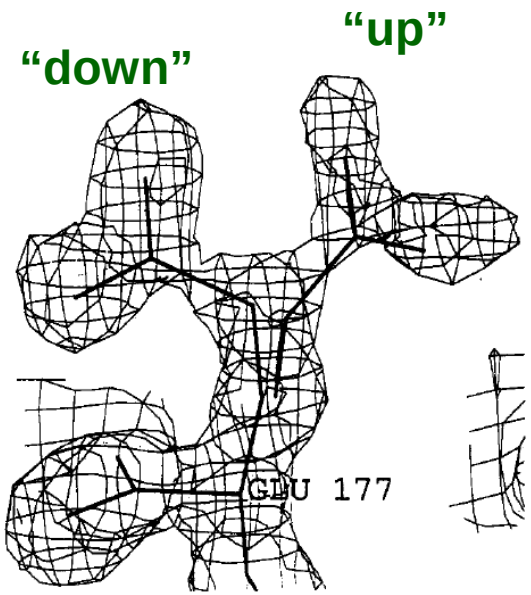

pH = 6.0

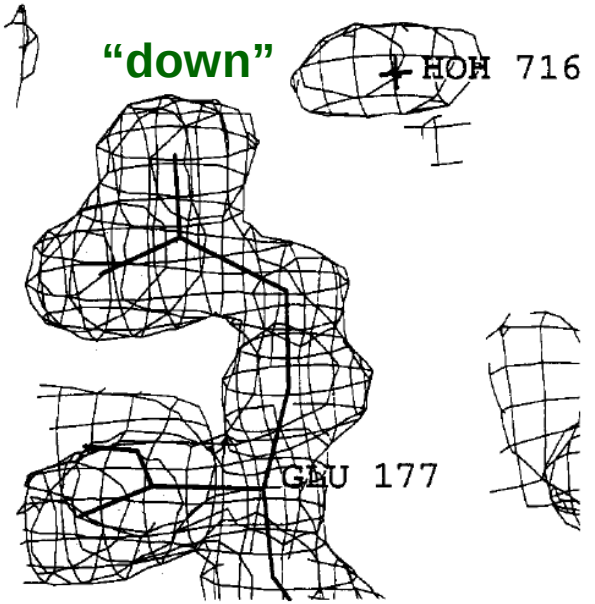

pH = 4.5

Törrönen & Rouvinen, *Biochemistry* 1995, **34**, 847-856

Increase in enzyme activity

XynII at three different pH: higher pH induces ‘low-barrier’ hydrogen bond, whereas low pH

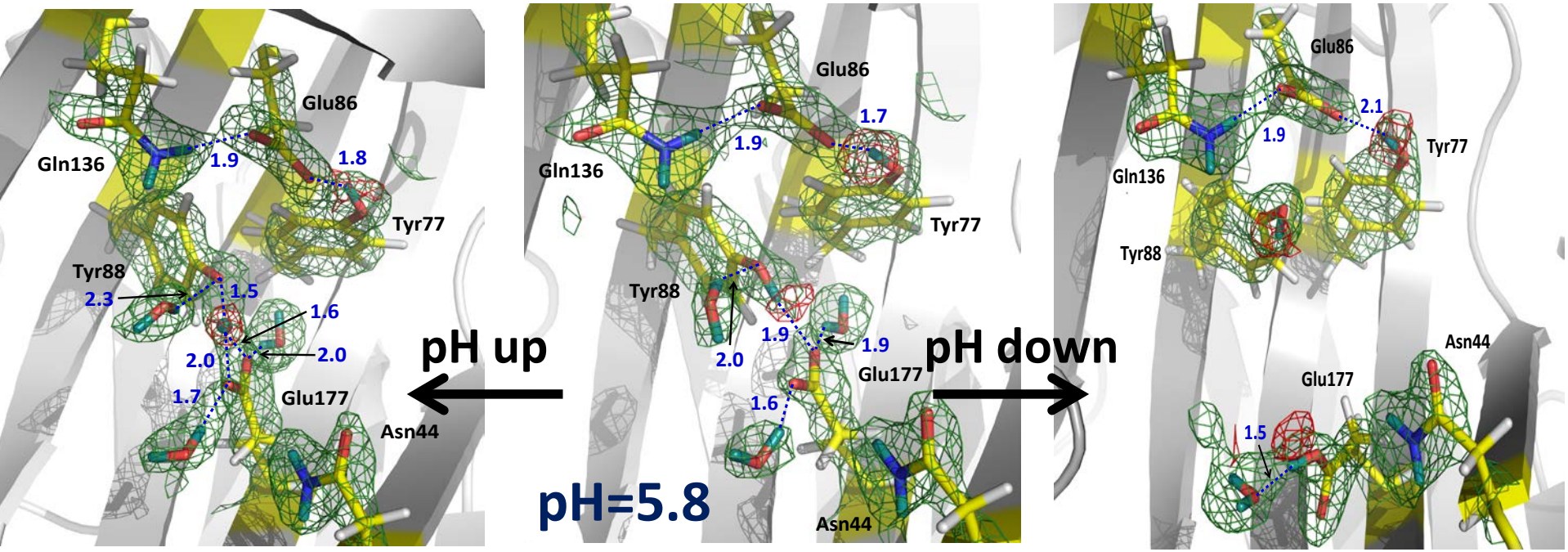

‘LBHB’

Conformational change of Glu177 and its protonation

Q. Wan et al. (2015) *Proc. Natl. Acad. Sci. U.S.A.* **112**, 12384-12389.

Proposed cycling of the general acid between two conformations controlling pK_a and protonation states in GH11 enzymes

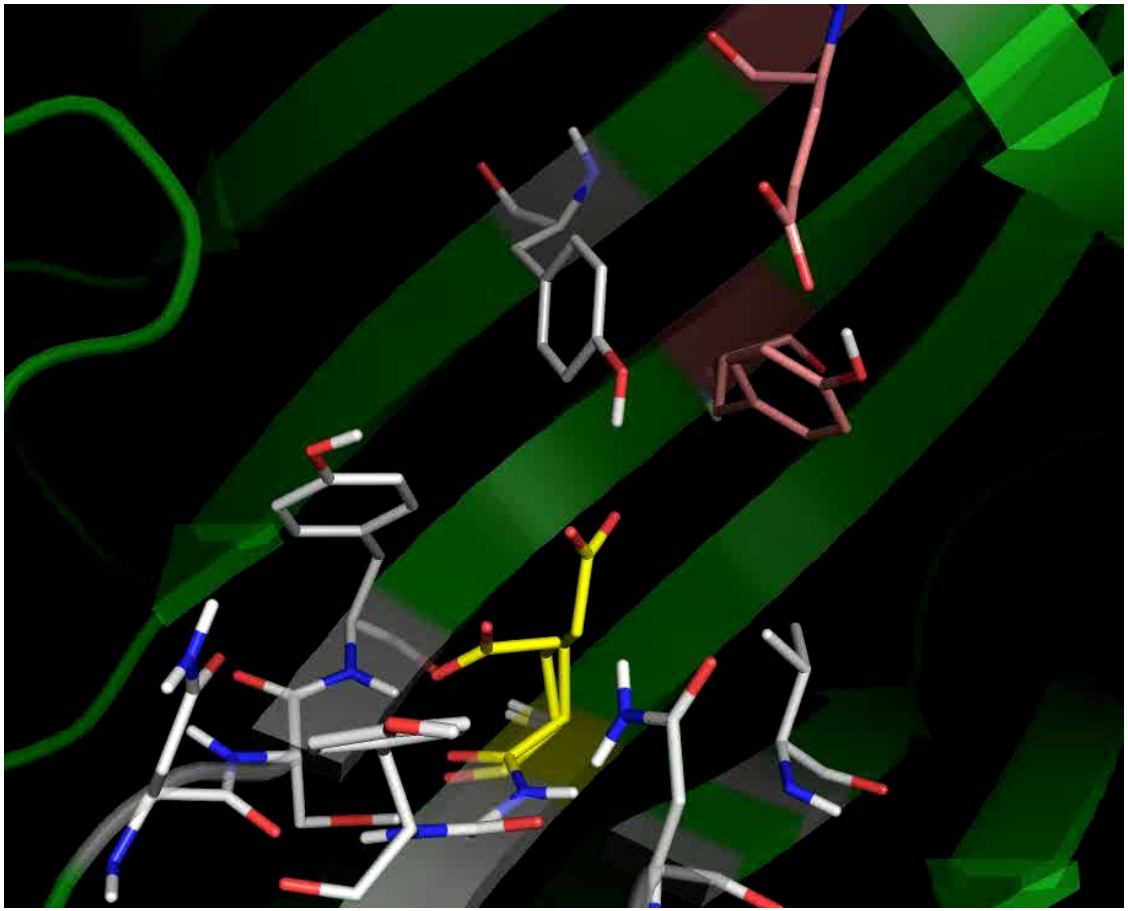

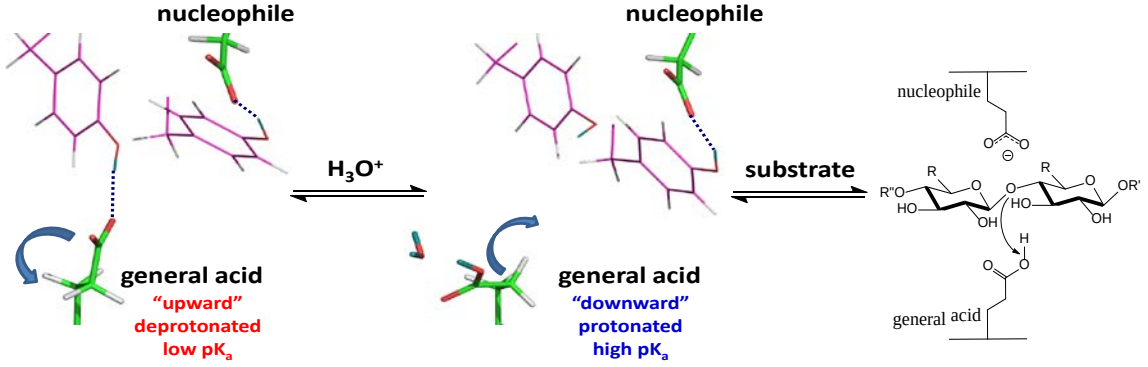

HIV-1 protease (PR)

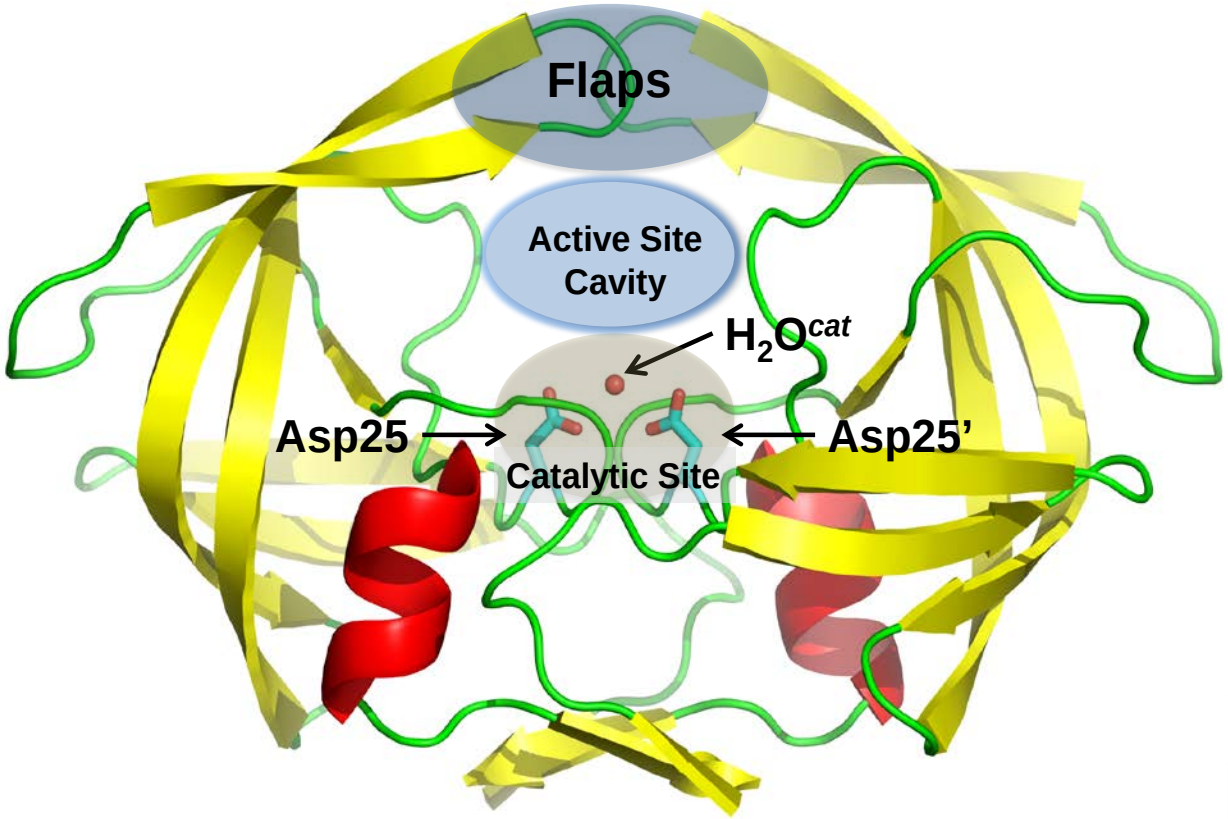

- **99-amino acid homodimeric PR processes Gag and Gag-Pol polyproteins into viral enzymes, structural proteins;**
- **aspartic proteases catalyze hydrolysis of the peptide bond by utilizing two closely co-located aspartic acid (Asp) residues;**
- **catalytic aspartic dyad has to be mono-protonated;**
- **proton transfer events are key in the catalytic mechanism.**

Visualizing H bonding in protease-amprenavir complex

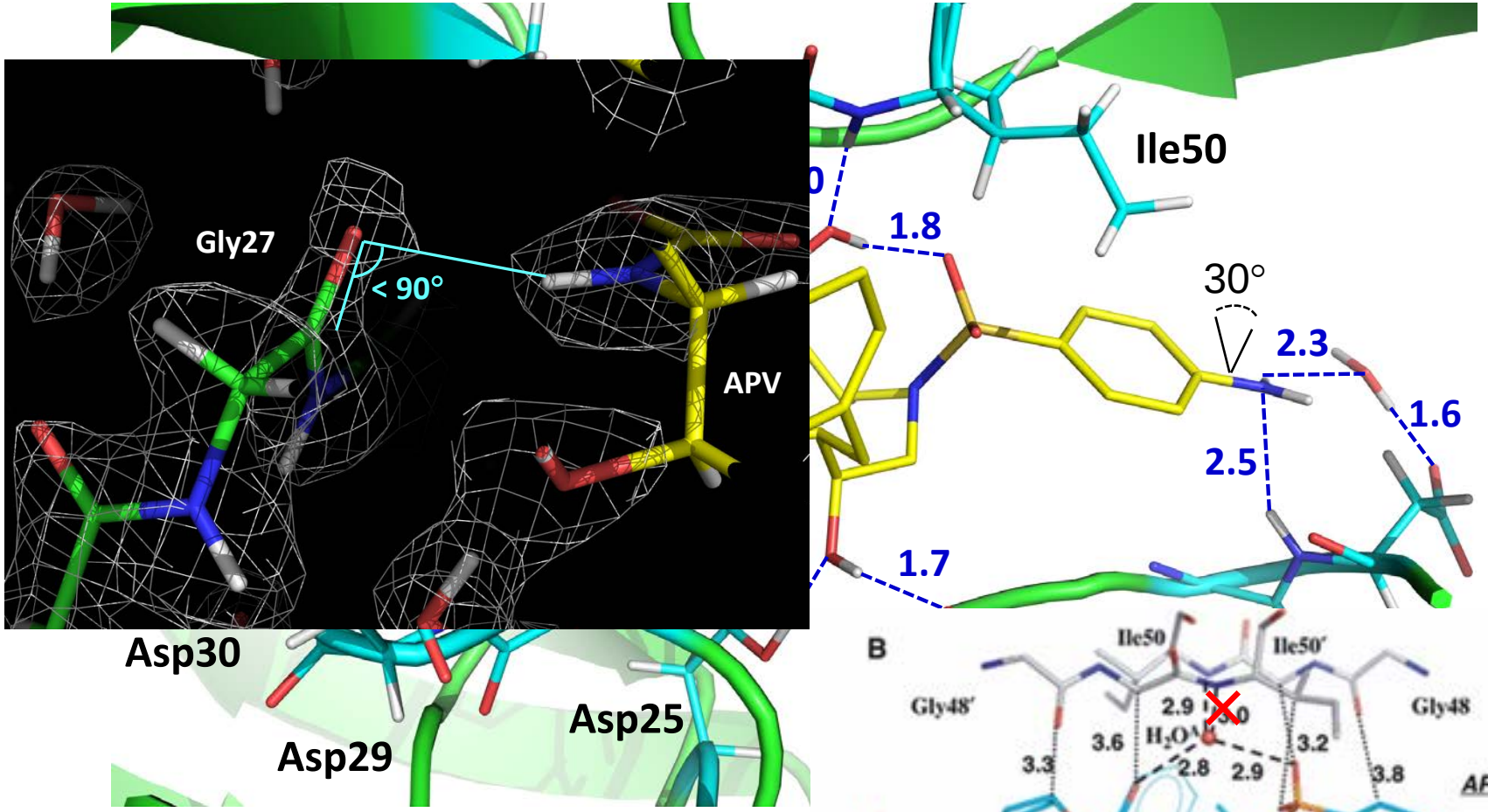

Neutron structure reveals that strong H bonding occurs only between central OH of APV and the catalytic Asp residues!

Shen et al., *FEBS J.* **277**, 3699-3714 (2010)
Weber et al., J. Med. Chem. 56, 5631-5635 (2013)

Accurate positions of protons in the PR catalytic site

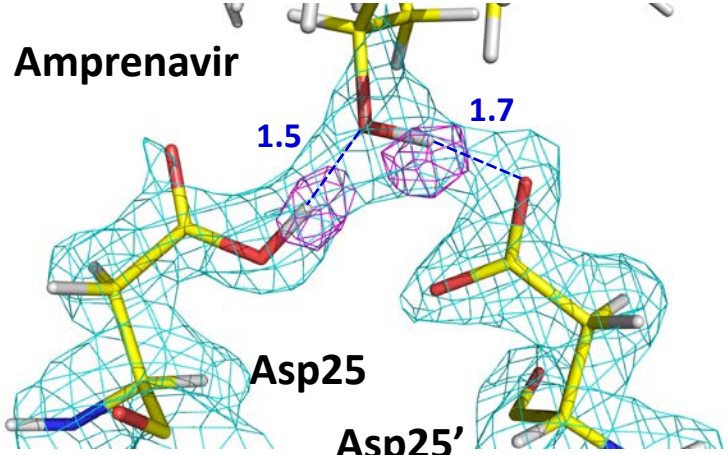

pH=6.0

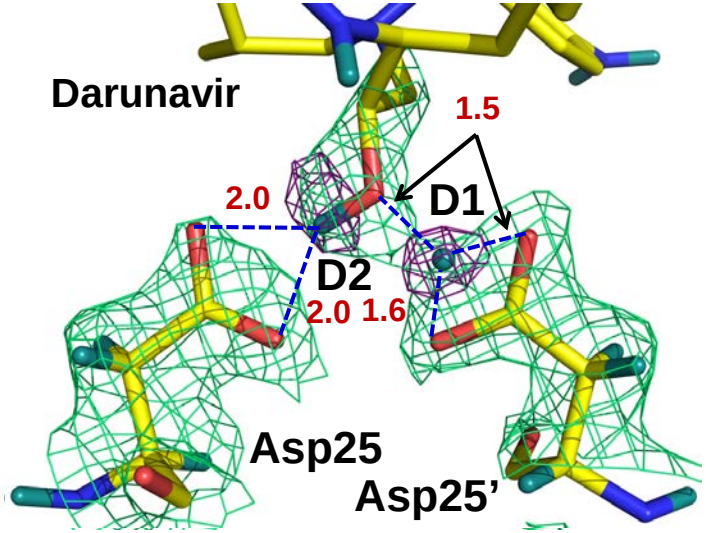

pH=6.0

pH ↓

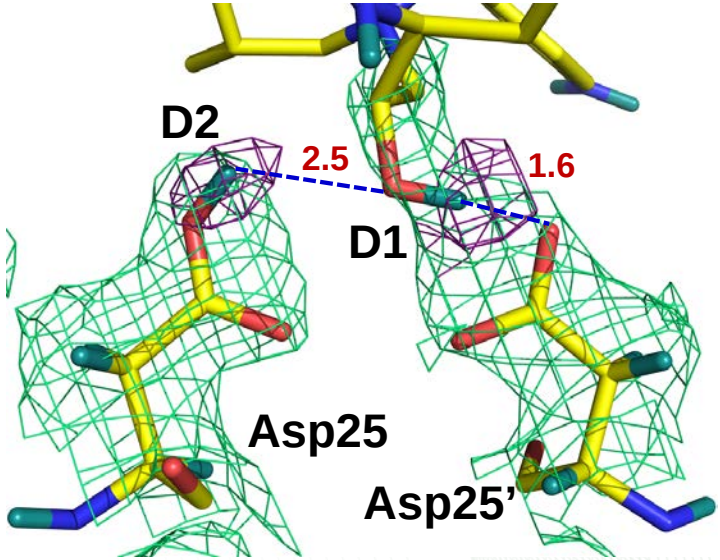

pH=4.3

pH drop in crystal leads to protonation of 4 surface residues

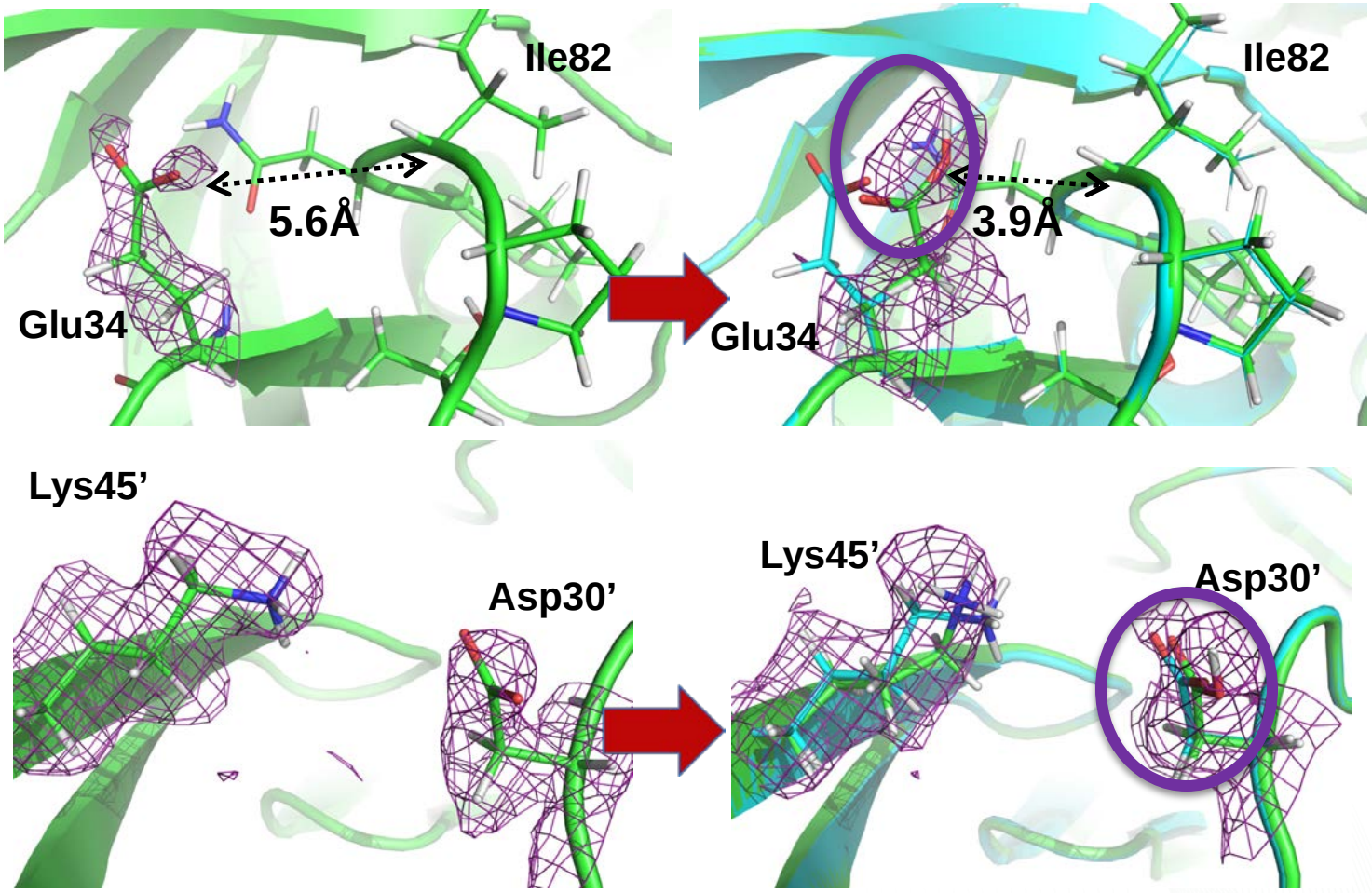

- **Asp30, Asp30', Glu34, Glu34', located 11-14 Å away from the catalytic site, are protonated at lower pH, significantly changing the enzyme charge.**

Long-range electrostatics-induced proton transfer

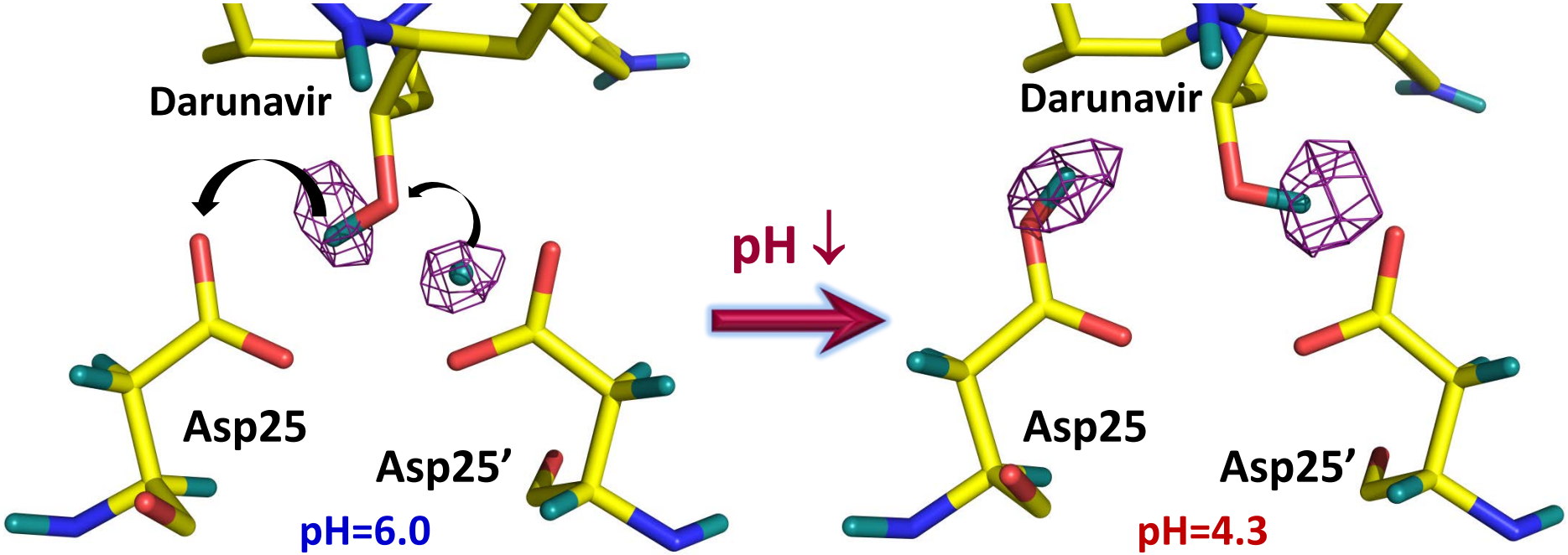

QM/MM calculations

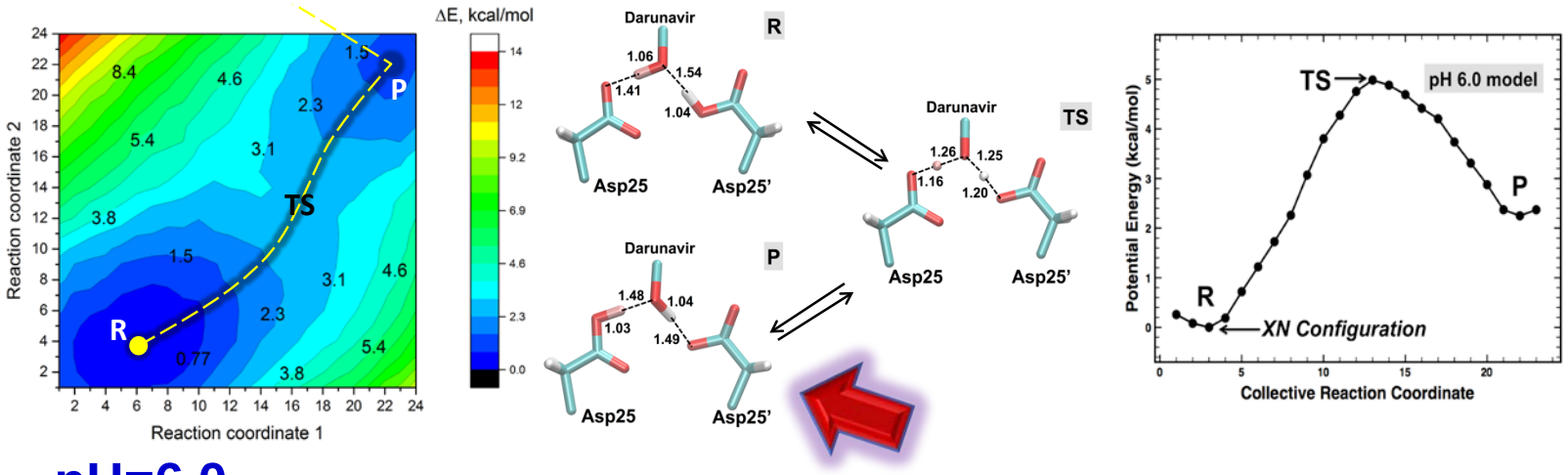

pH=6.0

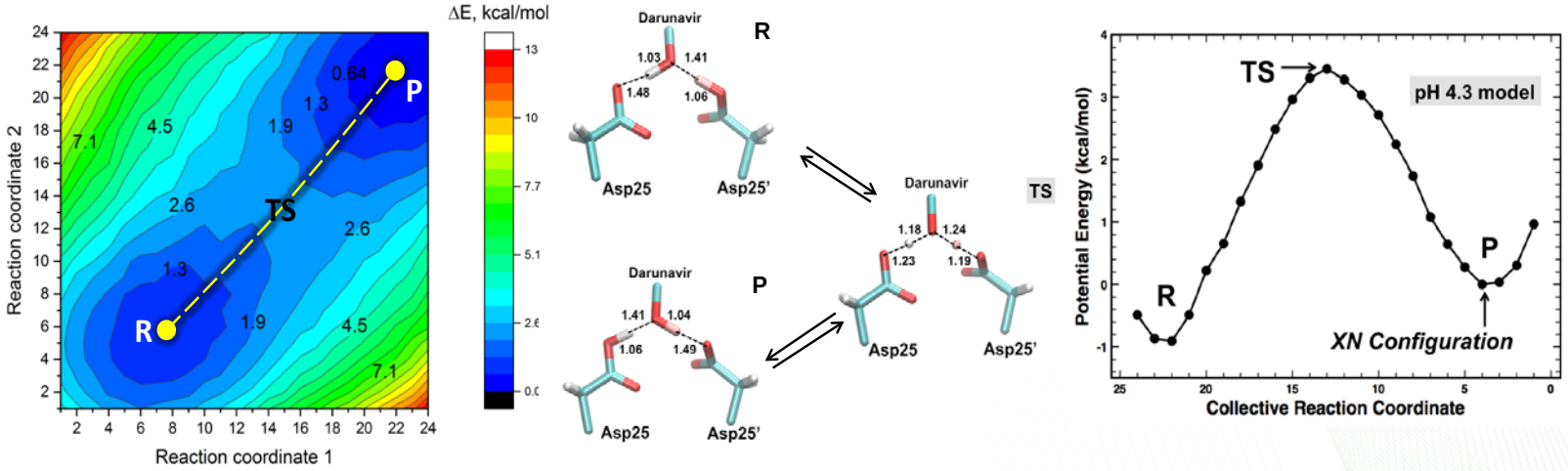

pH=4.3

Neutron crystallography of nucleic acids enabled by Se derivatization

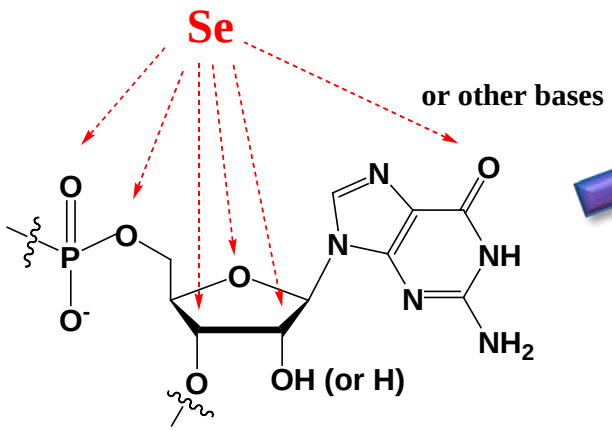

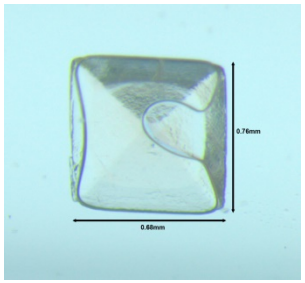

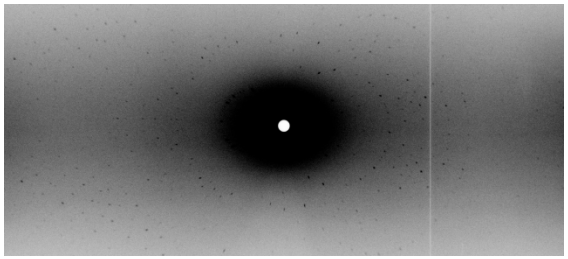

- Derivatization of 2’-group and bases facilitates crystal.

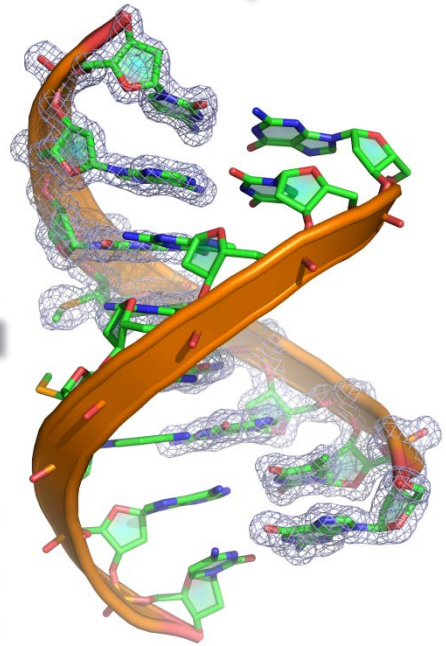

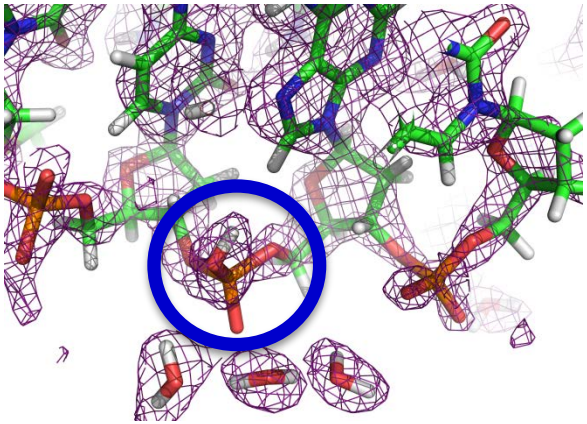

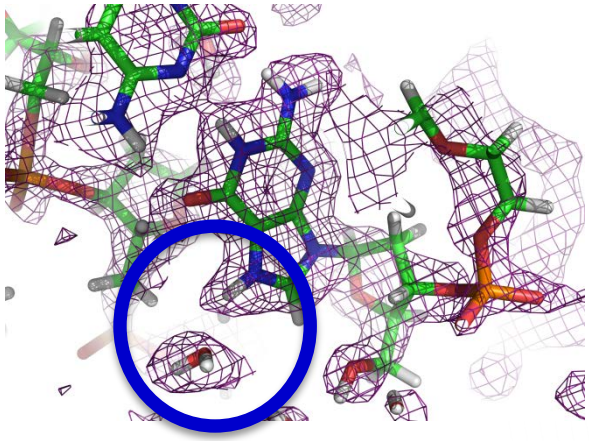

- Neutron structure at 1.9 Å at room temperature from a 0.2 mm^3 crystal.

5’-GTGG(^{Se}C)CAC-3’ @ 1.56 Å room-temp

Acknowledgements

BSMD
Oksana Gerlits
Amit Das
Qun Wan
Kevin Weiss
Leighton Coates

IMAGINE:
Flora Meilleur
Laskeisha Walker

Center for Mol. Biophys.:
Troy Wymore
Jerry Parks
Jeremy Smith

GSU:
Chen-Hsiang (Brian) Shen
Irene Weber

Purdue University:
Arun Ghosh

NIDDK, NIH:
John Louis

LANL:
Mary Jo Waltman
Matt Challacombe
Nick Bock

ESS
S. Zoe Fisher
Lund, Sweden

ILL:
Matthew Blakeley
Trevor Forsyth
Sax Mason

ISIS:
David Keen
Oxfordshire, UK

FRM-II:
Andreas Ostermann
Tobias Schrader
Munich, Germany

Lujan Center
LANSCE
Los Alamos, NM

Funding:

LANL LDRD
ORNL LDRD
DOE-BER
DOE-BES User Program

Small-Angle Neutron Scattering for Biomembranes

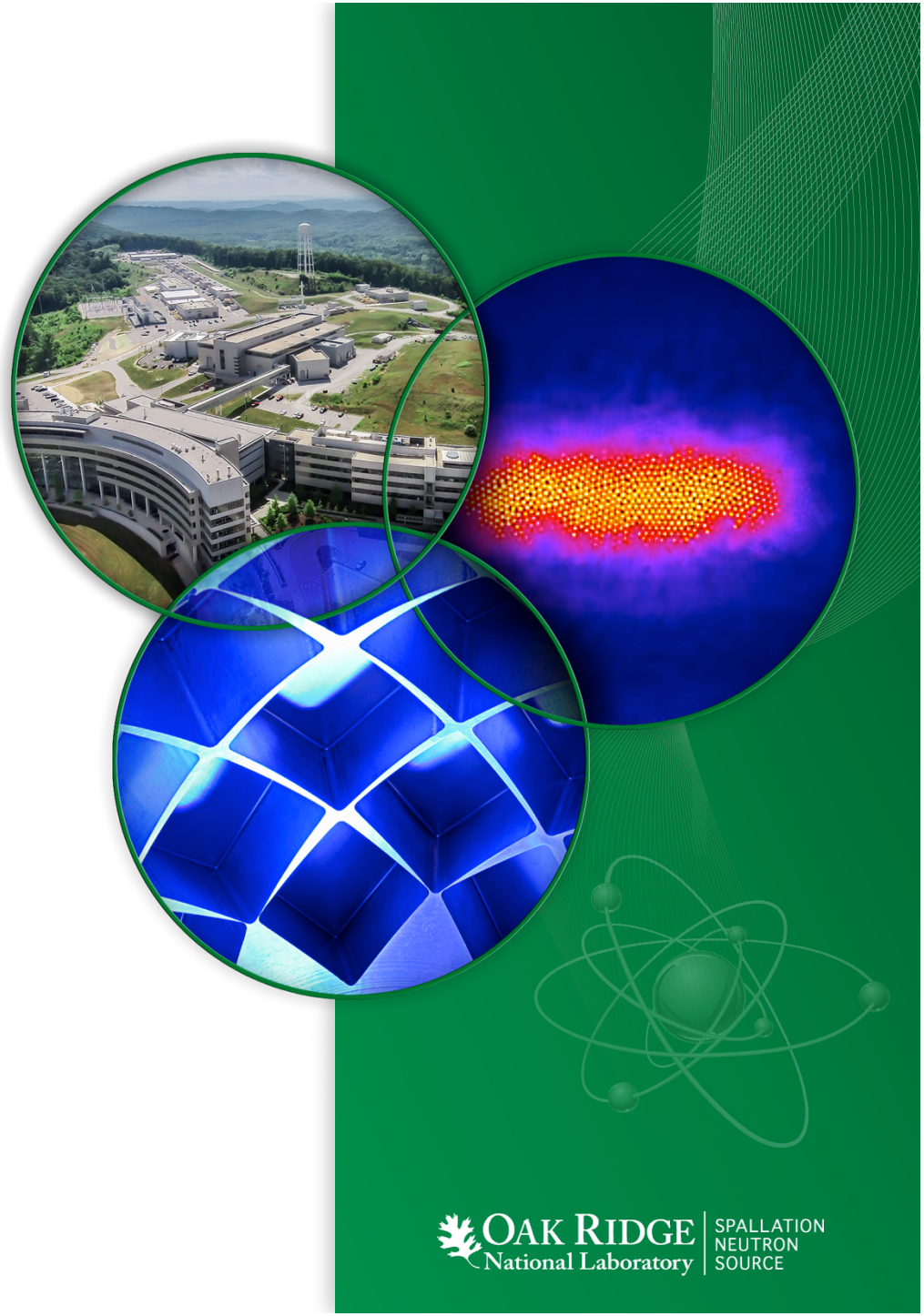

William T. Heller, Ph.D.

EQ-SANS Lead Instrument Scientist
Oak Ridge National Laboratory

ORNL-Georgia Tech Joint Workshop in Neutron Science and Scattering
Georgia Tech
January 27, 2016

ORNL is managed by UT-Battelle
for the US Department of Energy

OAK RIDGE National Laboratory | SPALLATION NEUTRON SOURCE

Small-angle Scattering

- **A structural technique**
  - **Broadly applicable to almost any kind of material**
  - **Broadly applicable to all states of matter**

- Size
- Shape
- Correlations
- Void fraction
- Fractal dimension
- Aggregation behavior

The list goes on...

SAS is a characterization tool for bulk materials that has proven indispensable for the Polymer and Materials Sciences

SAS is also well-suited to studies of biological materials

Small-angle Scattering

- **Small-angle scattering is a diffraction method**

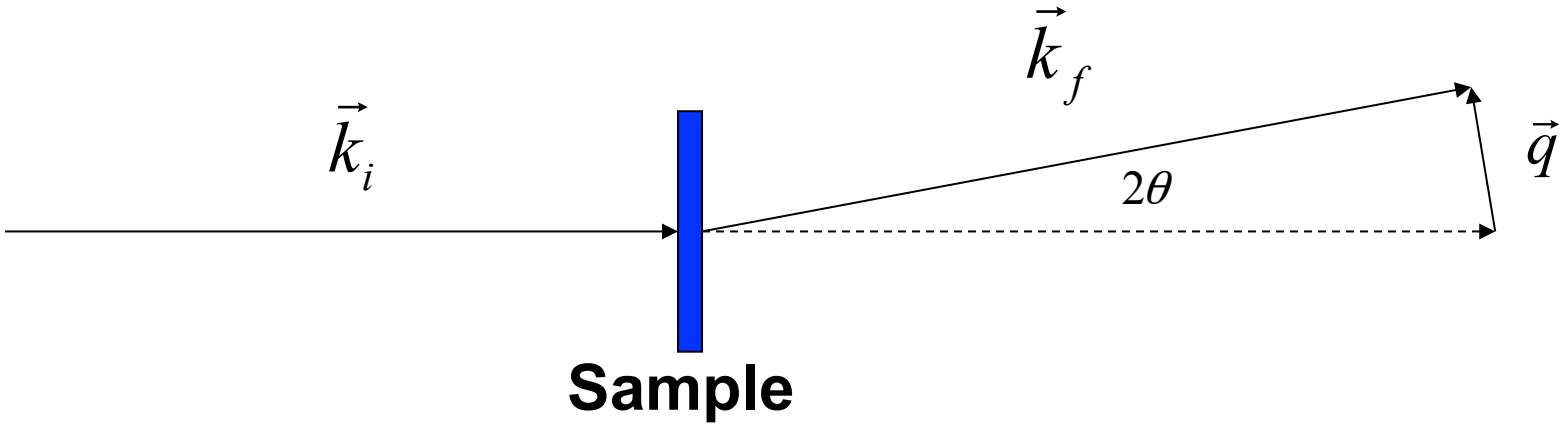

$$\left|\vec{k}_i\right| = \left|\vec{k}_f\right| = 2\pi/\lambda \qquad \left|\vec{q}\right| = (4\pi\sin\theta)/\lambda$$

q **is related to the distance, *d*, probed** $d = 2\pi/q$

SAS Instrumentation

SAS instruments are conceptually simple

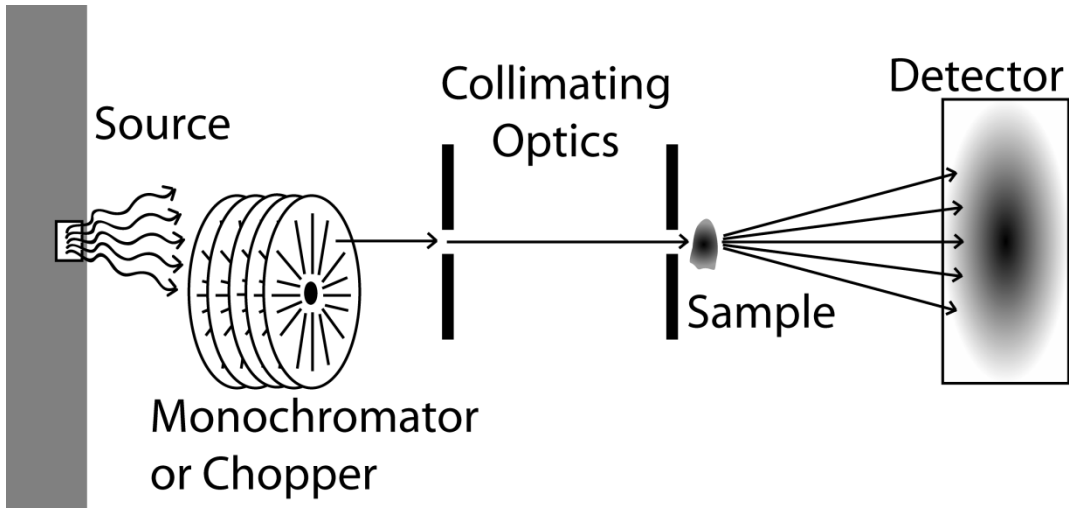

Source: x-ray generator, synchrotron, spallation source or reactor

Monochromator/Chopper: Defines wavelength(s)

Collimating Optics: Defines the angular divergence of the beam

Determines the maximum size probed

Detector: Collects the radiation scattered by the sample

Large detectors provide better angular coverage

Small-angle Scattering

- **When applied to problems in structural biology, SAS provides**

  - Structural information on macromolecular complexes and systems not amenable to other techniques
  - Traditional methods of data interpretation provide structural insight at the molecular (shape) level
  - Does not provide structural information at the same level of detail as crystallography and NMR

Why Neutrons for Biomaterials?

- **Nondestructive (no radiation damage)**
- **Sensitive to hydrogen and deuterium**

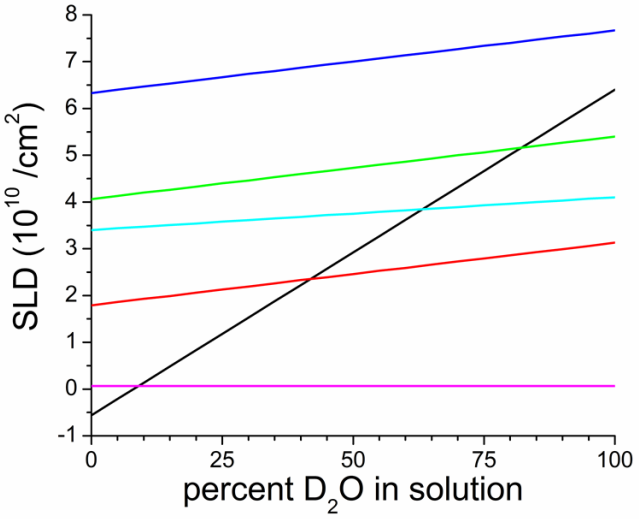

- Water
- Hydrogenated Protein
- 50% Deuterated Protein
- 100% Deuterated Protein
- DNA
- Phospholipid

Selective deuterium labeling makes it possible to highlight features in complex structures

Great for problems from biology!

The Cell Membrane

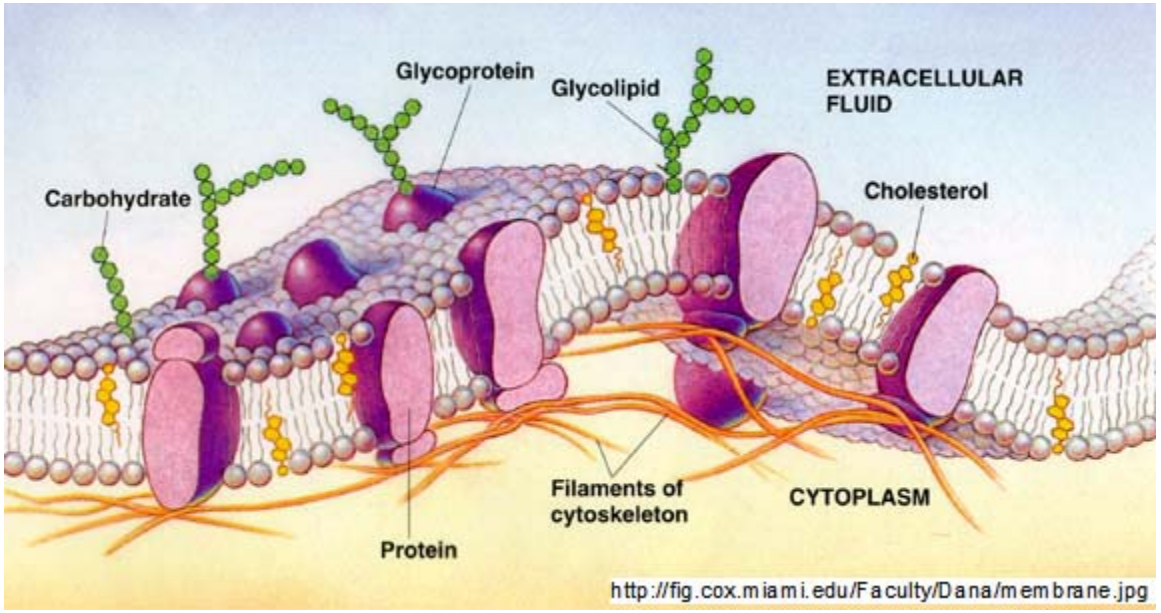

Pulled from www.colorado.edu via google.com

The membrane is a heterogeneous mixture of lipids, proteins and other molecules that spans the molecular and mesoscopic length scales

Structure and function derive from the interactions between the constituents of its tightly-regulated composition

The Cell Membrane

The structure of the assembly is driven by a competition between the various energy costs including electrostatic and hydrophobic Interactions

Hydrophobic interactions play a large role in determining the structure of the membrane and the functional structures within it

- **Between the various components and water**
- **Between the various components within the membrane**

Light Harvesting Complex II

The structure of the LHC-II in complex with the detergent was studied by SANS

LHC-II with detergent 'contrast matched'

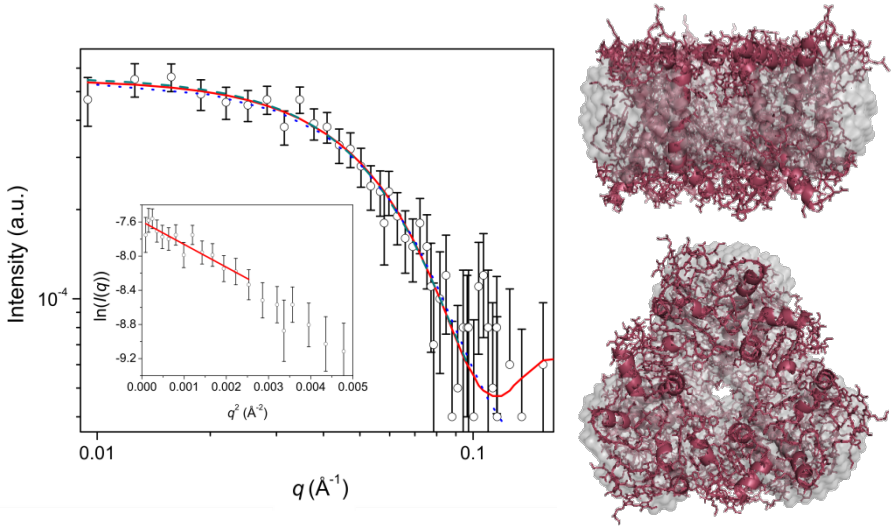

LHC-II with detergent in 100% D_2O

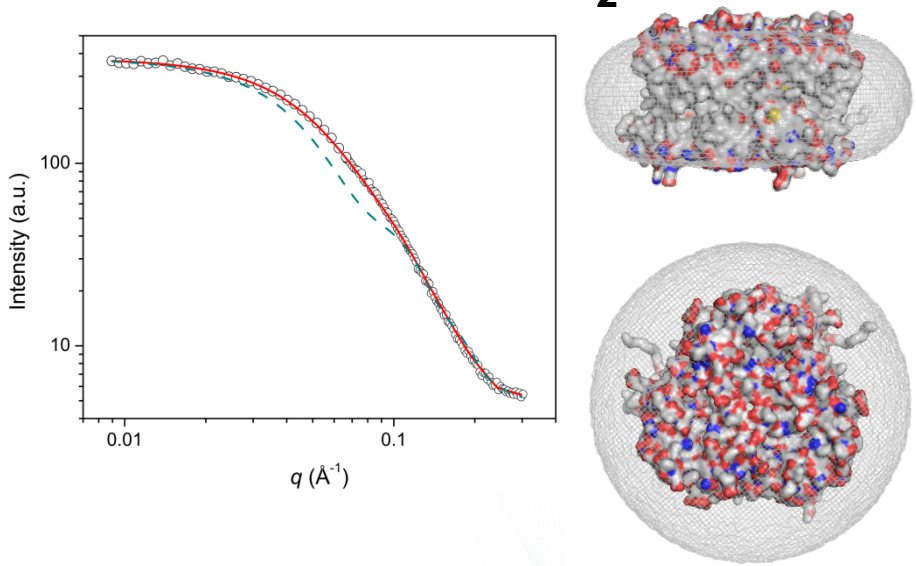

The detergent solubilized LHC-II retains its native structure with an irregular detergent 'belt'

Cardoso, M.B., et al (2009) *J. Phys. Chem. B* **113**: 16377

Bacterial Photosystem-I

The structure of the trimeric PS-I from T. elongatus also retains its native structure in detergent solution

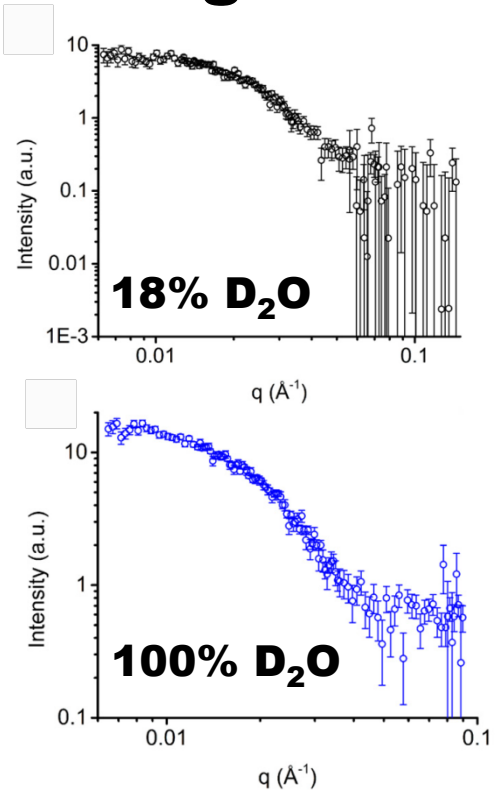

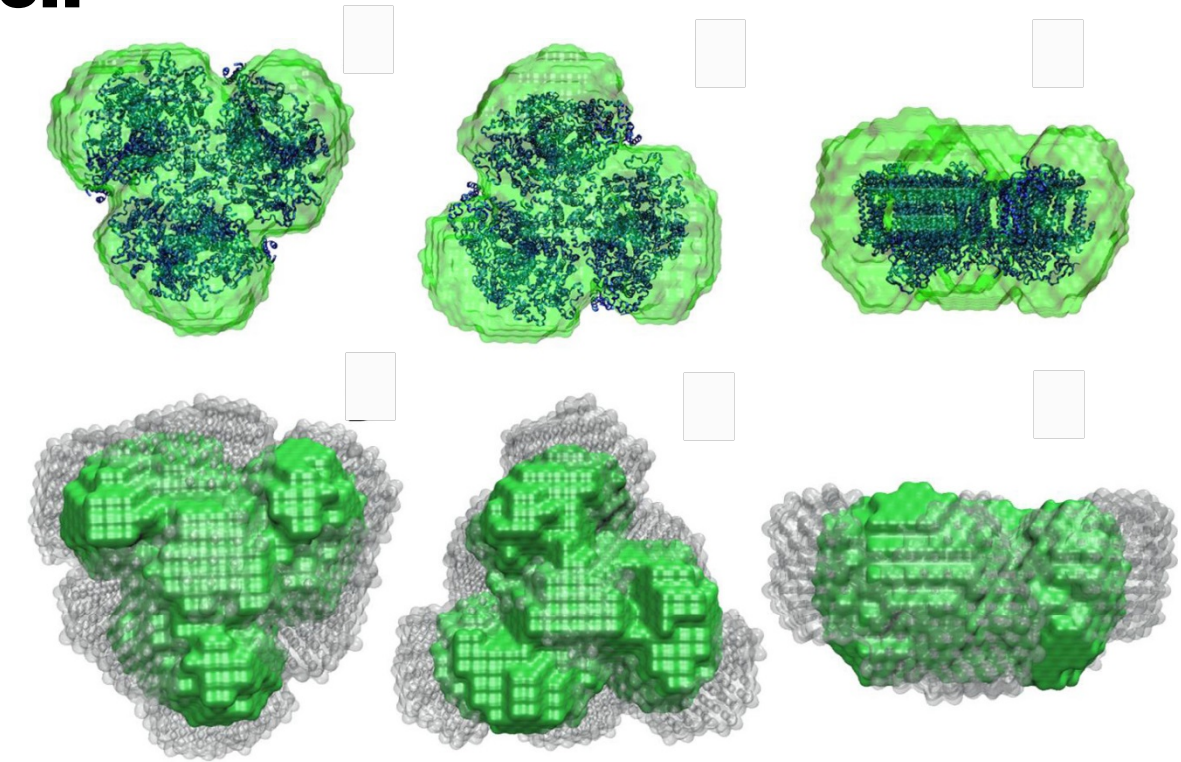

Again, there is an irregular detergent 'belt'

Le, R. K., et al (2014) *Arch. Biochem. Biophys.* **550-551**: 50

Sindbis Virus

Compared mammalian- and insect-grown virions

- **Still infectious after measurements!**

Sindbis – Arthropod borne virus

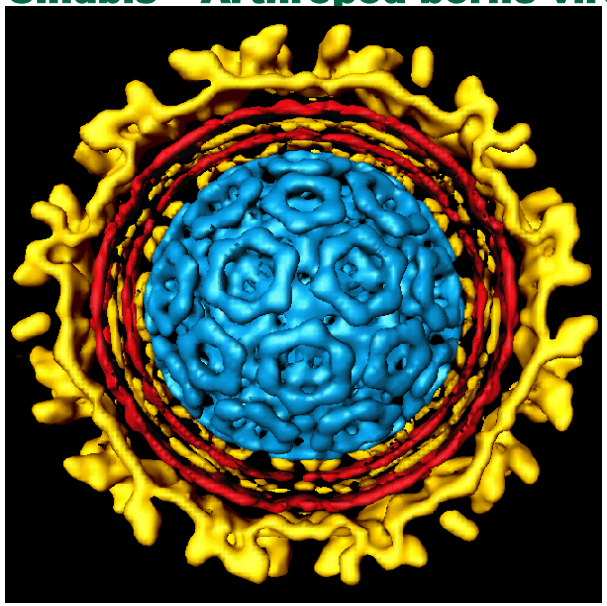

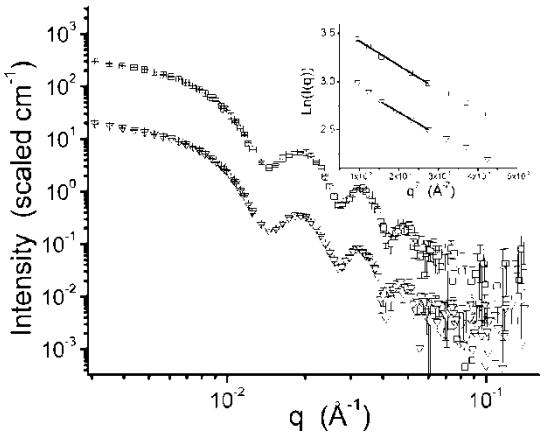

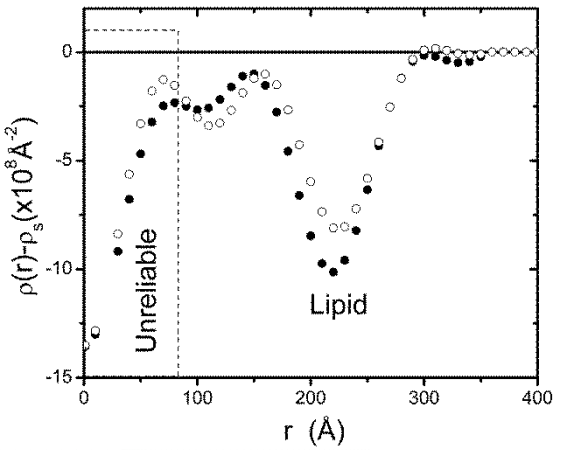

Paredes A.M. et al. ***Virology*** *(2004),324,373*

The lipid layer of the mammalian virus has a lower scattering length density than the insect form - cholesterol

He, L. L., et al. *J. Virology* **84**: 5270-5276 (2010)

Membrane Biophysics

A real membrane is a complex mixture, which makes it difficult to study the physics that govern how composition gives rise to structure

Membrane proteins are difficult to work with and obtain in quantities well-suited to neutron scattering

- **Use simplified model systems**

Membrane Biophysics

Synthetic lipids afford chemical uniformity and specific deuterium labeling

- **Phospholipids**
- **Cholesterol**

Membrane-active peptides (MAPs) interact with the lipid bilayer rather than a protein target

- **Antimicrobial peptides (e.g. magainin)**
- **Venom peptides (e.g. melittin)**

Membrane Biophysics

MAPs, such as alamethicin and melittin first make contact with a cell at the membrane surface

Alamethicin

- 20 amino acids
- Single negative charge at neutral pH
- Forms barrel-stave pores

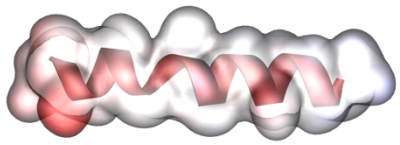

Melittin

- 26 amino acids
- Five positive charges at neutral pH
- Forms toroidal pores

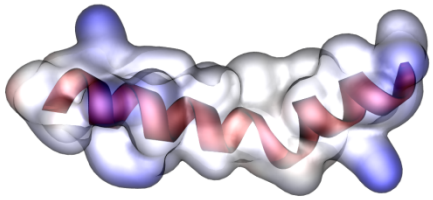

Does a MAP change the organization of specific lipids in a mixed-composition membrane?

Headgroup-Specific Interactions

Charged lipids are vital components of cell membranes

Do MAPs alter how charged lipids are distributed in PC/PG lipid bilayer vesicles?

- **Chain-perdeuterated DMPC and DMPG**
  - **Remove sensitivity to chain composition**
  - **Provide sensitivity to what is where**

Qian, S. and Heller, W. T. *J. Phys. Chem. B* **115**: 9831-9837 (2011)

Headgroup-Specific Interactions

Alamethicin

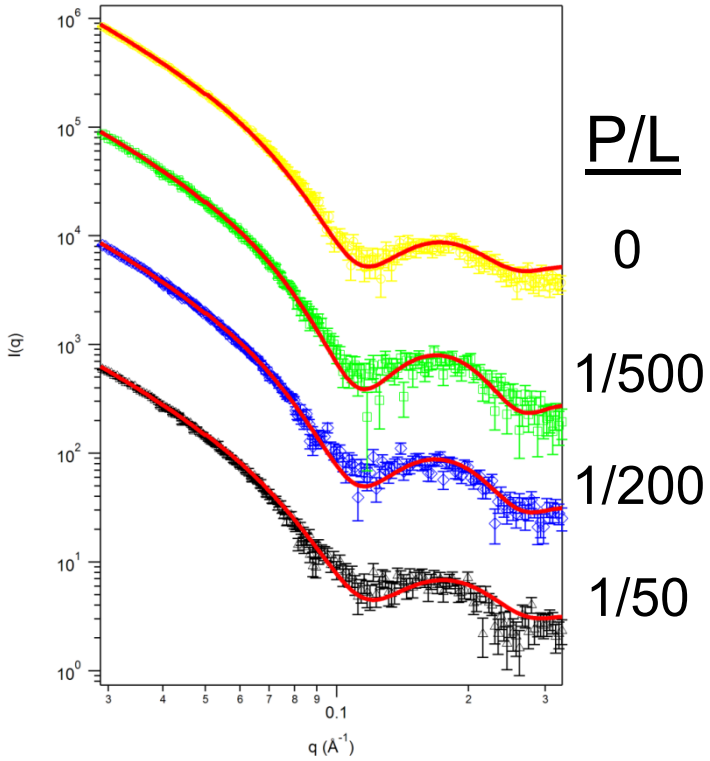

P/L

0

1/500

1/200

1/50

Melittin

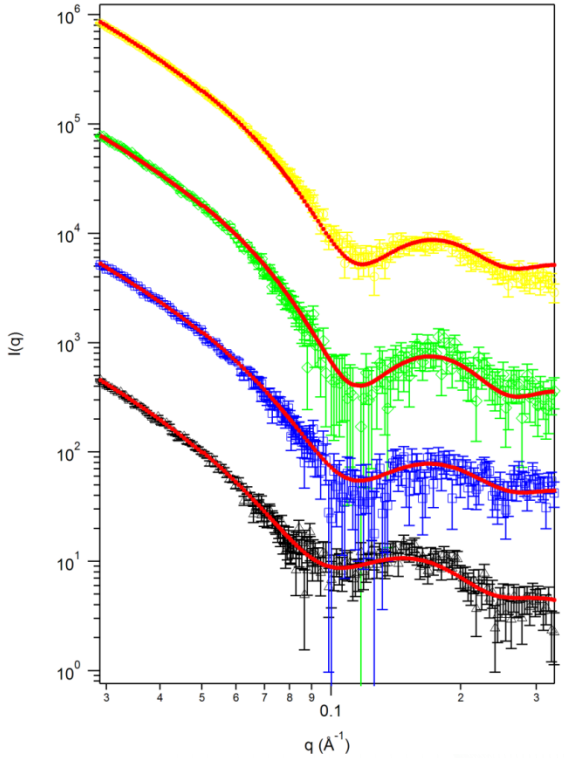

P/L

0

1/1000

1/500

1/200

The red curves are fits to the data using a sample 4-shell spherical vesicle model

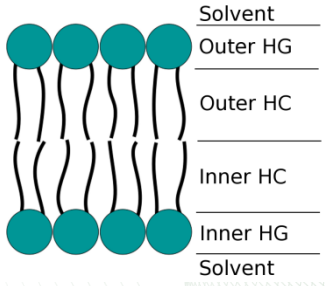

Qian, S. and Heller, W. T. *J. Phys. Chem. B* **115**: 9831-9837 (2011)

Headgroup-Specific Interactions

Alamethicin and Melittin impact the bilayer thickness differently

P/L		Lipid only	Ala 1/500	Ala 1/200	Ala 1/50	Mel 1/1000	Mel 1/500	Mel 1/200
Inner leaflet	Head group(Å)	8.10	8.10	8.0	7.84	8.10	8.10	8.20
	Chain(Å)	14.20	14.10	14.08	13.60	14.20	14.10	15.90
Outer leaflet	Chain(Å)	14.20	14.10	14.10	13.50	14.20	13.90	16.00
	Head group(Å)	8.10	8.15	8.00	7.86	8.10	8.10	8.30
Total Shell Thickness (Å)		**44.60**	**44.45**	**44.18**	**42.80**	**44.60**	**44.20**	**48.40**

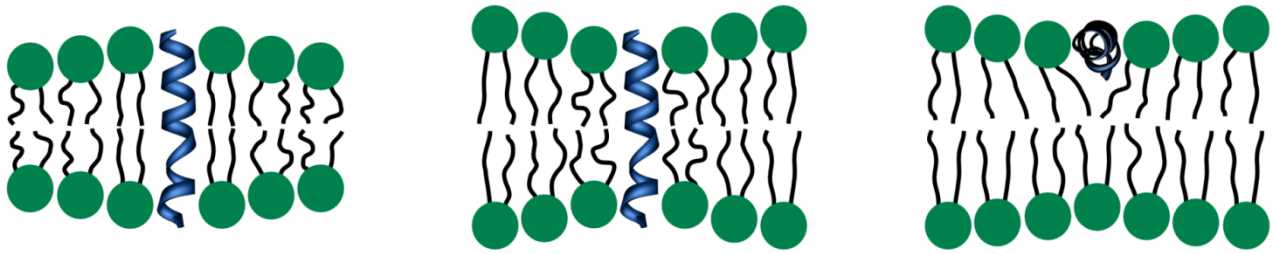

Hydrophobic matching schematic of the alamethicin crystal structure in bilayers of various thicknesses
PDB ID: 1AMT; Fox and Richards (1982) *Nature* **300**, 325-330.

Qian, S. and Heller, W. T. *J. Phys. Chem. B* **115**: 9831-9837 (2011)

Headgroup-Specific Interactions

Model the distribution of what is in each of the 4 layers of the model as well as the thicknesses of the layers

	P/L	Peptide insertion ratio (%)	DMPC in the inner leaflet (%)
Lipid only	0	0	76 ± 2
Alamethicin	1/500	0	78 ± 2
	1/200	50 ± 10	79 ± 2
	1/50	90 ± 10	85 ± 2
Melittin	1/1000	0	75 ± 2
	1/500	35 ± 15	79 ± 2
	1/200	60 ± 15	89 ± 2

A combination of electrostatics and peptide-induced curvature effects

Qian, S. and Heller, W. T. *J. Phys. Chem. B* **115**: 9831-9837 (2011)

Acknowledgements

A portion of this research was sponsored by the Laboratory Directed Research and Development Program of Oak Ridge National Laboratory, managed by UT-Battelle, LLC, for the U. S. Department of Energy. Research at ORNL's Center for Structural Molecular Biology (FWP ERKP291) was supported by the U.S. Department of Energy's Office of Biological and Environmental Research. Research at Oak Ridge National Laboratory's High Flux Isotope Reactor and Spallation Neutron Source was sponsored by the Scientific User Facilities Division, Office of Basic Energy Sciences, U. S. Department of Energy.

Polymer and Surfactant Self-Assemblies

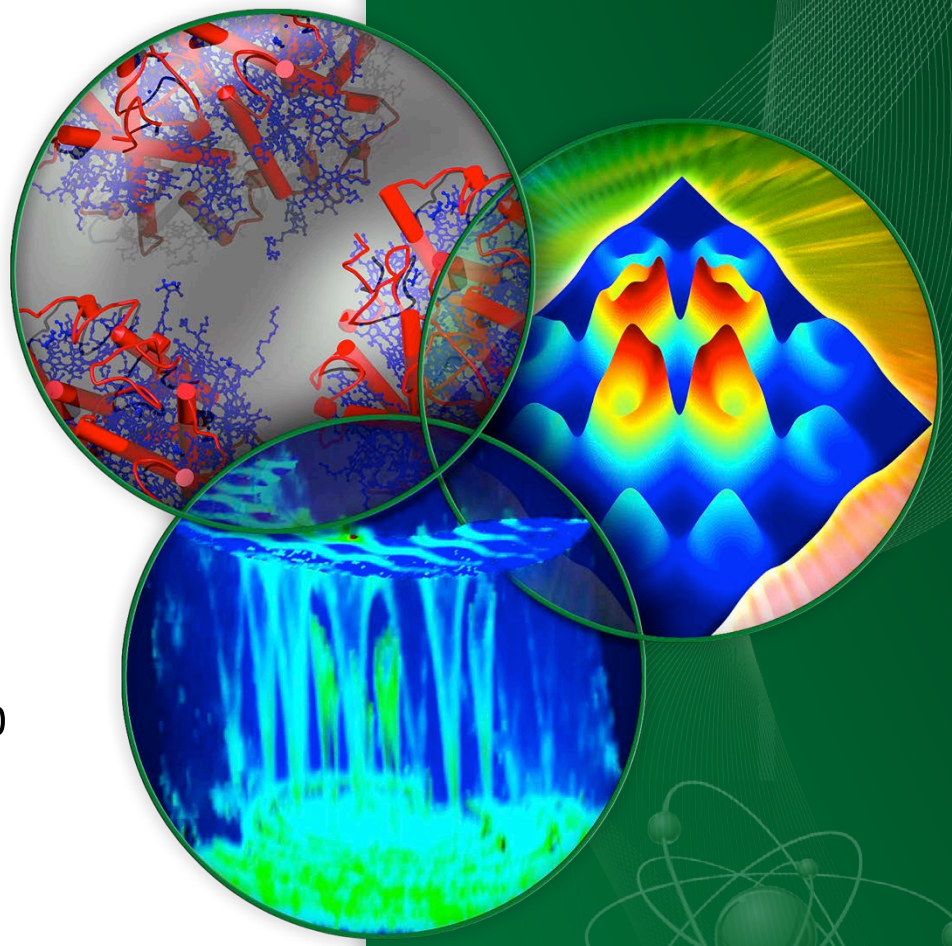

Changwoo Do

EQ-SANS Instrument Scientist
Structure and Dynamics of Soft Matter Group
Biology and Soft Matter Division
Oak Ridge National Laboratory

ORNL-Georgia Tech Joint Workshop in Neutron Science and Scattering
January 27, 2016

Nanofabrication via Self-Assembly

Self-Assembly: Spontaneous organization of molecular units into ordered structures

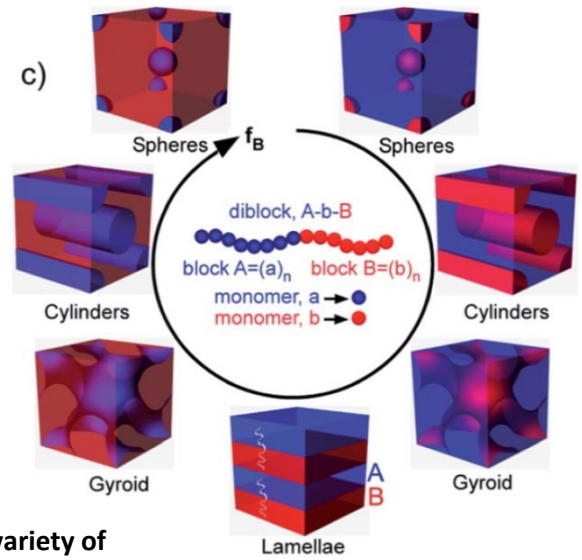

A variety of self-assembled architectures using block copolymers

H. Hu *et al*., *Soft Matter* **10** (2014) 3867

Hierarchical self-assembly

Powerful and effective way to create functional nanostructured materials with various architectures

Sensitive to environmental variations : stimuli-responsive & tunable architecture ("smart")

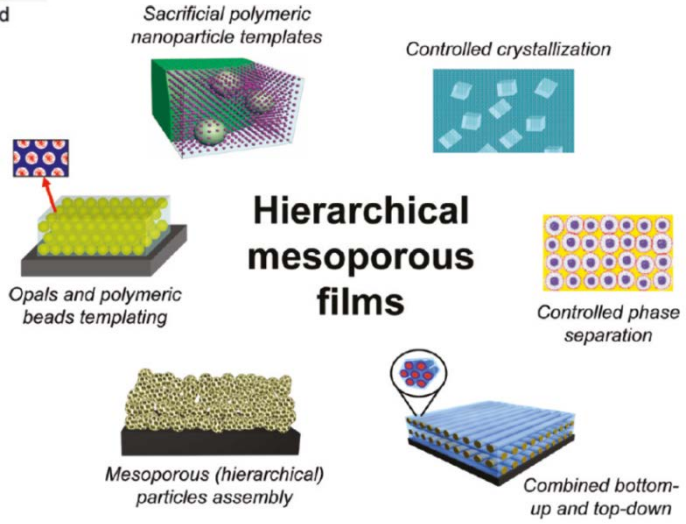

P. Innocenzi *et al*., *Chem. Mater.* **23** (2011) 2501-2509

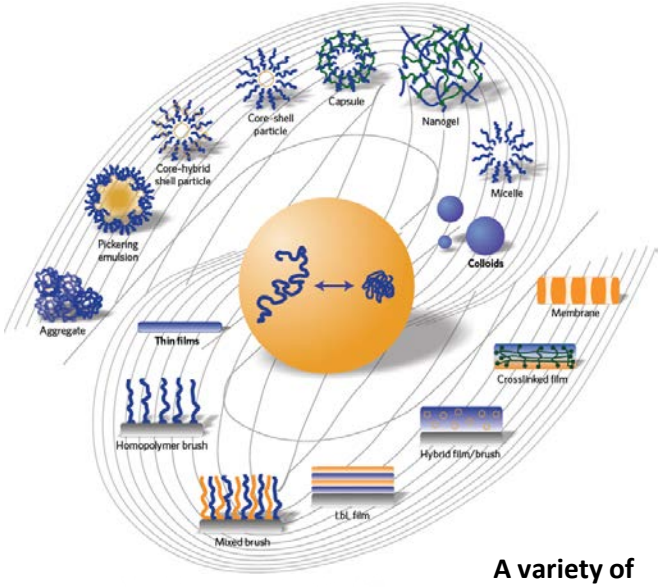

A variety of nanostructured polymer materials : Thin films and nanoparticles

M. Stuart *et al*., *Nature Materials* **9** (2010) 101-113

Recent Research at EQ-SANS

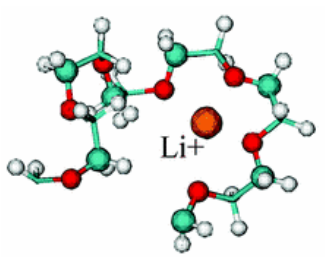

Understanding Li-batteries
Phys. Rev. Lett. **2013**, 111, 018301

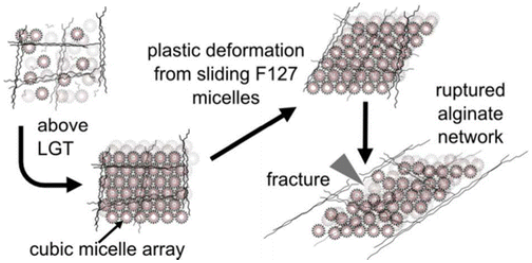

PEO-PPO-PEO Composite Hydrogel
Biomacromolecules. **2013**, 14, 4456

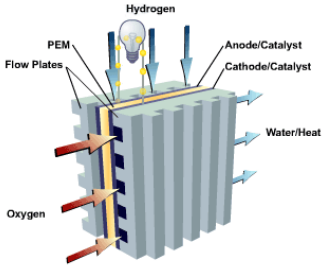

Proton Exchange Membranes
Polym. Eng. Sci. **2014**, 54, 2215

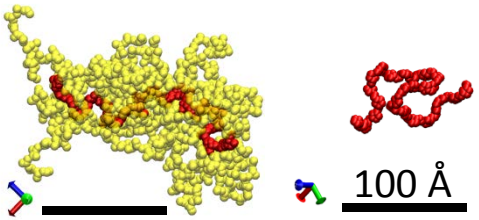

Self-assembled morphology
Macromolecules. **2014**, 47, 5808

Capabilities/performance

- $0.002 < Q < 1.4$ Å^{-1}
- **Largest dynamic Q-range for a SANS instrument at ORNL**
- **Measurement times as short as minutes for strongly scattering samples**

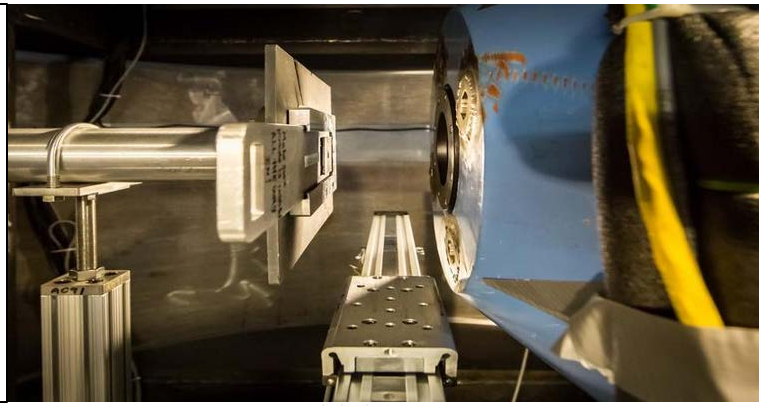

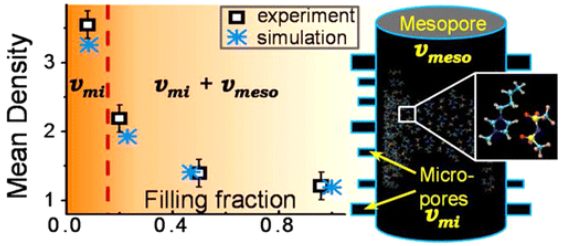

Ionic liquid in a hierarchical structure
Chem. Mater. **2014**, 26, 1144

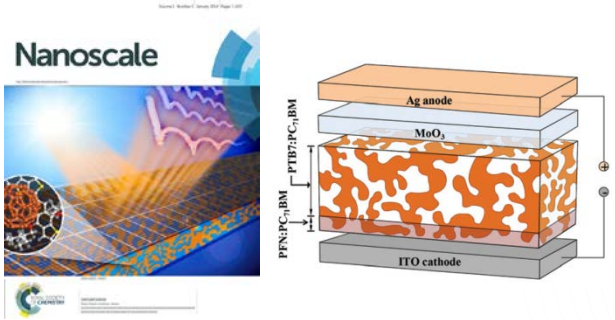

Structure-Power Conversion Efficiency
Nanoscale, **2015**, DOI: 10.1039/c5nr03332b

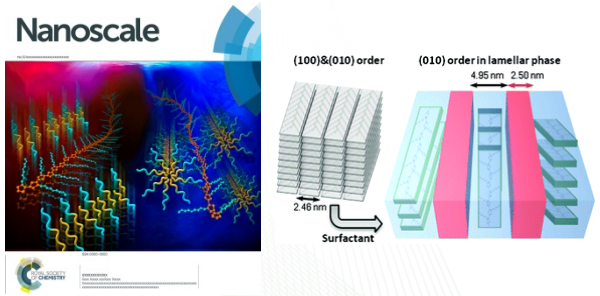

Molecular self-assembly of conjugate polymer with surfactant
Nanoscale, **2015**, Advance Article

Examples of SANS Study

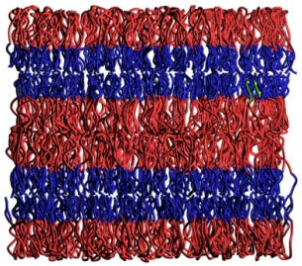

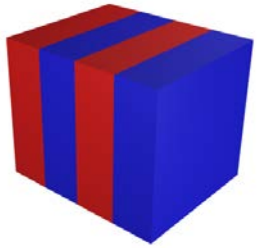

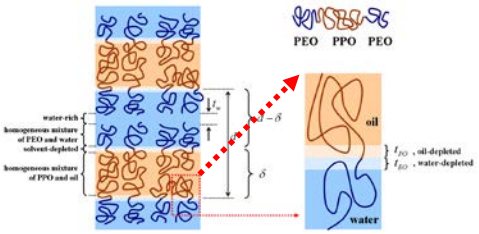

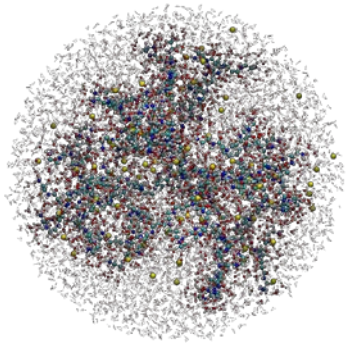

Research Examples

- **Sub-domain structure**
- **Water distribution**
- **Nano-building block**
- **Surfactant aggregates**

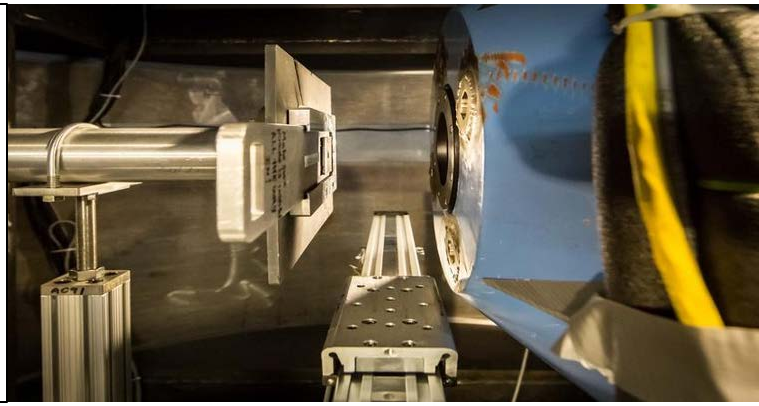

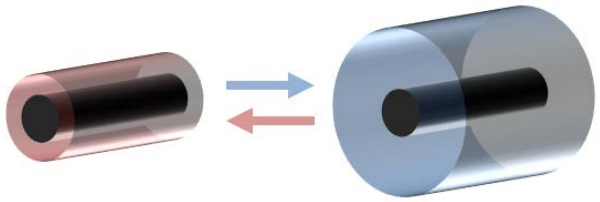

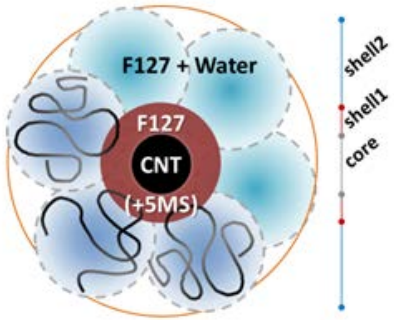

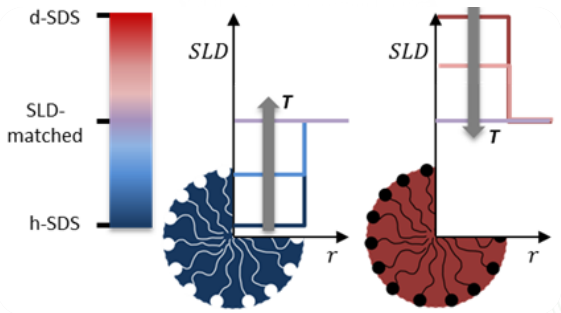

Subdomain Structures of Ternary System

P84: $EO_{19}PO_{43}EO_{19}$
+
water
+
oil (*p*-xylene)

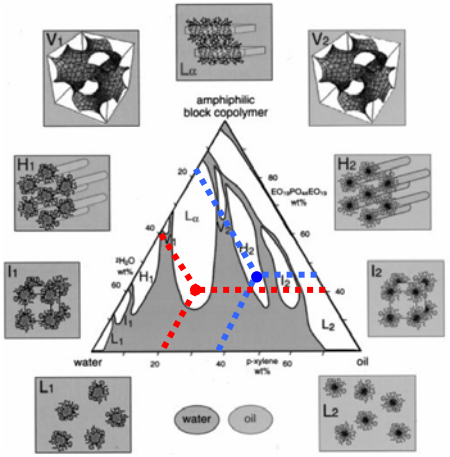

Alexandridis *et al.* Langmuir **14**, 2627 (1998)

They form various ordered phases. For examples, lamellar and reverse hexagolal phase.

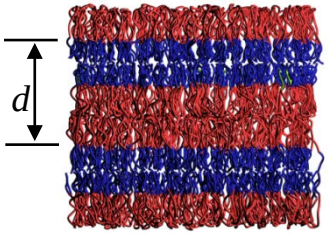

polar domain: PEO + water

apolar domain: PPO + oil

neutron sees

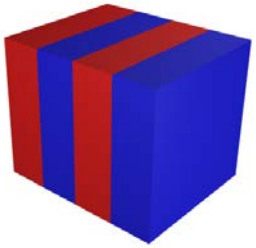

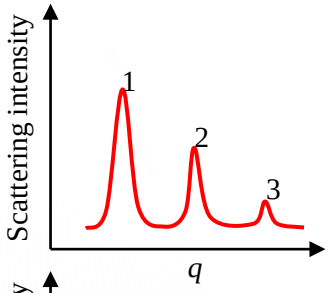

If the SLD of water is varied such that the average SLD of polar domain matches the average SLD of apolar domain,

neutron sees

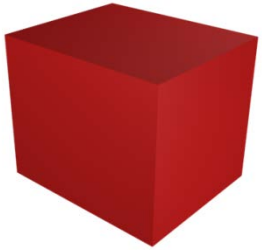

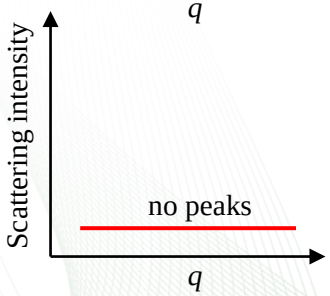

Subdomain Structures of Ternary System

- Isotope subsitution: Various mixtures of H2O:D2O for water

Neutron

P84/water/oil = 40/40/20 in mass

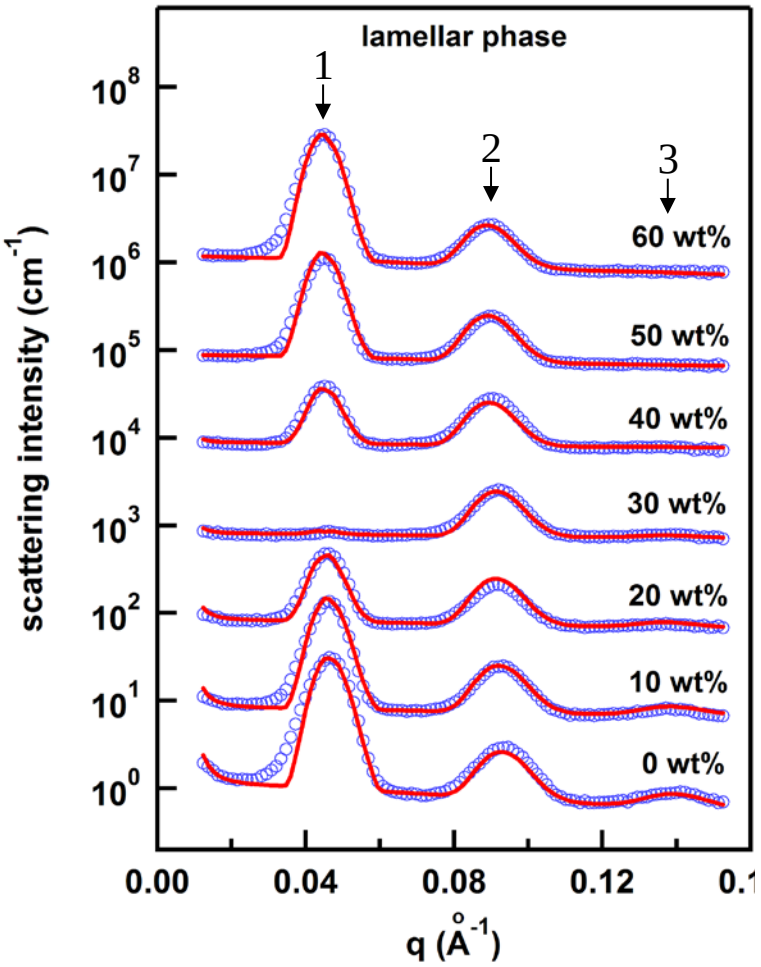

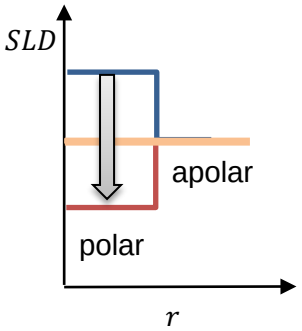

lamellar phase			
H_2O wt %	ρ_w	$\bar{\rho}_{polar}$	$\bar{\rho}_{apolar}$
0	6.33	4.63	3.00
10	5.58	4.11	3.00
20	4.84	3.59	3.00
30	4.12	3.09	3.00
40	3.41	2.59	3.00
50	2.72	2.10	3.00
60	2.03	1.62	3.00

X-ray

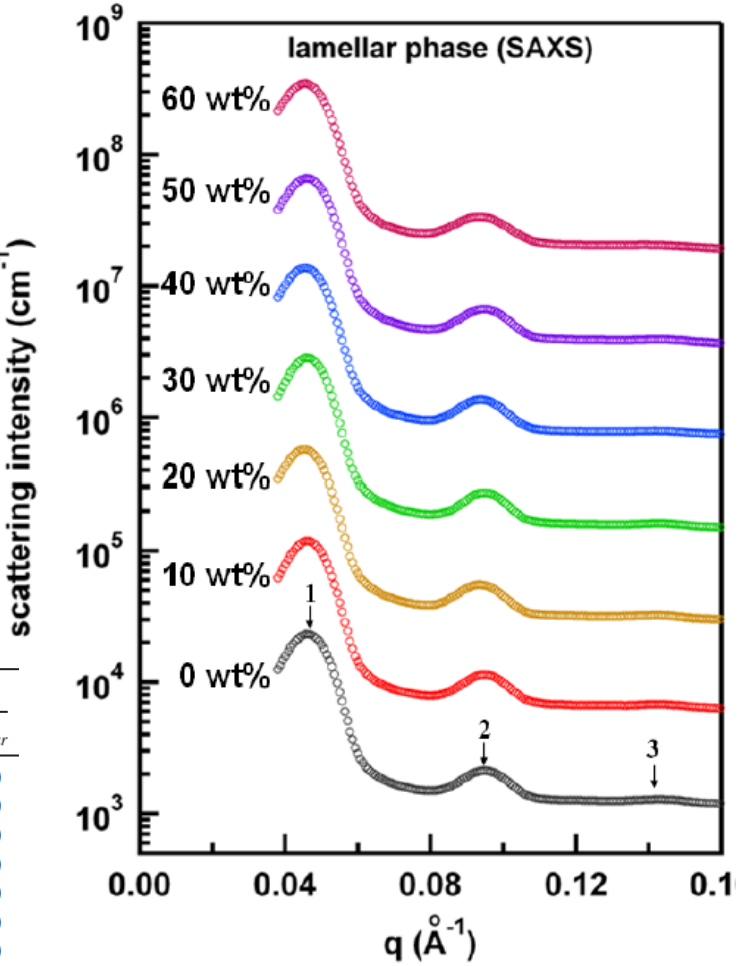

Subdomain Structures of Ternary System

SANS Results

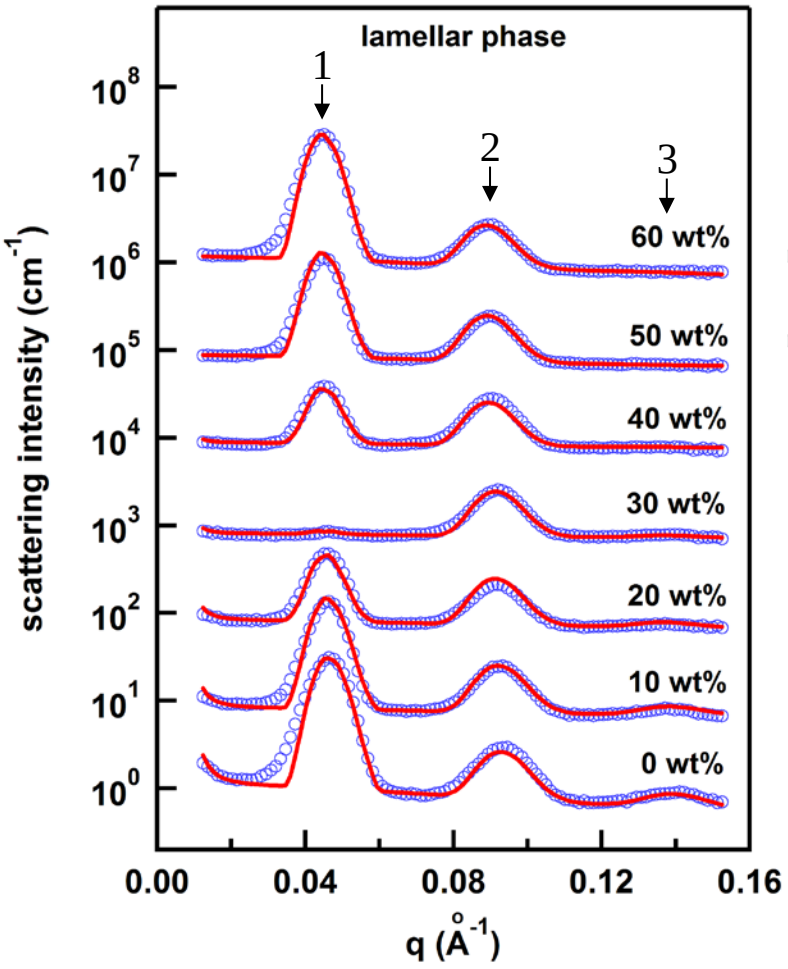

Proposed Model

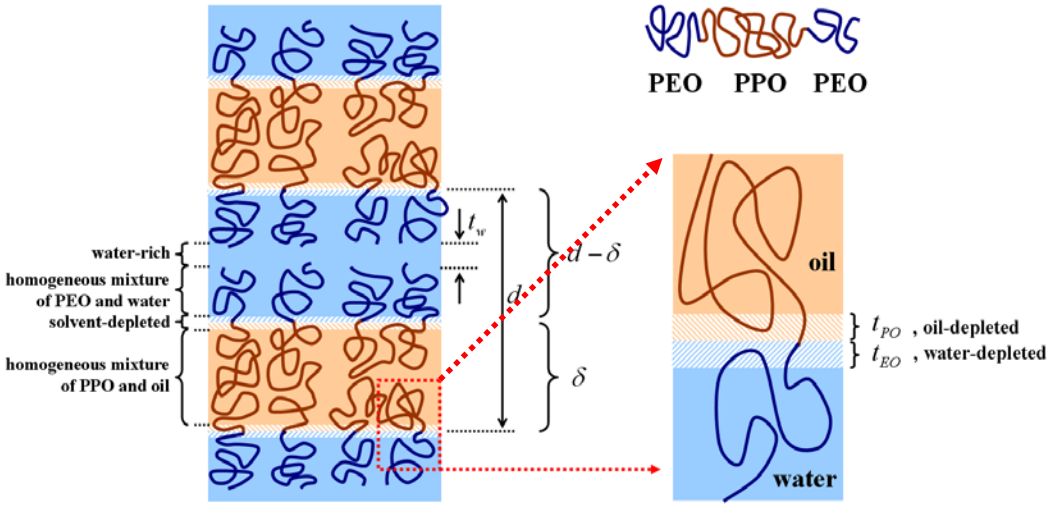

$$I(q) = S(q)|F(q)|^2/q^2 + b$$

$$S(q) = N + 2\sum_{k=1}^{k=N-1}(N-k)\cos(kqd)\exp(-k^2q^2\Delta^2/2)$$

Simultaneously fitting 7 curves with above model results in

d = 137.8 ± 2.3 Å
Δ = 2.4 ± 0.02 Å
t_w = 5.7 ± 0.06 Å
t_{EO} = 2.2 ± 0.01 Å
t_{PO} = 4.5 ± 0.01 Å

- **Sub-domain structure was revealed by contrast-varied SANS**

Do et al., *Macromolecules*, 43, 5411, **2010**

Distribution of Water Molecules in Dendrimers

- Dendrimers: Highly branched dendritic macromolecules
  - Structural duality: particle-like resemblance & flexible, porous polymeric architecture
  - Polyamidoamine dendrimers (PAMAM)
    - Ethylenediamine cores
    - Polyamidoamino units
  - Water distribution inside dendrimers determines both structure and dynamics of molecules
- Contrast varied SANS using mixtures of H2O and D2O

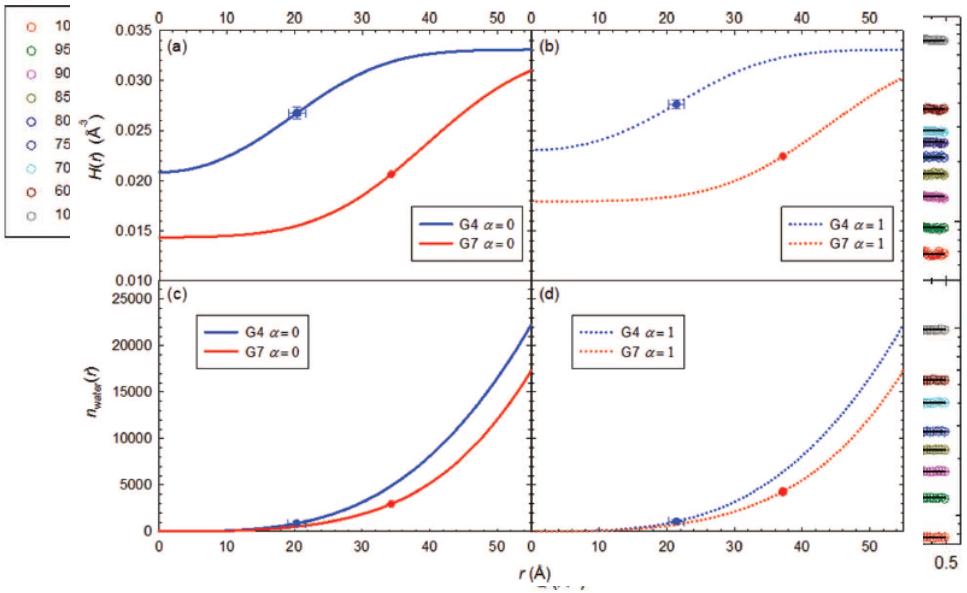

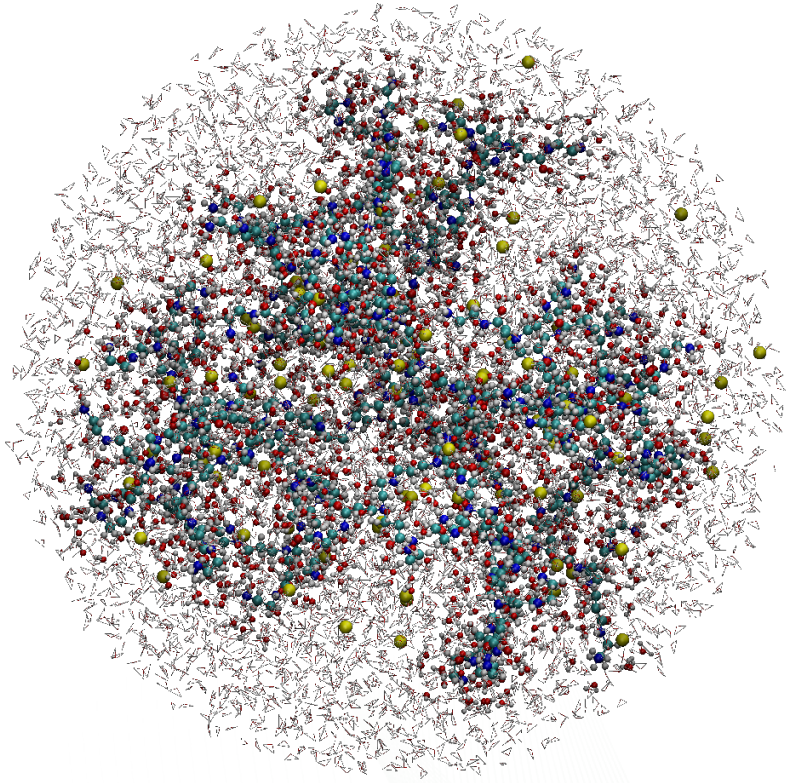

- **Dense-core molecular density profile**
- **Intra-molecular porosity is quantified**

Wu et al. *J. Chem. Phys.* **2011**, 135, 144903.

Smart Nano-sized Building Block

❑Polymer + Carbon nanotube (CNT) for functional materials

❑ Combination of their advantages complementary to each other

[CNTs]

- Remarkable physical properties
  - ✓ High thermal stability / tensile strength / elasticity
  - ✓ Extraordinary electrical and thermal conductivity
- Low percolation threshold
  - ✓ Unusual length-to-diameter ratio
- Poor solubility in commonly used solvents

[Pluronic Block copolymers]

- Good solubility in polar and organic solvents
- Rich phase behaviors (**Self-assembly**)
  - ✓ Various self-assembled architecture
  - ✓ Sensitive to environmental conditions : temperature, pH, etc
- Environment-friendly and biocompatible material
- Relatively poor mechanical and electrical properties

➔ Novel functional building block using CNT/polymer?

Thermo-responsive polymer shell + Rigid CNT core

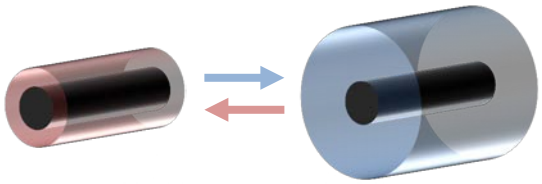

❑Sample preparation

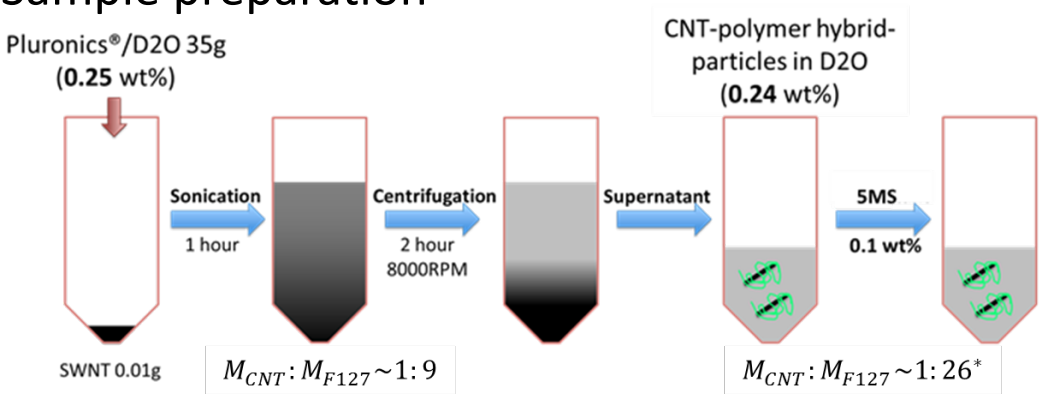

* Measured by TGA after freeze-drying

❑Materials

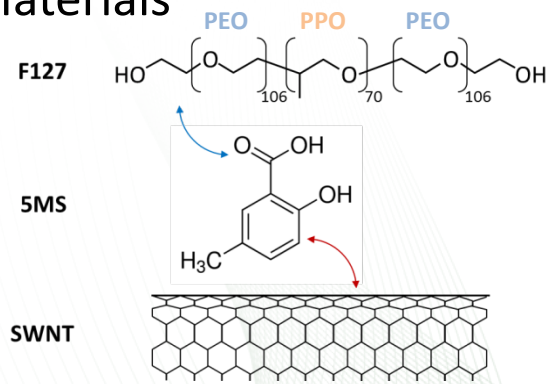

Y. Han, S. Ahn, Z. Zhang, G. S. Smith, and **C. Do*** *Macromolecules* **2015**, 48, 11, 3475–3480.

Tunable Encapsulation Structure

- Tunable encapsulation structure revealed by SANS

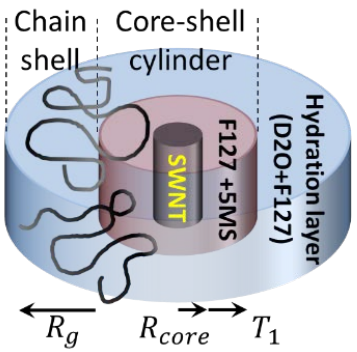

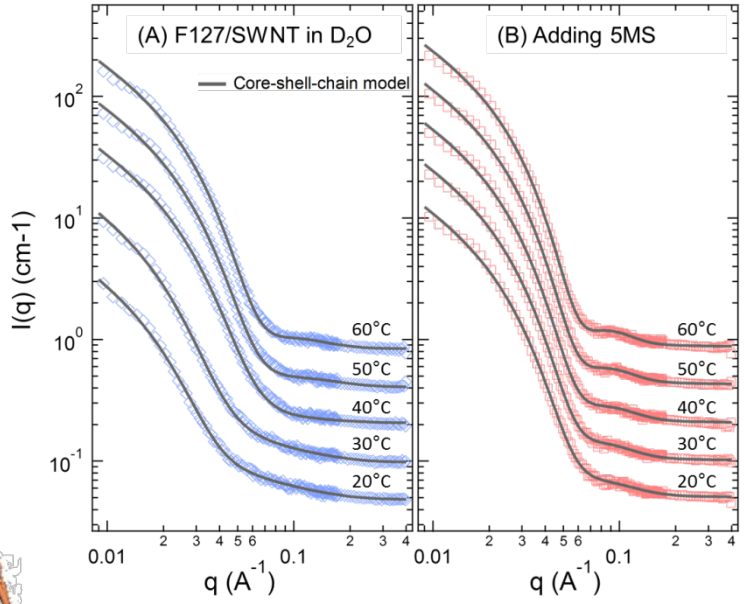

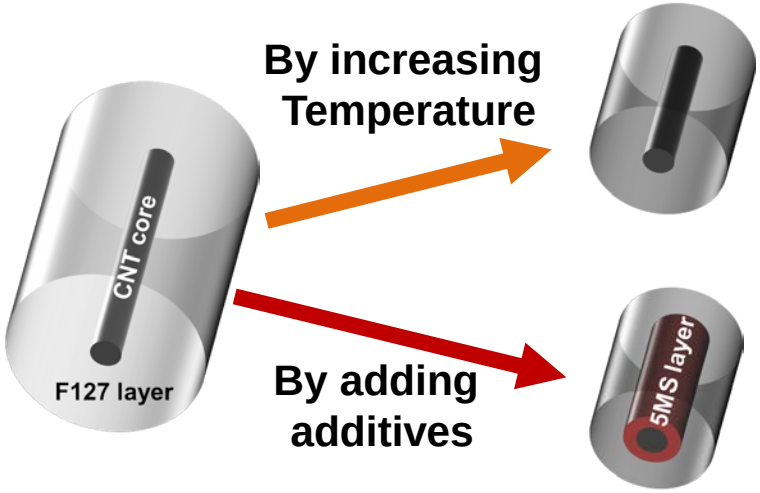

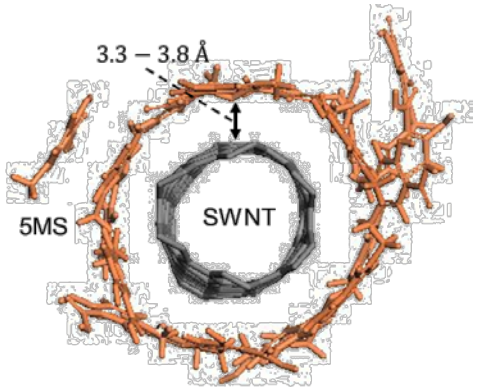

- UV-vis spectroscopy, AFM, TGA, MD simulation provide additional information that is helpful for SANS modeling
- Structure was revealed by taking advantages of different SLDs of CNT, polymer, solvent seen by neutrons

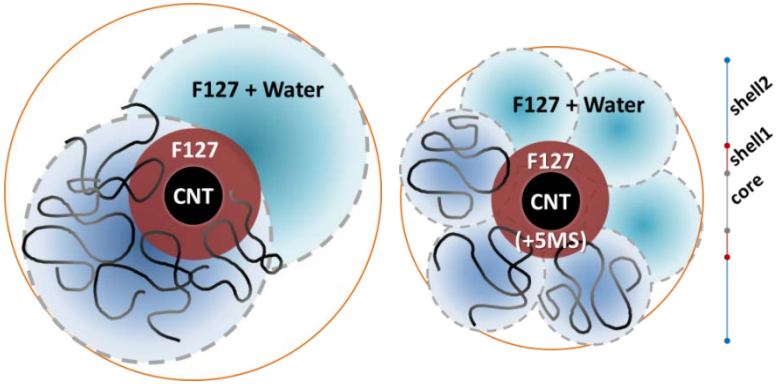

Self-Assembled Micelles: Relaxation Kinetics

- Critical micellization concentration, C^* (CMC)
  - Above a certain concentration, amphiphilic molecules (i.e. surfactants, block copolymers) self-assemble into micelles in aqueous solutions.

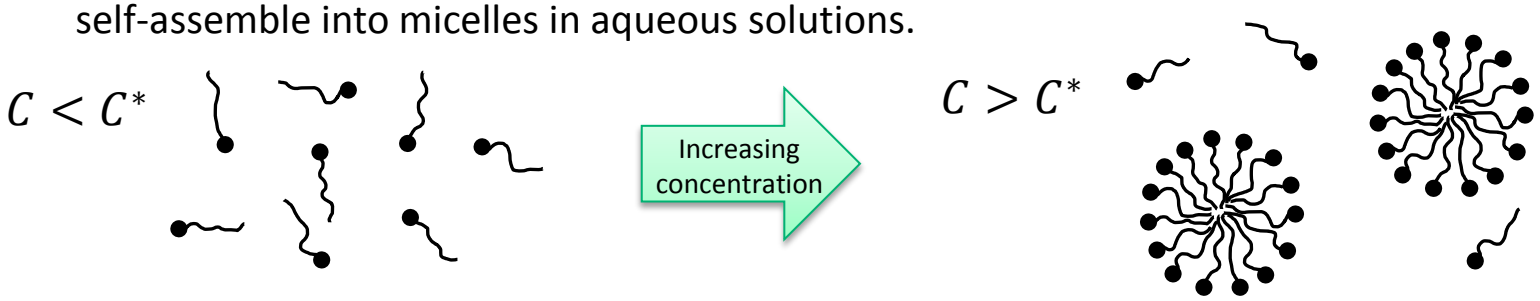

- Relaxation kinetics of micelles at dynamic equilibrium

  → Continuous redistributions of consistent molecules due to thermal fluctuations.

i) Association-dissociation process (exchange of individual molecules)

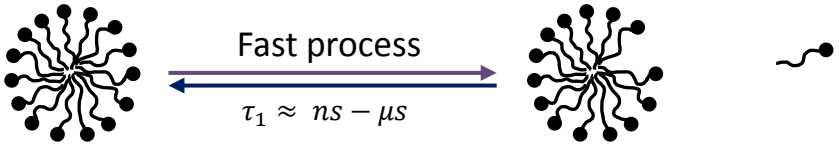

→ Fast process

N_{mic} : unchanged

ii) Micellization-dissolution process (breakup and formation of micellles)

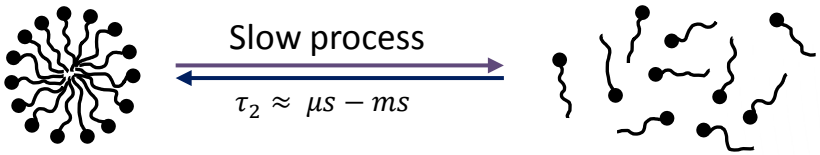

iii) Fusion-fission process

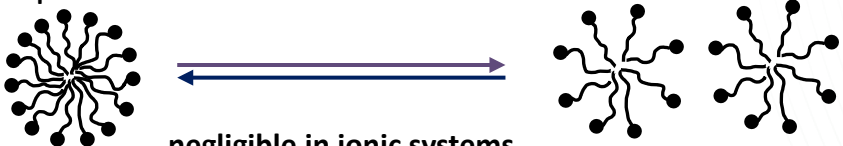

negligible in ionic systems

→ Slow process

N_{mic} : changed

A. Patist *et al. J. Colloid Interface Sci.* **245**, 1-15 (2002)

Time-Resolved SANS & Isotope Labeling

- Hydrogen isotopes (H vs. D)
  - Hydrogen
    : An important and major component in all soft and biological materials
  - Isotope labeling via H-D exchange
    : Very distinct neutron scattering lengths and cross sections

Deuterium (D)

$b_{coh} = +6.671 \times 10^{-15} m$

$b_{inc} = +4.04 \times 10^{-15} m$

Hydrogen (H)

$b_{coh} = -3.742 \times 10^{-15} m$

$b_{inc} = +25.274 \times 10^{-15} m$

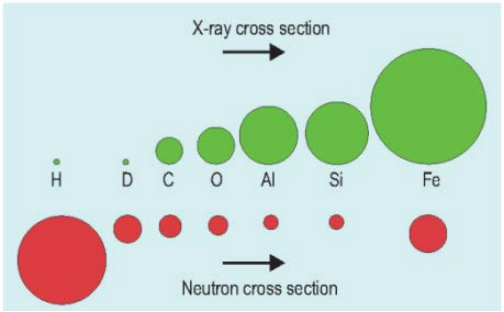

- Molecular exchange study via mixing H- and D-labelled micelles

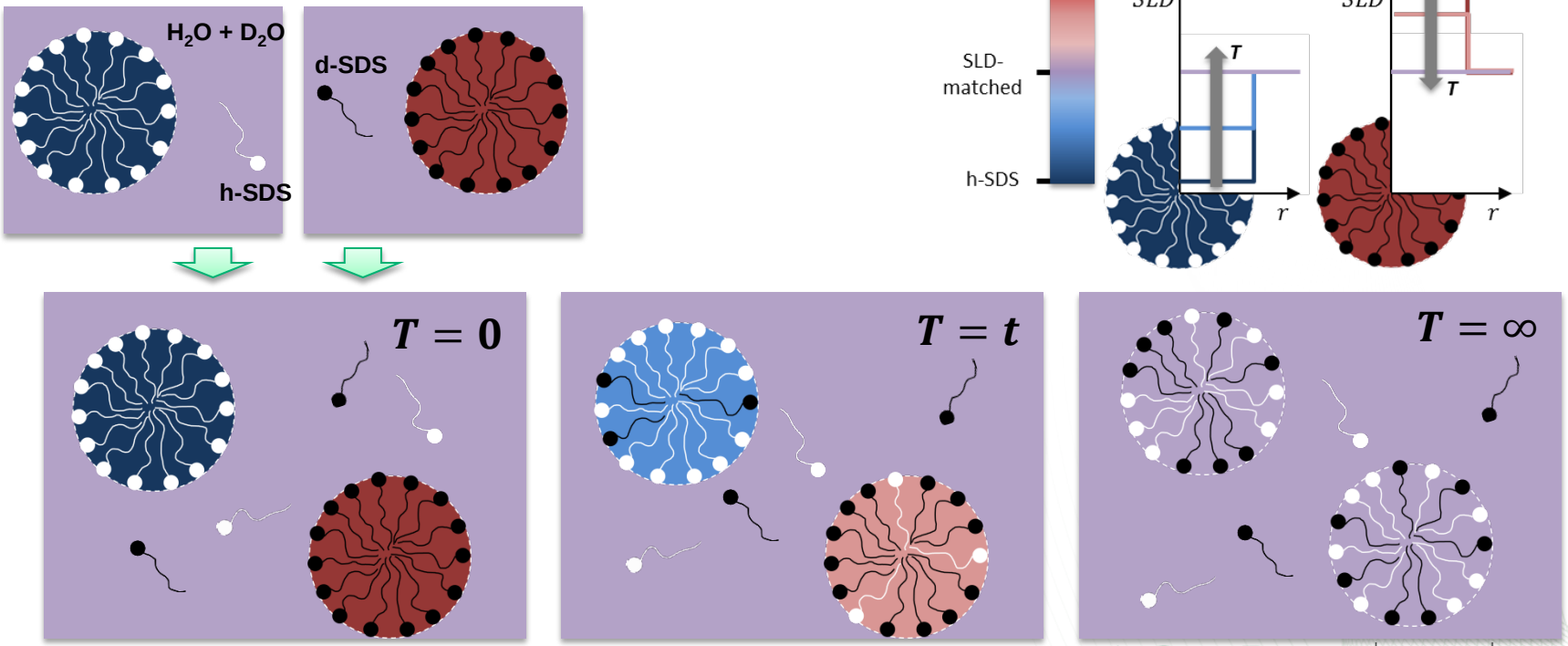

Contrast Matched Results

- SANS experiment
  - EQ-SANS beamline at SNS, ORNL
  - 1.3 m sample-to-detector distance
  - 5-8.5A neutron wave length band

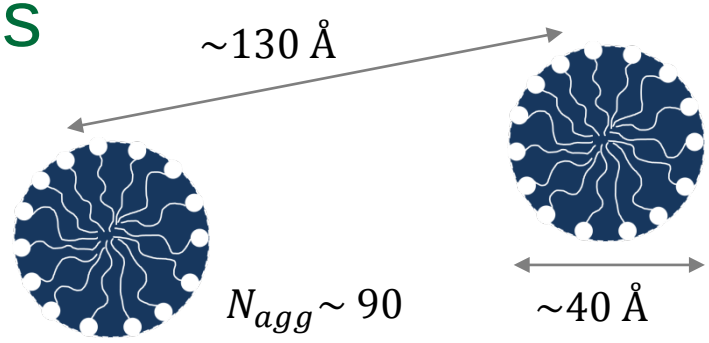

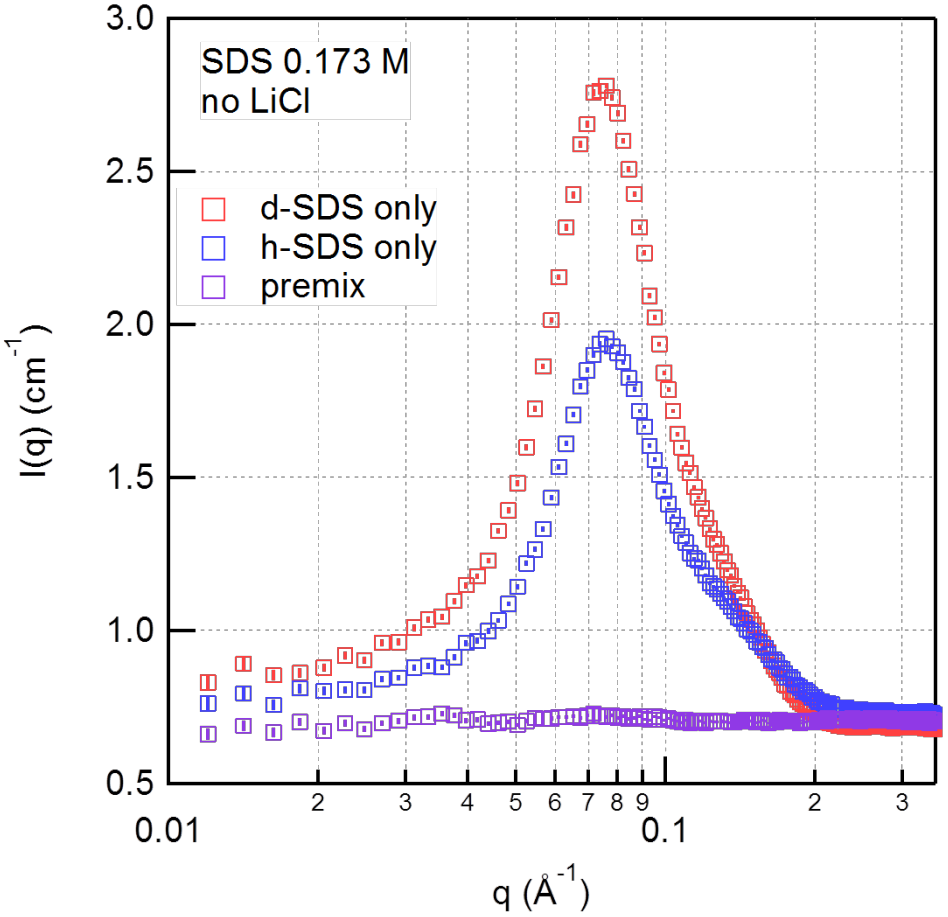

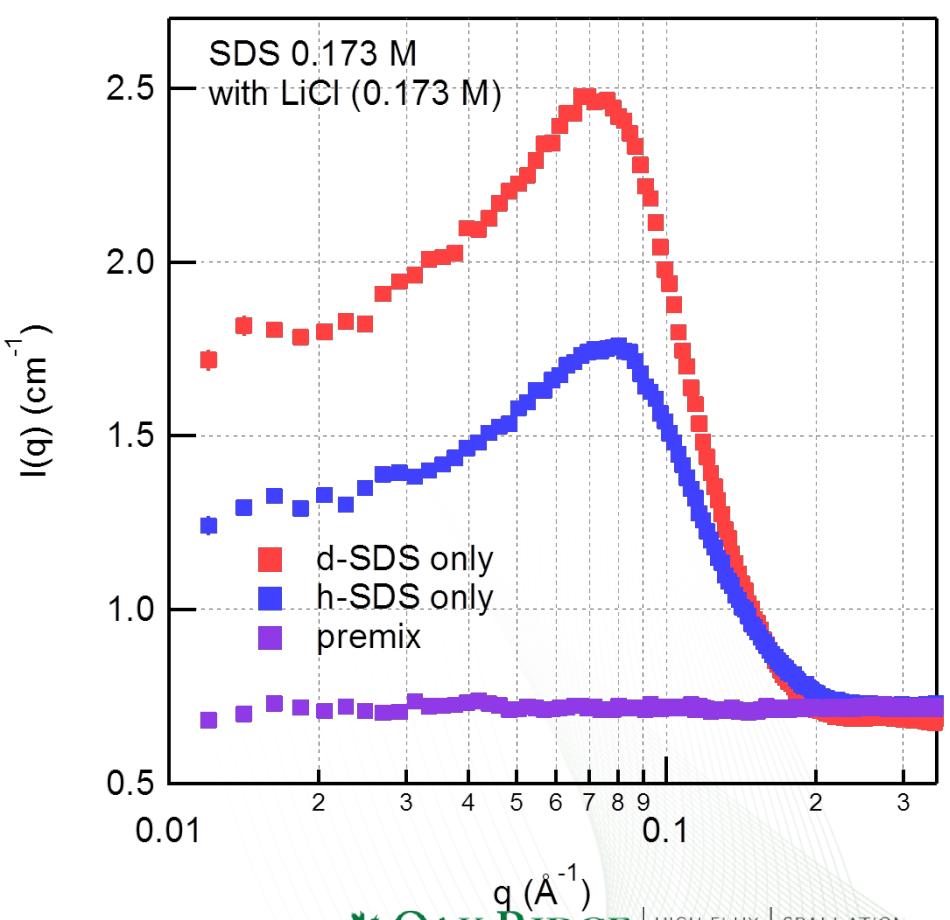

Time-Resolved SANS Results

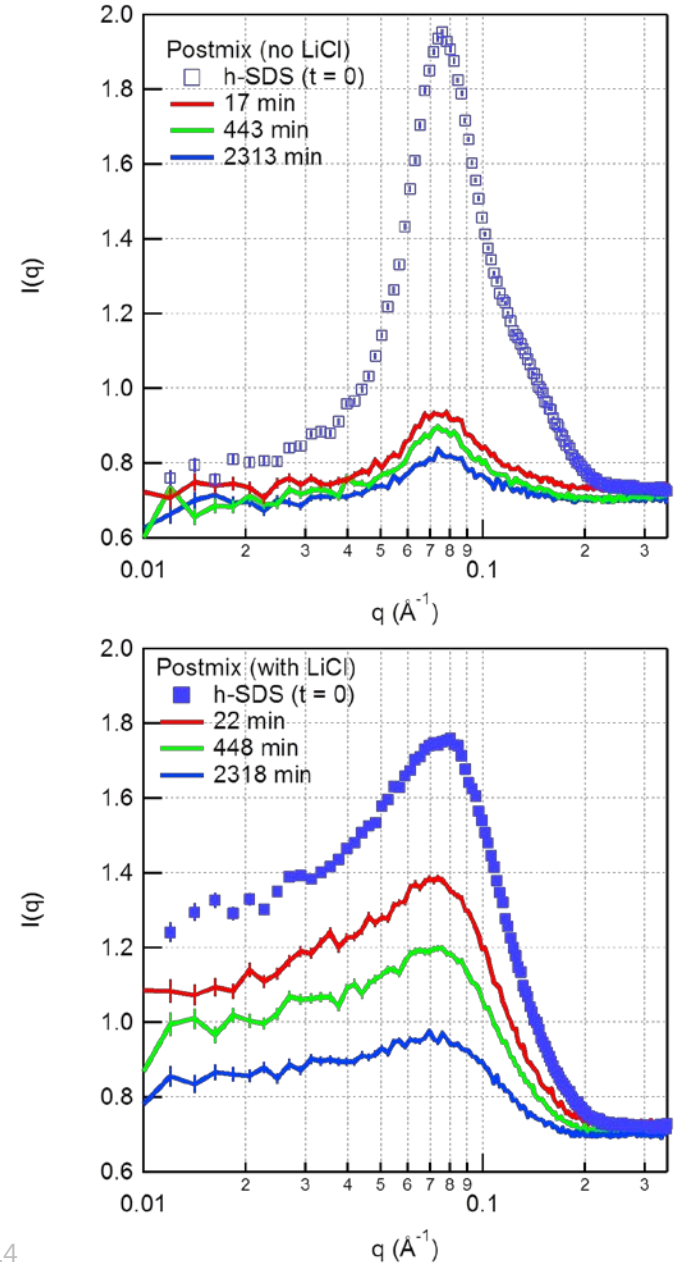

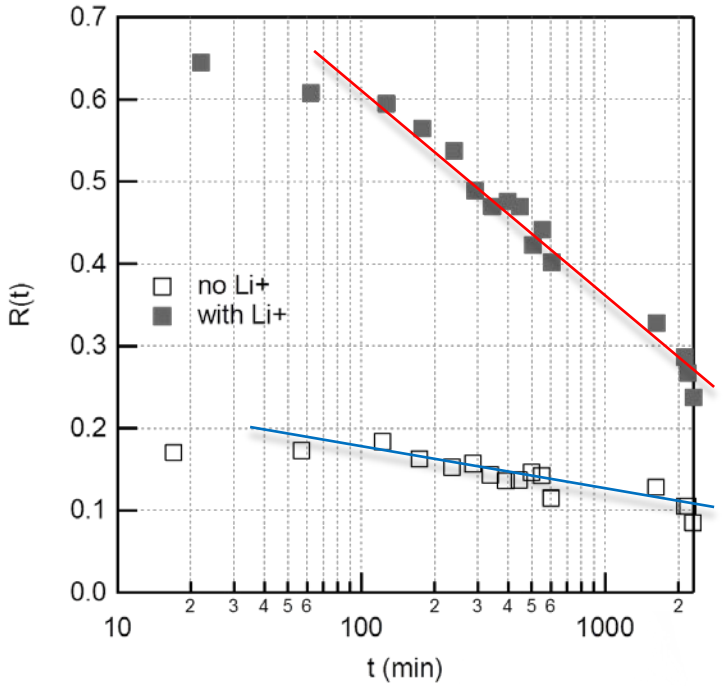

$$R(t) \equiv \frac{I(q_{peak}) - I_{bkg}(q_{peak})}{I_{h-SDS}(q_{peak}; T = 0) - I_{bkg}(q_{peak})}$$

- **Li+ ions significantly slow down the molecular exchange process**
- **More quantitative analysis is in progress**

A. Patist *et al*. *J. Colloid Interface Sci*. **245**, 1-15 (2002).
B. Hammouda, *J. Res. Natl. Inst. Stand. Technol*, *118*, 151-167 (2013).

Conclusion

- Neutron scattering investigation can provide unique structural information when it is combined with contrast variation techniques or isotope labelling
- Neutron's deep penetration power and low energy is ideal for studying soft materials

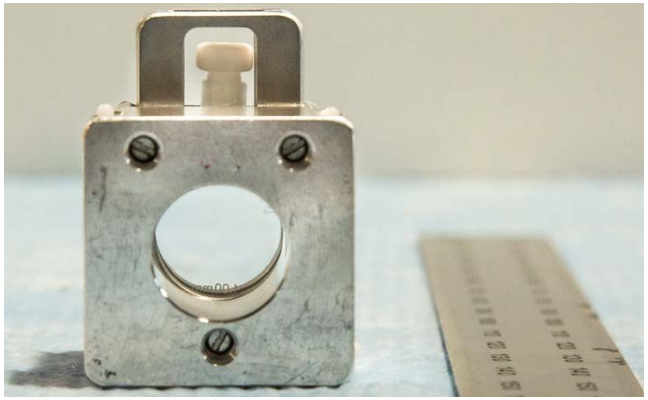

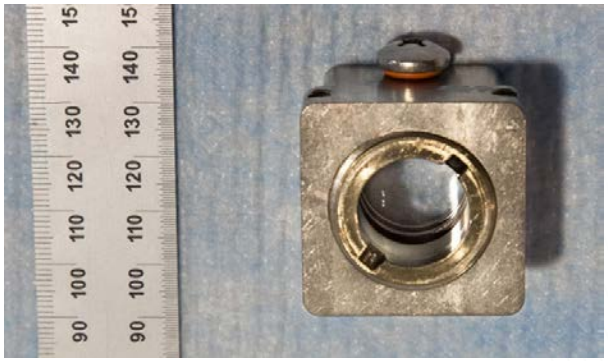

Acknowledgement

C. Do (BSMD, BL-6)
W.T. Heller (BSMD, BL-6)
W.R. Chen (BSMD)
G.S. Smith (BSMD)
Y. Han (BSMD)
Z. Zhang (BSMD)

P. C. Joshi (MSTD)
J.L. Banuelos (CSD)
P.F. Fulvio (CSD)
G. Rother (CSD)
S. Dai (CSD)
D.J. Wesolowski (CSD)

B.G. Compton
C.E. Duty

B. Wu

J. Chen
K. Hong
S.K. Ahn

G. Feng (CBE)
P.T. Cummings (CBE)

M. Ohl (JCNS-SNS, BL-15)

U.S. DEPARTMENT OF ENERGY
Office of Science

APPENDIX